THE PHYSICS OF SINGULAR DISLOCATION STRUCTURES IN CONTINUUM DISLOCATION DYNAMICS

A Dissertation

Presented to the Faculty of the Graduate School

of Cornell University

in Partial Fulfillment of the Requirements for the Degree of

Doctor of Philosophy

by

Woosong Choi

January 2013

THE PHYSICS OF SINGULAR DISLOCATION STRUCTURES IN CONTINUUM DISLOCATION DYNAMICS

Woosong Choi, Ph.D.

Cornell University 2013

Dislocations play an important role in the deformation behaviors of metals. They not only interact via long-range elastic stress, but also interact with short-range interactions; they annihilate, tangle, get stuck, and unstuck. These interaction between dislocations lead to interesting dislocation wall formation at the mesoscales. A recently developed continuum dislocation dynamics model that shows dislocation wall structures, is presented and explored in two and three dimensions. We discuss both mathematical and numerical aspects of simulating the model; the validity of our methods are explored and we show that the model has physical analogies to turbulence. We explain why and how the walls are formed in our continuum dislocation dynamics model. We propose modifications for more traditional slip dynamical laws, which lead them to form dislocation wall structures. Furthermore, we argue that defect physics may generate more singular structures than the density jumps that have traditionally been observed within fluid dynamics, and that development and enhancement of mathematical and numerical schemes will be necessary to incorporate the microscale defect physics that ought to determine the evolution of the singularity (replacing traditional entropy conditions).

BIOGRAPHICAL SKETCH

In the year 1981, Woosong Choi was born in Korea. This shy but curious boy grew up making transistor radios and writing computer software for many years, aspiring to be a scientist someday. He was a theorist at heart, backpack filled with heavy books, drafting ideas in his notebooks all the time, but was never hesitant to be an experimentalist at the same time, crafting gizmos and experimenting on whatever curiosity led to: at the age five he ironed the floor to see what happens – fortunately only the floors were burnt – and in his teens he blew up a mini bulb in an effort to observe how bright it would be on 100 volts – which is *very* bright although the bulb disappeared and he blacked out briefly.

During the middle school, he spent most of his time studying and practicing computer programming; he was sure he would become a computer scientist. However, since his stint of studying physics for the physics olympiad, his fascination for science revived again and he would spend four years (two years in high school and the first two years of college) focused on learning physics.

As his enormous of list of hobbies illustrates, he held intellectual interest in a large number of topics ranging through many scientific and engineering disciplines: to name a few, quantum computing, cellular dynamics, virtual reality, fluid dynamics simulations for geophysical flows, artificial intelligence and neuroscience, complex networks, etc. While working as a software engineer he developed a large scale search engine and spent the weekends those years studying bioinformatics, machine learning, and related subjects with friends. At this point, he decided that he needed to become a statistical physicist in order to better understand everything he is fascinated about from a fundamental perspective.

Then he came to Ithaca. He spent the first two years rummaging through books and trying to figure out what he should work on; then he joined Sethna group and started working on continuum dislocation dynamics. It turned out to be a very different journey than what he imagined and dreamed of until then; yet it led to exciting discoveries at times and surprising relations to – maybe because science and engineering is so intertwined – many topics that he previously had interest in.

He is now departing on a yet another adventure in a whole new field. It is unclear where that will lead him to, as it always has been, but in the end he is going to have fun, as he always had.

To my family

ACKNOWLEDGEMENTS

I would like to first thank my collaborators who contributed to each and every part of this thesis. Many of these projects would not have reached fruition without their contributions. Particularly, Jim Sethna, my advisor and collaborator, has been an endless source of inspiration in the scientific journey. Stefanos Papanikolaou has provided guidance and pushed me forward, especially when we worked together in figuring out the numerical methods. The whole set of projects on dislocation dynamics involved Yong S. Chen, and his perseverance led to various new findings. Our recent recruit, Matthew Bierbaum, contributed many things for the projects and he has assisted me in various fronts and research during my last year.

I have many colleagues to thank. We have regularly consulted Stefano Zapperi and Alexander Vladimirsky for various aspects in plasticity and hyperbolic conservation laws, and I thank both for their always positive opinions and helpful advices provided throughout. We would like to also thank Eric Siggia, Randall LeVeque, Chi-Wang Shu, Mattew Miller, and Paul Dawson for advices and guidance to fields which we were new to. I also thank my thesis committee members Chris Henley and Itai Cohen, for providing many helpful comments and guidance in writing of this thesis.

All of this work was made possible with support from US Department of Energy/Basic Energy Sciences grant no. DE-GF02-07ER46393, and we thank the Department of Energy for continued support on the research.

I would like to thank my family for that I would not have been able to achieve anything without them. My parents, Heejae Choi and Jongwon Kim, raised me to be here as an independent, self-criticizing, but confident person; all of these qualities have helped me survive and progress as a person and an

academic. My brother, Eunsong Choi, and I spent so much time together for the whole duration of my life. As he thrives to become a brilliant physicist himself, he has always been my friend and companion with whom I could talk about anything. I thank my grandmother for raising us brothers safely and warmly, and I would like to thank all my aunts, uncles, cousins, nieces and nephews who have cheered and supported my path here.

Lastly, I must thank my friend, a fellow physicist, colleague, and wife, Jeehye Lee, for the time we spent together as both of us struggled through our academic journeys.

TABLE OF CONTENTS

LIST OF TABLES

LIST OF FIGURES

CHAPTER 1

INTRODUCTION

1.1 Overview of the thesis

The prehistory of mankind experienced distinct "age" transitions from the stone age to the bronze age when *Homo sapiens* began mastering the art of manipulating copper and bronze. Subsequent transition took place from the bronze age to the iron age, and from then until the late 20th century the ability to obtain, forge, and utilize metal was the most important part of technology. It has become an overwhelmingly essential possession of the modern society; now we can not live or survive without all the metal tools, machines, and vehicles that form the infrastructure, structures, and machinery we rely on.

The history of metallurgy is not short – one could argue that it is one of the oldest engineering discipline – and tremendous amount of knowledge has been accumulated on how metals behave when they are cast, forged, rolled, and mixed(or alloyed). But our fundamental understanding of the whys and hows of material characteristics has remained primitive due to the limitations of our experimental and numerical tools. During the last century, however, technological advances in all fronts has led to exhilarating discoveries in the field of metallurgy.

New experimental tools provide eyes into smaller scales, reaching micrometers and nanometers. X-ray diffraction analysis in various forms led to studies of texture (crystal orientation distributions) and internal stresses, while the transmission electron microscope (TEM) allowed a microscopic view of a variety of

defects in crystalline structures.

Defects of several different forms are of great interest because of their effects on hardness and yield strength. Effects of solute atoms (precipitates) and vacancies are studied extensively in the field, but of primary importance are the dislocations. A dislocation is a line-like defect in a crystal; the mismatch in crystalline order at the "end of an extra inserted plane". Dislocations are crucial for *plasticity*. Crystalline metals have very strong bonds and deforming a perfect crystal far enough to break bonds would require an enormous stress. Not so when dislocations are present: crystals use their dislocation defects to deform plastically, by *moving* the dislocations.

Through the use of experimental techniques (TEM and EBSD) and theoretical and computational studies (elasticity, first principles and atomistic simulations), the properties of a single dislocation and the interactions of several dislocations have been understood in detail. For examples, the barriers for a dislocation to move (the Peierls barrier), how dislocation junctions behave, the speed of dislocation motion, and so forth. However, traditional macroscopic crystal plasticity, and augmented gradient theories developed to apply at smaller length scales, are yet far from the atomic and few-dislocation scales that are understood microscopically using these experiments and theoretical studies. Various attempts have been made to bridge the scales, but neither theory nor experiment has been able to convincingly provide a solid bridge across the micron scale, which is the focus of this thesis.

One of the most interesting physics that happen in the intermediate (meso) scales is the formation and evolution of dislocation structures. Dislocations are known to not only nucleate and glide, but also annihilate, form junctions (tan-

gle), cross-slip, climb, and get stuck (and unstuck) for various other reasons. These complex short-range interactions, in addition to the long range interaction between dislocations through stress, conspire to produce dislocation patterning and dislocation wall structures.

Dislocation wall structures have also been an area with many enlightening discoveries, with models using phase field [40, 87, 52, 41], Potts models [15, 83], level-set methods [66], and front-tracking methods. However, these models are focused on studying the behaviors of dislocation walls whose existence and properties are presumed known from extensive experimental and numerical studies. These methods can not answer the questions of why and how the dislocations structures form and evolve. On the other hand, coarse grained continuum theories of the microscopics have yet to be fully successful, with many remaining difficulties.

In this thesis, we focus on a particular continuum model of dislocation dynamics that exhibits dislocation wall formation [49, 16]. The model has its own share of subtle issues, however, and we will focus our discussion on justifying our methods for numerically solving and understanding the model. We explore and illustrate the physics behind wall formation observed in our model; we provide a generic mechanism which could be responsible for dislocation wall formation; and we argue that existing numerical methods need to expand their horizons, allowing for singularity evolution laws to be incorporated based on the physical properties.

1.2 Chapters of the thesis

We start in chapter 2 by introducing our continuum dislocation dynamics model. We find that dislocation wall structures are formed in 2D simulations, and with glide-only dynamics they exhibit fractal self-similar patterns. We compare our results to various TEM measurements analyzed with different models and methods, and propose that self-similar correlated dislocation patterns analyzed with fractal analysis and scaling need not disagree.

Chapter 3 focuses on explaining how the simulations of our continuum dislocation dynamics are analogous to those of turbulence. Analogies are drawn based on their numerical behaviors in the limit of infinitely fine mesh and low viscosity. We propose that, as in the case of turbulence, the limit of vanishing viscosity leads naturally to spatio-temporal nonconvergence. Nevertheless, also as in turbulence, we argue that successful numerical methods should provide statistical behaviors that are consistent and convergent.

In chapter 4 we explore in detail how we perform simulations of the continuum dislocation dynamics model. The applicability of existing methods is already a concern for this problem, exhibiting several issues: nonlocality, questionable hyperbolicity, the appearance of δ-shock, and spatio-temporal nonconvergence. We discuss each of these concerns and argue that the simulations represent the physical behavior of the equation faithfully. Detailed analysis that were performed in the process of studying the equation are presented in this chapter; sometimes forming the basis of more speculative work described in later chapters. Particularly, questions we addressed in checking the validity of the numerical methods – self-skepticism prompted by the turbulent and singu-

lar behaviors – are addressed here in detail.

In chapters 5 and 6 we discuss the generic ways δ-shocks walls can appear in systems of conservation laws. We show in chapter 5 that existing plasticity models can be modified in natural ways to exhibit wall formation. We argue in chapter 6 that the physics of the singularities may not be derivable as a 'weak limit' of the continuum equations, and that prescribing the singularities' dynamics from microscopic considerations demands departure from the traditional notion of solutions for hyperbolic conservation laws.

Lastly, we will describe how the simulations performed in this thesis have been accelerated greatly by the use of massively-parallel GPU computing technology in appendix A.

1.3 Choosing a method, choosing a model

This thesis focuses mainly on implementation and validation of the numerical methods, and while it is argued that the numerical methods works well and gives consistent and physically meaningful solutions, we are still left with questions. Particularly, we show that solving the equations in different form leads to different solutions (Chapter 6 and Appendix B), although qualitatively they might be the same. We also argue that depending on the microphysics of the singularities, new numerical methods may be necessary to cope with the fact that the "viscosity solutions" are not the physical solutions in chapter 6. Lastly, while our continuum dislocation dynamics simulations do provide a theoretical view of cell wall formation and evolution, it remains to be seen whether it is the only explanation (mechanism) of the behavior, or if it is physically relevant at

all.

How do we choose a method? How do we determine whether the method and/or the model is suitable and physical? This question is pertinent to any theoretical and numerical methods applied to any model intended to describe a physical phenomenon; traditionally, the answer to this is to confirm the predictions of the model and the method with experiments. This, however, is only in theory a good answer, as it still remains to question what experiments does one compare to, and what predictions do indeed provide validations.

For example, many continuum theories of dislocations are augmented with *constitutive relations*; these additional constraints in essence provide coarse-grained effective terms to the dynamics so as to exhibit "correct" physical behavior, such as the stress-train curves and yield strength. It must be asked, obviously, whether the model and the method is indeed capable of replicating targeted physical property; it would simply be a bad model (or method) if it did not do so. However, it must be noted that the model (or method) must then be validated for other physical properties, for applications with different targets.

What physical properties are we interested in? Are the models and the methods we used faithfully reproducing the physics of interest?

As we have asserted throughout, dislocations exhibit complex collective behaviors such as dislocation cell walls. The sequence of our contribution in continuum dislocation dynamics (Refs. [50, 51, 17] and Chapters 2, 3, 4, and 5) have focused on the behaviors of dislocation wall structures.

Unfortunately, what dislocation cell walls do and how they form have not been experimentally observed. Comparison of our 2D simulations to TEM mi-

crographs (as studied in Chapter 2) hints that the model may indeed be moving in the correct direction, but there are yet too many properties to be explained. Rome was not built in a day, however, and a roadmap of models could guide us through the steps as we build on previous work.

As physicists, we are more intrigued by universal fundamental behaviors. Also, models and theories based on microscopic physics, rather than phenomenology, are preferred since we are interested in the phenomena themselves. However, it is also clear that real materials and real systems ought to be explained by the models, and some higher-order theories that correct for the real world deviations from the minimalistic theory are exceedingly valuable as well. This flexibility in the complexity of the model allows for generic applicability and usability of the models, as it could be used from understanding generic behaviors to predicting material specific properties.

CHAPTER 2

BENDING CRYSTALS: EMERGENCE OF FRACTAL DISLOCATION STRUCTURES[1]

2.1 Introduction

Structural engineering materials have a bewildering variety of microstructures, which are often controlled by deformation and annealing during the formation process. An imposed distortion generates a complex morphology even for a single crystal of a pure material – polycrystalline grains form at high temperature where dislocation climb allows for polygonization, cell structures form at low temperatures when climb is forbidden. Cell walls (Fig. 2.1c,d) are distinct from grain boundaries in that they have smaller misorientations, different origins, are morphologically fuzzier, and the cells refine (get smaller) under shear. Experiments differ in characterizing the cell structures; some show convincing evidence of fractality [61, 77, 29] with structure on all length scales (Fig. 2.1c), while others show structures with a single characteristic scale setting their cell size and cell wall misorientation distributions [36, 34, 35] (Fig. 2.1d).

Dislocation avalanches [58], size-dependent hardness (smaller is stronger) [84] and cellular structures [61, 34] all emerge from collective dislocation interactions on the micron scale. We expect that these mesoscale phenomena should be captured by an appropriate continuum theory of dislocation dynamics. Computationally, such a theory is crucial for multiscale modeling, as atomistic and discrete dislocation simulations are challenging on these scales of length and strain.

[1] This chapter has been published in Physical Review Letters [16]. The content of this chapter has also been incorporated in Yong Chen's thesis.

Here we present a minimal model for cellular structures, which eventually can be extended to include the pinning and entanglement needed for avalanches and hardness, and the slip systems and statistically stored dislocations needed for realistic descriptions of texture evolution and cross-slip [53]. Our model gives the elegant, continuum explanation for the formation and evolution of cellular dislocation structures. It exhibits both the experimentally observed fractal structures and scaling collapses hitherto thought incompatible. Finally, it provides the fundamental distinction between cell walls and grain boundaries; cell walls are intrinsically branched in a fractal fashion.

Within a continuum theory of dislocation dynamics [74, 49], incorporating only elastic self-interactions with a minimally modified gradient dynamics, we study the relaxation of a smoothly deformed crystal and its subsequent evolution under external strain (Fig. 2.1a and b). When climb is allowed, we find the distortion neatly evolves into a stress-free collection of grain boundaries. When climb is forbidden, cell wall structures evolve with power-law correlations and self-similarity – providing a clear morphological distinction between cell walls and grain boundaries, a tangible model for the experimentally observed fractal structures [61, 77, 29], and an alternative to those that predict microstructure without a wide range of scales [65]. The resulting morphology, however, is self-similar only after rescaling both space *and amplitude*. Performing the experimentalist's analysis of the misorientations and cell size distributions [36, 34, 35] yields good agreement with the observed scaling form (albeit with significantly different scaling functions and exponents). By directly exhibiting key features of the emergent experimental behavior in a continuum, deterministic dislocation density theory, our simulations pose a challenge to theories based on stochasticity in the continuum laws [29, 27] or in the splittings and rotations of the

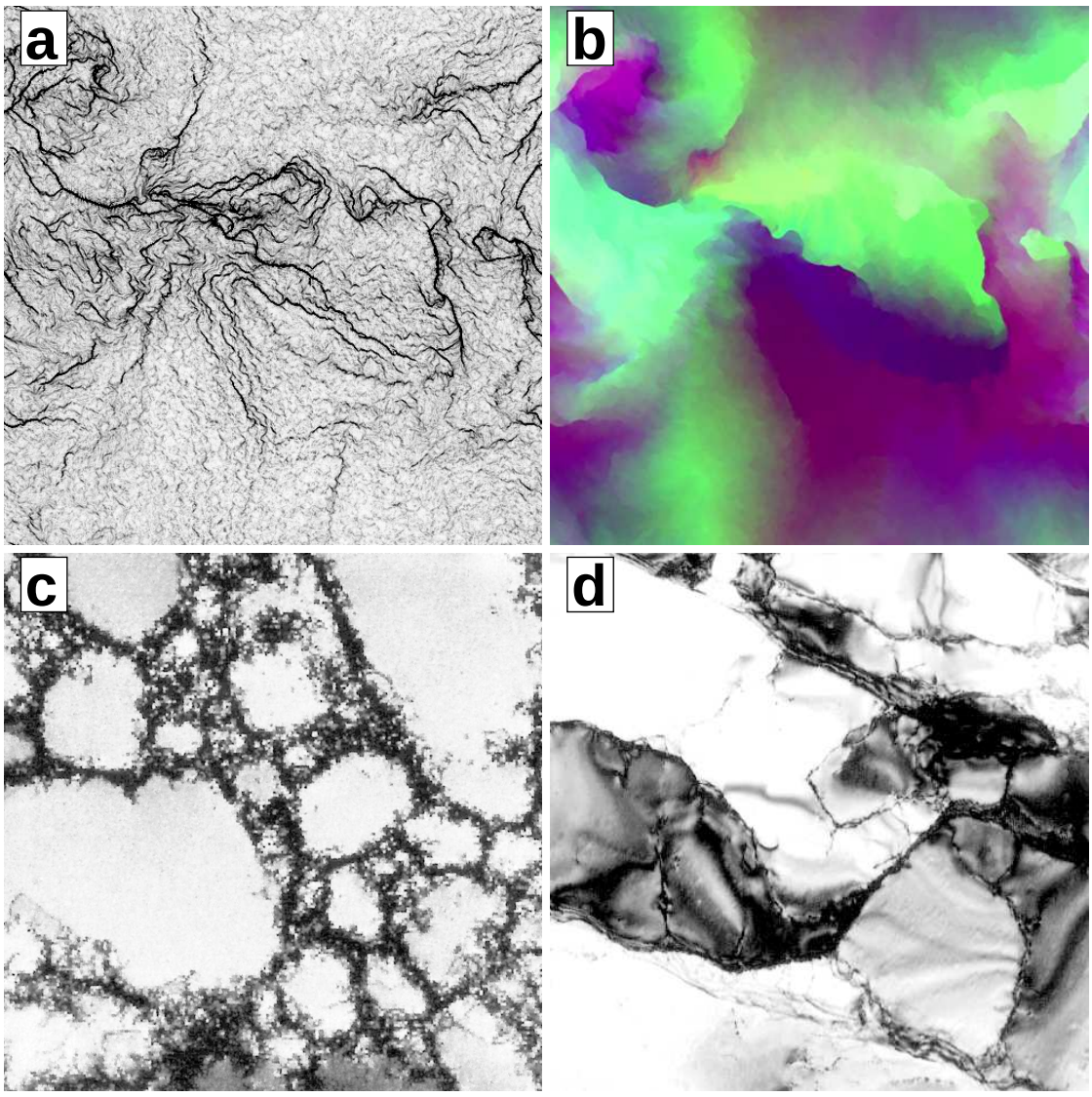

Figure 2.1: **Theoretical and experimental dislocation fractal morphologies**. *Top:* Simulated fractal cell wall pattern after uniaxial strain of $\epsilon_{zz} = 4\beta_0$. (a) Dislocation density plot; (b) Local orientation map. *Bottom:* TEM micrographs taken from: (c) a Cu single crystal [61] after [100] tensile deformation to a stress of 75.6 MPa and (d) an Al single crystal following compression to $\epsilon = 0.6$ [34], respectively. Gray scales have been adjusted to facilitate visual comparisons. Note the striking morphological similarity between theory and experiment.

macroscopic cells [68, 50]. Can these stochastic theories describe our chaotic dynamics after coarse graining?

2.2 Minimalistic isotropic continuum dislocation dynamics

Our order parameter is the plastic distortion tensor β^{P}. Together with the resulting elastic distortion β^{E} derivable from β^{P} via the long-range fields of the dislocations [49], β^{P} both gives the deformation $\mathbf{u}$ of the material (through $\partial_i u_j = \beta^{\mathrm{E}}_{ij} + \beta^{\mathrm{P}}_{ij}$) and gives a three-index variant of the Nye dislocation density tensor [64] $\rho_{ijk}(\mathbf{x}) = \partial_j \beta^{\mathrm{P}}_{ik} - \partial_i \beta^{\mathrm{P}}_{jk}$ (defining the flux of dislocations with Burgers vector along the coordinate axis $\hat{\mathbf{e}}_k$ through the infinitesimal surface element along $\hat{\mathbf{e}}_i$ and $\hat{\mathbf{e}}_j$). β^{P} thus fully specifies the dislocation wall morphologies, the crystal rotation (the Rodrigues vector $\mathbf{\Lambda}$ giving the axis and angle of rotation), and the stress field σ (the external load plus the long-range stresses from the dislocations, given by a kernel [49, 62] $\sigma_{ij}(\mathbf{r}) = \sigma^{\mathrm{ext}}_{ij} + \int K_{ijkl}(\mathbf{r} - \mathbf{r}')\rho_{kl}(\mathbf{r}')\, d\mathbf{r}'$).

Following Roy and Acharya [74], we assume the flow of $\rho_{ijk}(\mathbf{x})$ is characterized by a single velocity $\mathbf{v}(\mathbf{x})$. Allowing both climb and glide, we can take the velocity $\mathbf{v}$ to be proportional to the Peach-Kohler force $\mathcal{F}$ on the entire population of dislocations times a mobility $D(|\rho|)$ $v_a = D(|\rho|)\mathcal{F}_a = D(|\rho|)\rho_{ast}\sigma_{st}$, where σ is the stress; we then define $\partial {\beta^{\mathrm{P}}}_{ij}/\partial t = J_{ij} = v_a \rho_{aij}$. (This provides the same equation of motion derived later by Limkumnerd and Sethna [49].) To remove dislocation climb (mass transport via frozen-out vacancy diffusion), we must set the trace of the volume change $J_{ii} = 0$, suggesting a dynamics which moves only the traceless portion of the dislocation density:

$$\frac{\partial \beta^{P}_{ij}}{\partial t} = J_{ij} = v_a \rho_{aij} - \frac{1}{3}\delta_{ij} v_a \rho_{akk}. \tag{2.1}$$

In this case, to guarantee that energy monotonically decreases we are led to choose the velocity based on the Peach-Kohler force on this traceless part $v_a = D(|\rho|)(\rho_{ast} - \delta_{st}\rho_{abb}/3)\sigma_{st}$, making the rate of change of the energy density the negative of a perfect square [17]. (This differs from our earlier glide-only

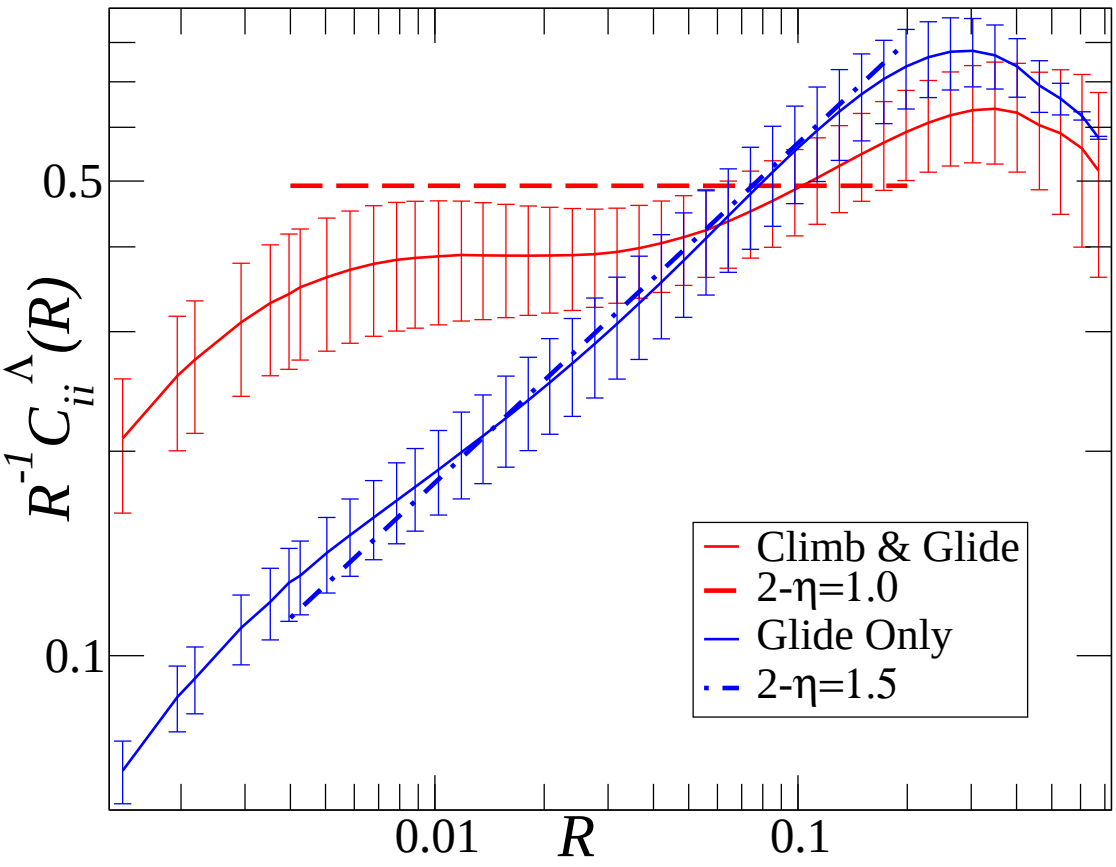

Figure 2.2: **Scaling of the correlation function** (1024^2 simulations). The trace of the orientation-orientation correlation function $C_{ij}^{\Lambda}(R) = \langle(\Lambda_i(\mathbf{x}) - \Lambda_i(\mathbf{x}+\mathbf{r}))(\Lambda_j(\mathbf{x}) - \Lambda_j(\mathbf{x}+\mathbf{r}))\rangle$ is averaged over all pairs of points at distance $|\mathbf{r}| = R$. Notice that the simulation allowing climb has $C_{ii}^{\Lambda}(R) \sim R$ as expected for non-fractal grain boundaries. Notice that the glide-only simulations show $C_{ii}^{\Lambda}(R) \sim R^{2-\eta}$ with $\eta \approx 0.5$, indicating a fractal, self-similar cell structure, albeit cut off by lattice and system size effects.

formulation [49].) To ensure that the velocity is proportional to the force per dislocation, we choose $D(|\rho|) = 1/|\rho| = 1/\sqrt{\rho_{ijk}\rho_{ijk}/2}$. Our theory does not incorporate effects of disorder, dislocation pinning, entanglement, glide planes, crystalline anisotropy, or geometrically unnecessary dislocations. It is designed to provide the simplest framework for understanding dislocation morphologies on this mesoscale.

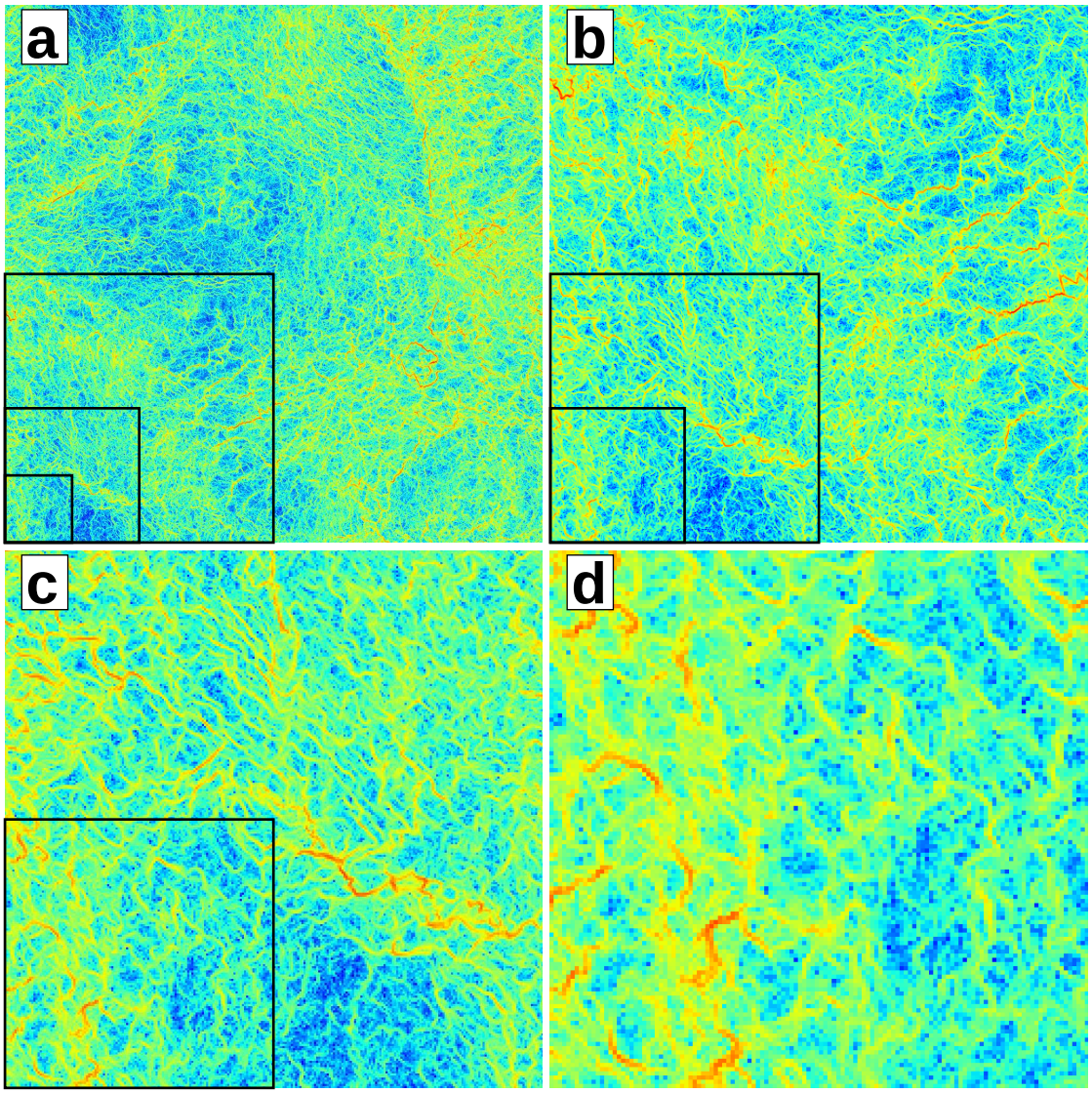

Figure 2.3: **Self-similarity in real space**. Each frame represents the lower left-hand quarter of the previous frame. Frame (a) is a 1024×1024 simulation; (b), (c), and (d) are thus of length $L = 512$, 256, and 128. All are rescaled in amplitude by $(L/L_0)^{-\eta/2}$ with $\eta = 0.5$ (see Fig. 2.2 and Table 2.1). The scale is logarithmic with a range of almost 10^7. Notice the statistical self-similarity. Other regions, when expanded, can show larger differences between scales, reflecting the macroscopic inhomogeneity of the dislocation density.

2.3 Numerical method and turbulent behavior

Our simulations show a close analogy to those of turbulent flows. As in three-dimensional turbulence, defect structures mediate intermittent transfer of mor-

Table 2.1: **Critical exponents** measured for different correlation functions. **GO:** Glide Only; **CG:** Climb&Glide; **ST** Scaling Theory [17].

Correlation functions	GO	CG	ST
$C^{\Lambda}_{ii}(\mathbf{r}) = \langle \sum_i [\Lambda_i(\mathbf{r}) - \Lambda_i(0)]^2 \rangle$	1.5 ± 0.1	1.1 ± 0.1	$2 - \eta$
$C^{\rho}(\mathbf{r}) = \langle [\rho_{ij}(0)\rho_{ij}(\mathbf{r})] \rangle$	0.4 ± 0.1	0.9 ± 0.3	η

phology to short length scales. (Unlike two-dimensional turbulence, we find no evidence of an inverse cascade – our simulations develop structure only at scales less than or equal to the initial correlation length of the deformation field.) As conjectured [70] for the infinite-Reynolds number Euler equations, our simulations develop singularities in finite time [49]. It is unclear whether our physically motivated equations have weak solutions; our simulations exhibit statistical convergence, but the solutions continue to depend on the lattice cutoff (or on the magnitude of the artificial diffusion added to remove lattice effects) in the continuum limit (See chapters 4 and 3). Since our simulations exhibit structure down to the smallest scales, we conjecture that this is a kind of sensitive dependence on initial conditions – but here amplified not by passage of time, but by passage through length scales. Since the physical system is cut off by the atomic scale, we may proceed even though our equations are in some sense unrenormalizable in the ultraviolet.

We simulate systems of spatial extent L in two dimensions with periodic boundary conditions; our deformations, rotations, strains, and dislocations are fully three-dimensional. The initial plastic distortion field β^{P} is a Gaussian random field with decay length $L/5$ and initial amplitude $\beta_0 = 1$. We apply a second order central upwind scheme designed for Hamilton-Jacobi equations [43] on a finite difference grid. The unstrained simulations presented are at late time, where the elastic energy density is small and smoothly decreasing to zero, (see

Supplementary Movies 1 and 2 [2]). The strained simulations in Fig. 2.4, (see Supplementary Movie 3 [2]), have uniaxial strain in the out-of-plane direction, which is increased by adjusting the external stress $\sigma_{zz}(t)$ to hold $\epsilon(t)$ fixed. The strain rate is $\dot{\epsilon} = 0.05\beta_0^2$.

2.4 Correlation functions and self-similarity

Figure 2.2 shows the orientation-orientation correlation function. Here we see that the cellular (climb-free) structures have non-trivial power-law scaling, but we see non-fractal behavior in the grain boundary morphology allowing climb. In Supplementary Movie 2 [2], the complex structure of cell walls (climb-free) shows a few primary large-angle boundaries with high dislocation density and many low-angle sub-boundaries, leading to fuzzy cell walls that are qualitatively different from the grain boundaries (climb & glide, seen in Supplementary Movie 1 [2]). Table 2.1 includes also the correlation function of the total dislocation density; one can show [17], if the elastic strain is zero [50], that $C^{\rho}(\mathbf{r}) = -\partial^2 C^{\Lambda}_{ii}(\mathbf{r}) - \partial_i\partial_k C^{\Lambda}_{ik}(\mathbf{r})$, so $C^{\Lambda}_{ij}(\mathbf{r}) \sim |\mathbf{r}|^{\alpha}$ tells us that $C^{\rho}(\mathbf{r}) \sim |\mathbf{r}|^{\alpha-2}$, implying the exponent relation $\alpha = 2-\eta$ in the last column of Table 2.1. The scaling for the correlation function for the total plastic distortion β^{P} is not as convincing [17]. Both are consistent with a renormalization-group transformation that rescales the dislocation density by a factor of $b^{-\eta/2}$ when it rescales the length scale by a factor of b. Figure 2.3 gives a real-space renormalization-group illustration of this self-similarity; the cell walls form a self-similar, hierarchical structure.

[2] http://link.aps.org/supplemental/10.1103/PhysRevLett.105.105501.

2.5 Comparison to experiments

Can we reproduce the experimental fractal characterization of cell boundaries? Box-counting applied to the dislocation density (as in Fig. 2.1a) gives dimensions that depend strongly on the amplitude cutoff (the dislocation density is self-similar, not a simple fractal). If we first decompose our simulation into cells as in Fig. 2.4b, and apply box-counting to the resulting cell boundaries, we obtain a fractal dimension of around 1.5 over about a decade [17], compared to the experimental values of $1.64 - 1.79$ [29]. Such a measurement, however, ignores the important variation of wall misorientations with scale (capturing the spatial scaling but missing the amplitude scaling).

Can we reconcile our self-similar cell morphologies with the experimental analyses of Hughes and collaborators [36, 34, 35]? Using our boundary-pruning algorithm to identify cell walls, Fig. 2.4c and d show the cell size and misorientation distributions extracted from an ensemble of initial conditions. The misorientation distribution we find is clearly more scale free (power-law) than that seen experimentally. Under external strain, we do observe the experimental cell structure refinement (Fig. 2.4b), and we find the experimental scaling collapse of the cell-size and misorientation distributions (Fig. 2.4c and d) and the observed power-law scaling of the mean size and angle with external strain (Fig. 2.4e and f), albeit with different scaling functions and power-laws than those seen in experiments [36, 34, 35].

Because we ignore slip systems, spatial anisotropy, and immobile and geometrically unnecessary dislocations, we cannot pretend to reflect real materials. But by distilling these features out of the analysis, we have perhaps elucidated

the fundamental differences between cell walls and grain boundaries, and provided a new example of non-equilibrium scale invariance.

Acknowledgements

We would like to thank S. Limkumnerd, P. Dawson, M. Miller, A. Vladimirsky, R. LeVeque, E. Siggia, and S. Zapperi for helpful and inspiring discussions on plasticity and numerical methods and N. Hansen, D.C. Chrzan, H. Mughrabi and M. Zaiser for permission of using their TEM micrographs. We were supported by DOE-BES through DE-FG02-07ER46393. Our work was partially supported by the National Center for Supercomputing Applications under MSS090037 and utilized the Lincoln and Abe clusters.

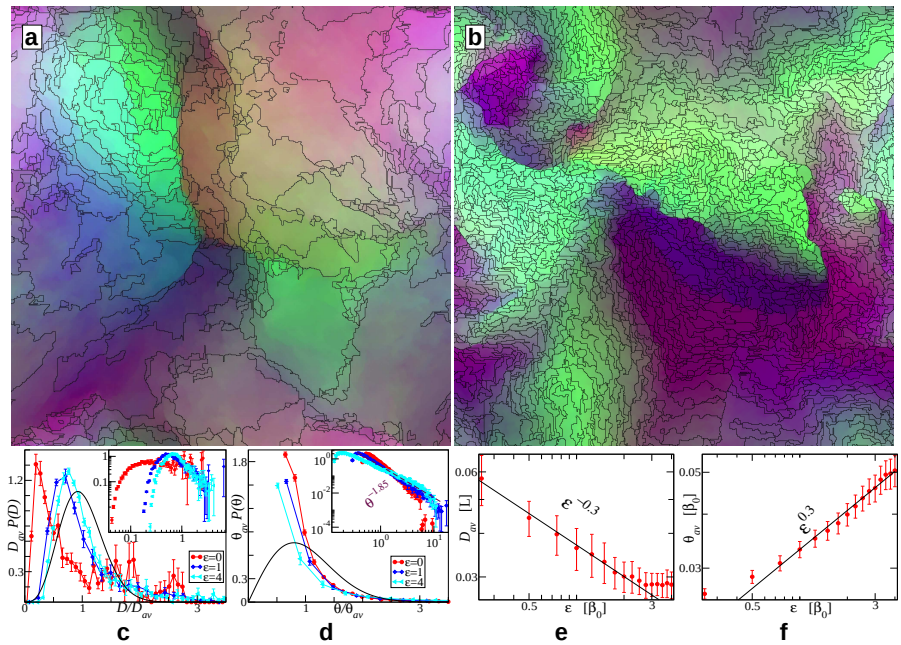

Figure 2.4: **Cellular structures under strain: size and misorientation distributions**. (a) An unstrained state formed by relaxing a random deformation, decomposed into cells determined by our boundary pruning method: we systematically remove boundaries in order of their average misorientation angle, and then prune cells based on their perimeter/area ratio and misorientation angle (see Supplementary Movie 4 [a]). Boundaries below a threshold root-mean-square misorientation $\theta_c = 0.015\beta_0$ are removed. (b) The final state after a strain of $\epsilon_{zz} = 4\beta_0$ is applied; notice the cell refinement to shorter length scales. (c) The cell size distribution (square root of area), scaled by the mean cell size and weighted by the area, at various external strains. (d) The misorientation angle distribution, weighted by cell boundary length, scaled by the mean. For each curve, data starts at θ_c. This distribution appears to be closer to a power-law (inset) than the experimental distributions (solid curves [36, 34, 35]). (e,f) Mean cell size D_{av} and misorientation angle θ_{av} as functions of external strain. We find these same power-laws $D_{av} \sim \epsilon^{-0.26\pm0.14}$ and $\theta_{av} \sim \epsilon^{0.26\pm0.04}$, with errors reflecting over a range of θ_c and for a variety of pruning algorithms and weighting functions. Notice that the product $D_{av}\theta_{av}$ is approximately constant, as observed experimentally [36]. The power-law dependence $\epsilon^{0.3}$ is weaker than the powers $\epsilon^{1/2}$ and $\epsilon^{2/3}$ observed experimentally for incidental dislocation boundaries and geometrically necessary boundaries, respectively.

[a] http://link.aps.org/supplemental/10.1103/PhysRevLett.105.105501.

CHAPTER 3

CONTINUUM DISLOCATION DYNAMICS ANALOGIES TO TURBULENCE[1]

3.1 Introduction

From horseshoes and knives to bridges and aircrafts, mankind has spent five millennia studying how the structural properties of metals depend not only on their constituents, but also how the atoms are arranged and rearranged as metals are cast, hammered, rolled, and bent into place. A key part of the physics of this plastic distortion is played by the motion of intrinsic line defects called *dislocations*, and how they move and rearrange to allow the crystal to change shape.

Here, we describe the intriguing analogies we found between our model of plastic deformation in crystals and turbulence in fluids. Studying this model led us to remarkable explanations of existing experiments and let us predict fractal dislocation pattern formation. The challenges we encountered resemble those in turbulence, which we describe here with a comparison to the Rayleigh-Taylor instability.

For brevity, we offer a minimal problem description that ignores many important features of plastic deformation of crystals, including yield stress, work hardening, dislocation entanglement, and dependence on material properties [62]. We focus on the complex *cellular structures* that develop in deformed crystals, which appear to be fractal in some experiments [29]. These fractal

[1]This chapter has been published in Computing in Science and Engineering [18].

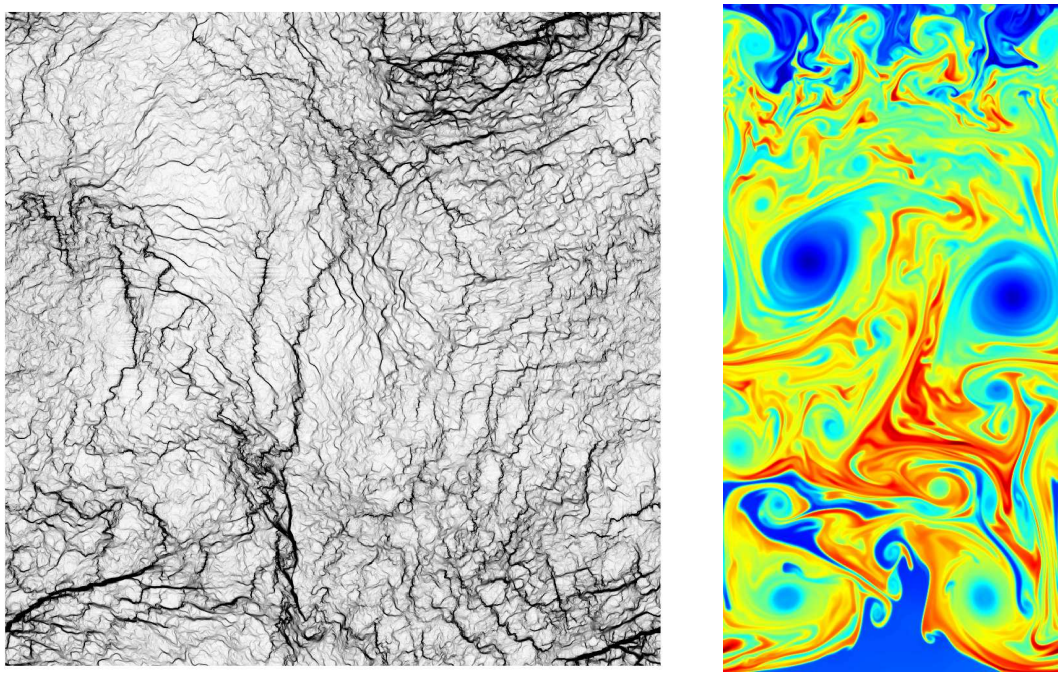

(a) Continuum Dislocation Dynamics (b) Turbulence

Figure 3.1: **Comparison of our continuum dislocation dynamics (CDD) with turbulence.** (a) Dislocation density profile as it evolves from a smooth random initial condition. The structures form fractal *cell wall* patterns. Dark regions represent high dislocation density. (b) Rayleigh-Taylor instability at a late time. The fluid (air) with two layers of different densities mix under the effect of gravity. The emerging flows exhibit complex swirling *turbulent* patterns. The color represents density (red for high, blue for low).

structures are reproduced by our continuum dislocation dynamics (CDD) [16] theory (see Figure 3.1a).

Not only do the resulting patterns match the experimental ones, but the theory also has rich dynamics, akin to turbulence. This raises a question: Is the dislocation flow turbulent? Here, we focus on exploring this question by building analogies to an explicit turbulence example: the Rayleigh-Taylor instability. As we describe, our theory displays similar conceptual and computational challenges as does this example, which reassures us that we're on firm ground.

3.2 Model

3.2.1 Continuum Dislocation Dynamics

This CDD model [49, 1, 16] provides a deterministic explanation for the emergence of fractal wall patterns [49, 16] in mesoscale plasticity. The crystal's state is described by the deformation-mediating dislocation density ϱ_{ij} – where i denotes the direction of the dislocation lines and j their Burgers vectors [62] – and our dynamical evolution moves this density with a local velocity V_ℓ, yielding a partial differential equation (PDE):

$$\partial_t \varrho_{ij} - \varepsilon_{imn}\partial_m(\varepsilon_{n\ell k} V_\ell \varrho_{kj}) = \nu \partial^4 \varrho_{ij} \tag{3.1}$$

Here V_ℓ is proportional to the net force on it (overdamped motion), coming from the other dislocations and the external stress. That is,

$$V_\ell = \frac{D}{|\varrho|}\sigma_{mn}\epsilon_{\ell mk}\varrho_{kn}$$

where σ is the local stress tensor, the sum of an external stress σ_{ij}^{ext} and the long-range interactions between dislocations. $\sigma_{ij}^{\text{int}} = \int K_{ijmn}(r - r')\varrho_{mn}(r')dr'$, with K_{ijmn} the function representing the stress at r generated by ϱ at r' [62]. The term proportional to ν is the regularizing quartic diffusion term for the dislocation density (an artificial viscosity), which we'll focus on here. (In fact, the equation we simulate here is further complicated to constrain the motion of the dislocations to the glide plane while minimizing the elastic energy [49, 16].) The details of our equations aren't crucial: dislocations move around with velocity $\vec{V}$, pushed by external loads and internal stresses to lower their energies. Our equation is *nonlinear*, and it's exactly this non-linearity that makes our theory different from more traditional theories of continuum plasticity.

3.2.2 Turbulence

Turbulence is an emergent chaotic flow, typically described by the evolution of the Navier-Stokes equations at high *Reynolds numbers*:

$$\begin{aligned} \rho\left(\partial_t \vec{v} + \vec{v}\cdot\nabla\vec{v}\right) &= \mu\nabla^2\vec{v} + \vec{f} \\ \partial_t\rho + \nabla\cdot(\rho\vec{v}) &= 0 \end{aligned} \tag{3.2}$$

where ρ is the local density of the fluid with velocity $\vec{v}$ under the application of local external force density $\vec{f}$. The term proportional to μ is the fluid viscosity, and μ is inversely proportional to the Reynolds number.

Despite this Navier-Stokes equation's enormous success in describing various experiments, there are many mathematical and numerical open questions associated with its behavior as $\mu \to 0$. In this regime, complex scale-invariant patterns of eddies and swirls develop in a way that isn't fully understood: turbulence remains one of the classic unsolved problems of science.

How is ν related to μ? Eq. (3.2) can be written differently by dividing the whole equation by ρ, in this equation μ/ρ (in the incompressible case) is called the *kinematic viscosity* (usually denoted as ν). Our artificial viscosity ν in Eq. (3.1) is analogous to this kinematic viscosity. For turbulence, μ in Eq. (3.2) is given by nature. In contrast, our ν in Eq. (3.1) is added for numerical stability; it smears singular walls to give regularized solutions. This is physically justified because the atomic lattice always provides a cutoff scale. How do we know that this artificial term gives the 'correct' answer (given that there can be many different solutions to the same PDE)? Numerical methods for shock-admitting PDEs are validated by showing that the vanishing grid spacing limit $h \to 0$ gives the same solution as the $\nu \to 0$ limit (that is, the *viscosity solution*). We will argue that both our model of plasticity and the Navier-Stokes equations do not have convergent

solutions as μ or $\nu \to 0$. We're reassured from the turbulence analogy and are satisfied with extracting physically sensible results from our plasticity theory – viewing it not as *the* theory of plasticity, but as an *acceptable* theory.

3.3 Methods

To solve Eq. (3.1), we implemented a second order central upwind method [43] especially developed and tested for conservation laws, such as Eqs. (3.1) and (3.2). The method uses a generalized approximate Riemann solver which doesn't demand the full knowledge of characteristics [43]. For the simulations of Navier-Stokes dynamics (Eq. (3.2)) we use PLUTO [57], a software package built to run hydrodynamics and magnetohydrodynamics simulations, using the Roe approximate Riemann solver.

Accurately capturing singular flows is a challenge in computational fluid dynamics. A classic example of such singularities is the sonic boom that happens when an object passes through a compressible fluid (described by a version of Navier-Stokes) faster than its speed of sound. The sonic boom is a sharp jump in density and pressure, which causes the continuum equations to become ill-defined. Our PDEs, depending on gradients of ϱ, become ill-defined when ϱ develops an infinite gradient at a dislocation density jump.

The numerical methods we use are designed to appropriately solve the so-called Riemann problem: the evolution of a simple initial condition with a single step in the conserved physical quantities. For hyperbolic conservation laws, exact solutions of the Riemann problem can be obtained by decomposing the step into characteristic waves. However, in most non linear problems, finding

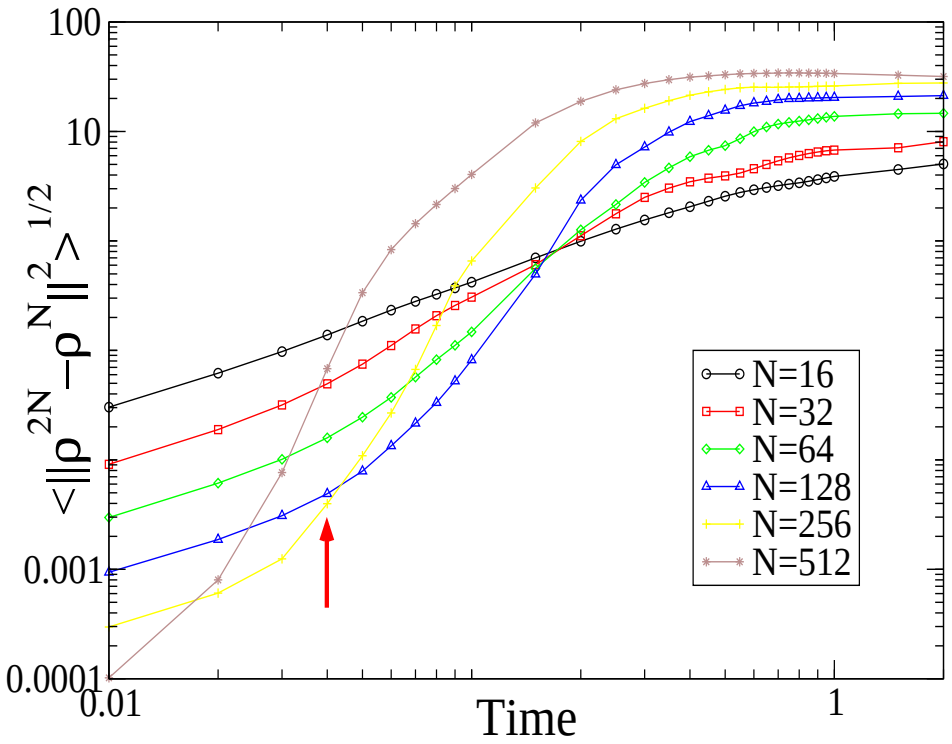

(a) Non-convergence in dislocation dynamics (see Eq. (3.1))

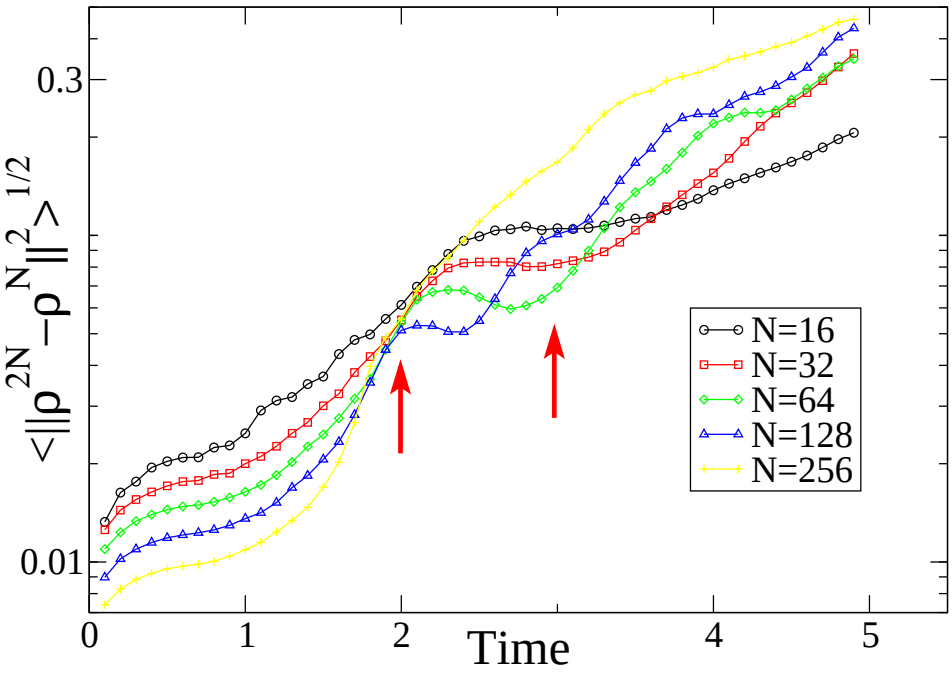

(b) Non-convergence in turbulence dynamics (Rayleigh-Taylor instability)

Figure 3.2: **Non-convergence exhibited in both plasticity and turbulence.** As time progresses, the curves, which are initially monotonically decreasing, flip order and become non-convergent (where the lines cross each other). Red arrows show where the convergence is lost.

(a) $h = 1/128$ (b) $h = 1/256$ (c) $h = 1/512$

Figure 3.3: **Continuum dislocation dynamics.** Simulation results at $t = 1.0$ of our CDD Eq. (3.1) at different grid sizes (h), starting from a smooth initial condition. We use periodic boundaries in both horizontal and vertical directions, and all physical quantities are constant along the perpendicular direction.

exact Riemann solutions involves iterative processes th at are either slow or (practically) impossible, and thus approximate solutions are employed instead. Both methods we use are approximate in different ways, but are qualitatively similar.

These sophisticated methods are designed to handle the kind of density jumps seen in sonic booms. In our dislocation dynamics, though, we have a more severe singularity that forms – a sharp wall of dislocations that becomes a δ-function singularity in the dislocation density (as $\nu \to 0$). These δ-shocks are naturally present in crystals – they describe, for example, the grain boundaries found in polycrystalline metals, which (in the continuum limit) form sharp walls of dislocations separating dislocation-free crystallites. Unfortunately, the mathematical and computational understanding of PDEs forming δ-shocks is relatively primitive; there are only a few analytic and numerical studies in one dimension (for an example, see [81]). Currently, to our knowledge, there's no numerical method especially designed for δ-shock solutions. Moreover, in a

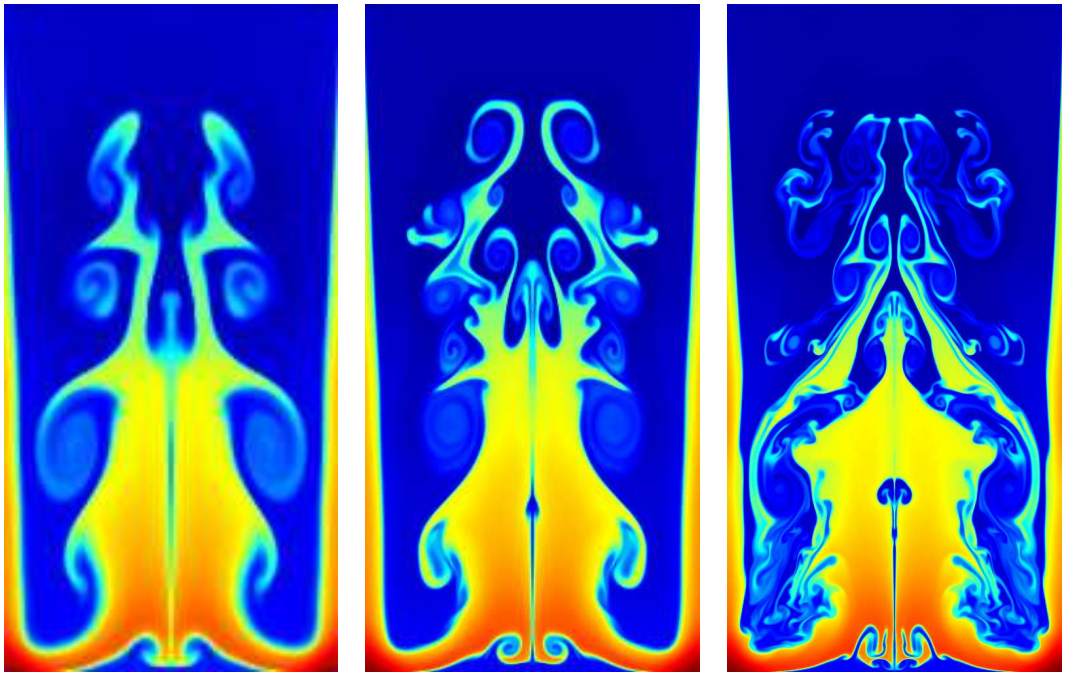

(a) $h = 1/128$ (b) $h = 1/256$ (c) $h = 1/512$

Figure 3.4: **The Rayleigh-Taylor instability of the Navier-Stokes equation.** The Rayleigh-Taylor instability is a fluid mixing phenomenon that occurs when an interface between two different fluid densities is pulled by gravity. These simulation results here are the Rayleigh-Taylor instability at $t = 4.0$, for $\mu \to 0$, at different grid spacings (h) with periodic boundaries in the horizontal direction and fixed boundaries along the vertical. The initial condition has density interface with a single mode perturbation in the vertical velocity. The system size is $(L_x, L_y) = (1.0, 2.0)$.

strict mathematical sense, several properties of Eq. (3.1) – nonlocality and mixed hyperbolic and parabolic features – haven't been proven to permit a successful application of shock-resolving numerical methods.

In the simulations presented here, we won't add an explicit viscosity (so $\mu = \nu = 0$); instead, we have an effective numerical dissipation [43] that depends on the grid spacing h as h^n, where n depends on the numerical method used. (Eq. (3.2) with $\mu = 0$ is the compressible Euler equation. Although we present our simulations as small numerical viscosity limits of Navier-Stokes,

they could be viewed as particular approximate solutions of these Euler equations.)

3.4 Results

Figure 3.1 shows typical emerging structures in simulations of both the CDD Eq. (3.1) and the Navier-Stokes dynamics Eq. (3.2): both are complex, displaying structures at many different length scales; sharp, irregular walls in the CDD and vortices in Navier-Stokes. Although it might not be surprising to professionals in fluid mechanics that nonlinear PDEs have complex, self-similar solutions, it's quite startling to those studying plasticity that their theories can contain such complexity (even though this complexity has been observed in experiments [29]): traditional plasticity simulations do not lead to such structures.

3.4.1 Validity of solutions

These rich and exotic solutions demand scrutiny. How do we confirm the validity of our solutions? For continuum PDEs solved on a grid, an important problem that needs to be addressed is the effect of the imposed grid. Traditionally, it's expected that as the grid becomes finer, the solution is likely to be closer to the real continuum solution. For differential equations that generate singularities, one cannot expect simple convergence at the singular point! How do we define convergence when singularities are expected? For ordinary density-jump shocks like sonic booms, mathematicians have defined the concept of a *weak solution*: it's a solution to the integrated version of the original equation,

bypassing singular derivatives.

For many problems, researchers have shown that adding an artificial viscosity and taking the limit to zero yields a weak solution to the problem. For some problems, the weak solution is unique, while for others there can be several: different numerical methods or types of regularizing viscosities can yield different dynamics of the singularities. This makes physical sense: if a singular defect (a dislocation or a grain boundary) is defined on an atomic scale, shouldn't the details of how the atoms move (ignored in the continuum theory) be important for the defect's motion? In the particular case of sonic booms, the microscopic physics picks out the *viscosity solution* (given by an appropriate $\mu \to 0$ limit), leading mathematicians to largely ignore the question of how micro-scale physics determines the singularities' motion.

However, our problems here are more severe than picking out a particular weak solution. Neither our dislocation dynamics nor the Navier-Stokes equation (with very high Reynolds number) converge in the continuum limit even for gross features, whether we take the grid size to zero in the upwind schemes or we take $\nu \to 0$ (or $\mu \to 0$) as a mathematical limit.

3.4.2 Spatio-temporal non-convergence

Figure 3.2a shows a quantitative measure of the our simulation's convergence as a function of time, as the grid spacing $h = 1/N$ becomes smaller. We measure convergence using the L_2 norm

$$\|\widehat{\varrho^{2N}} - \varrho^N\|_2 \equiv \left(\int \|\widehat{\varrho^{2N}} - \varrho^N\|^2 \, dx \right)^{1/2}$$

where $\widehat{\varrho^{2N}}$ has been suitably smeared to the resolution of ϱ^N. (Normally we'd check the difference between the current solution and the true answer, but here we don't know the true answer.) Here, We study the relaxation of a smooth but randomly chosen initial condition – that is, a perfect single crystal beaten with mesoscale hammers with round heads – as a function of time. We see that for short times these distances converge rapidly to zero, implying convergence of our solution in the L_2 norm. However, at around $t = 0.02$ to 0.2, the solutions begin to become increasingly different as the grid spacing $h \to 0$.

This worried us at the beginning because it suggests that the numerical results might be dependent somehow on the artificial finite-difference grid we use to discretize the problem, and therefore might not reflect the correct continuum physical solution. We checked this by adding the aforementioned artificial viscosity ν in Eq. (3.1). We found that it converges nicely when ν is fixed as the grid spacing goes to zero. However, this converged solution is not unique: it keeps changing as $\nu \to 0$. So, it's our fundamental equation of motion (Eq. (3.1)) and not our numerical method that fails to have a continuum solution. This would seem even more worrisome: How do we understand a continuum theory whose predictions seem to depend on the smallest studied length scale (the atomic size)?

3.4.3 Spatio-temporal non-convergence in Turbulence

It's here that the analogy to turbulence has been crucial for understanding the physics. It's certainly not obvious that the limit of strong turbulence $\mu \to 0$ in Navier-Stokes (Eq. (3.2)) should converge to a limiting flow. Actually, our short

experience suggests that there is no viscosity solution for Eq. (3.2). Turbulence has a hierarchy of eddies and swirls on all length scales, and as the viscosity decreases (for fixed initial conditions and loading) not only do the small-scale eddies get smaller, but also the position of the large-scale eddies at fixed time change as the viscosity or grid size is reduced.

Figure 3.2b depicts the convergence behavior of a simulation of the Rayleigh-Taylor instability (as in Fig. 3.2a). The instability triggers turbulent flow, and like our dislocation simulations, convergence is lost after $t \sim 2.0$ as the grid spacing h gets smaller. Our choice of the Rayleigh-Taylor instability for comparison is motivated by the presence of robust self-similar features (such as the "bubbles" and "spikes" in Fig. 3.4 [78]), and by the spatio-temporally non-converging features of the initially well-defined interface.

The interface between two fluid densities is analogous to our dislocation cell walls. Even though the Rayleigh-Taylor instability is different from homogeneous turbulence in important ways, we also verified that the latter shows similar spatio-temporal non-convergence but statistical convergence (simulating the Kelvin-Helmholtz instability for compressible flow in 2D). The Rayleigh-Taylor instability provides the best visualization of the analogy between the two phenomena, but this non-convergence appears to be more general. Fig. 3.4 shows density profiles at intermediate times for the Rayleigh-Taylor instability. The figure shows the formation of vortices (swirling patterns), and the simulations look significantly different as the grid spacing decreases. Again, this is analogous to the corresponding simulations of our dislocation dynamics shown in Fig. 3.3, where larger cells continue to distort and shift as the grid spacing decreases.

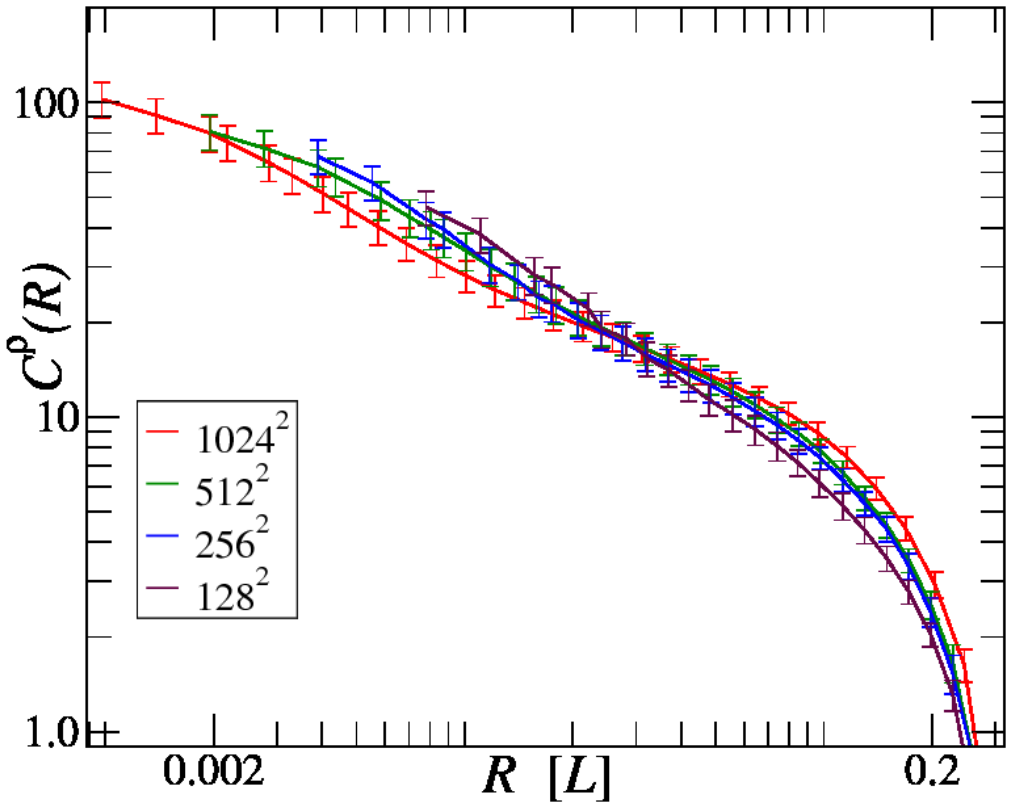

Figure 3.5: **Statistical properties and convergence** Although the continuum dislocation dynamics (CDD) simulations with different grid sizes are non-convergent (Fig. 3.2a), the statistical properties are the same. The dislocation density correlation function is plotted here for different simulation sizes at the same time, exhibiting consistent power laws.

3.4.4 Validation through Statistical properties

If the simulations aren't convergent, how can we decide if the theory is physically relevant and can be trusted to interpret experiments? In turbulence, it has long been known that, as vortices develop, self-similar patterns arise in the flow and exhibit power laws in the energy spectrum and in the velocities' correlation functions [25]. A successful simulation of fully developed turbulence isn't judged by whether the flow duplicates an exact solution of Navier-Stokes! Turbulence simulations study these power laws, comparing them to analytical

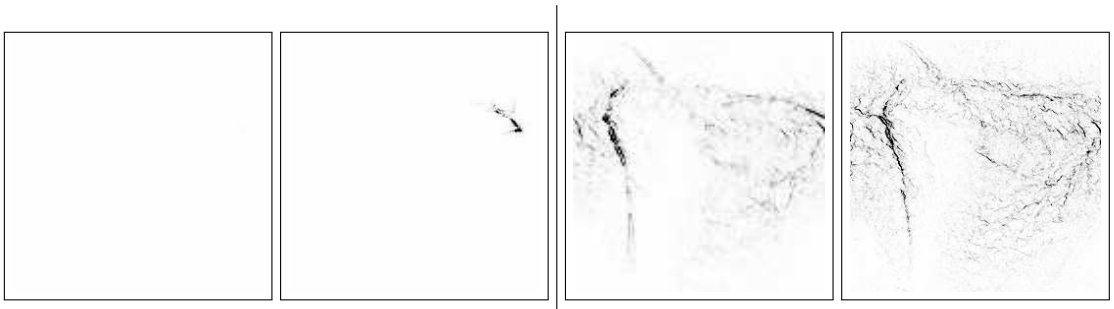

(a) $h = 1/256$ (b) $h = 1/512$ (c) $h = 1/256$ (d) $h = 1/512$

$t = 0.04$ $t = 1.00$

Figure 3.6: **Non-convergence and singularity for CDD** For (a) and (b), $t = 0.04$; for (c) and (d), $t = 1.00$. The two-norm difference between h and $h/2$ are plotted. At short time, $t = 0.04$, the differences are small: (a) is empty and (b) nearly so. At later times, $t = 1.00$, the two-norm difference becomes significant esepcially where the walls are forming (see Fig. 3.3 for wall locations).

predictions and experimental measurements.

Our primary theoretical focus in our plasticity study [16] has been to analyze power-law correlation functions for the dislocation density, plastic distortion tensor, and local crystalline orientation. As Fig. 3.5 shows, like turbulence simulations, these statistical properties seem to converge nicely in the continuum limit.

It's worth noting that, in both cases, non-convergence emerges when small scale features appear on the wall (see Fig. 3.6) or the interface (see Fig. 3.7):

3.4.5 Singularity and convergence

In the case of our simulations of plastic flow (Eq. 3.1), starting from smooth initial density profiles, finite time singularities develop in the form of δ-shocks. The existence of finite-time singularities was shown in a 1D variant of these

(a) $h = 1/64$ (b) $h = 1/128$ (c) $h = 1/256$ (d) $h = 1/64$ (e) $h = 1/128$ (f) $h = 1/256$

$t = 2.0$ $t = 3.0$

Figure 3.7: **Non-convergence and vortices for Navier-Stokes** For (a), (b), and (c) $t = 2.0$; for (d), (e), and (f) $t = 3.0$, corresponding to the two red arrows in Figure 3.2b. The two-norm difference between h and $h/2$ is plotted. At $t = 2.0$, small structures start to become strong, as in (c), and the same is true at $t = 3.0$ for $h = 1/128$, as in (e).

equations, which is associated with the Burgers equation [51]. Figure 3.6 shows how this effect occurs by considering the two-norm differences (the integrand in space of the L_2 norm discussed earlier). At $t = 0.04$ (see Fig. 3.2a) when the $N = 512$ curve starts to cross all the other curves, singular features start to appear around a wall (Fig. 3.6b). Although the boundaries are non-convergent when specific locations and times are considered (Fig. 3.2a), the statistical properties and associated self-similarity (Fig. 3.5) are convergent.

In the case of Navier-Stokes simulations (see Fig. 3.7), the existence of finite-time singularities is a topic of active research: even though local-in-time analytic solutions are easily shown to exist, global-in-time analytic solutions can be proven to exist only for special cases, such as in the 2D incompressible genuine Euler equation [8]. In 3D, the mechanism of vortex stretching is conjectured to lead to finite-time singularities [71], even though there are still crucial open questions. Despite its complexity, turbulence can be concretely studied in special cases. For our example of the Rayleigh-Taylor instability, the two-fluid

interface gets distorted and "bubbles" form (Fig. 3.4); over time, the bubbles exhibit emergent self-similar characteristics [78], showing *statistical convergence*. However, there is no spatio-temporal convergence, because the interface develops complex, turbulent features as the grid becomes finer (see Figs. 3.2b and 3.7).

3.5 Conclusion

Sometimes science seems to be fragmented, with independent fields whose vocabularies, toolkits, and even philosophies almost completely separate. But many valuable insights and advances arise when ideas from one field are linked to another. Computational science is providing a new source of these links, by tying together fields that can fruitfully share numerical methods.

Our use of well-established numerical methods from the fluids community made it both natural and easy to utilize their analytical methods for judging the validity of our simulations and interpreting their results.

Acknowledgement

We thank Alexander Vladimirsky, Randall LeVeque, Chi-Wang Shu, and Eric Siggia for helpful and inspiring discussions on numerical methods and turbulence. The US Department of Energy/Basic Energy Sciences grant no. DE-FG02-07ER46393 supported our work, and the US National Center for Supercomputing Applications partially provided computational resources on the Lincoln and

Abe clusters through grant no. MSS090037.

CHAPTER 4

NUMERICAL METHODS FOR CONTINUUM DISLOCATION DYNAMICS

4.1 Introduction

At meso and atomistic scales, it is an undisputed fact that dislocations form complicated structures that make coarse-grained modeling challenging. Dislocations are known to tangle and interact in subtle ways at atomistic scales, and collectively forming cell structures under deformation. These cell structures vary in structure and patterns, strongly dependent on the material properties and processing history.

Nevertheless, most continuum models to date are simplified – or complexified – to be unaffected by these issues. However, to bridge the scale from atomistics to phenomenological models properly, it is imperative that we develop a simple coarse grained description that can naturally connect the shorter and longer length-scale models. Particularly, because both single dislocations and the emergent dislocation walls are singular line-like or surface-like entities, it is necessary to use a numerical method that can capture and evolve these sharp features properly.

Phase field models, level-set methods, and front tracking methods [87, 15, 60, 83, 52] are standard approaches used to study dislocation wall structures (especially grain boundaries); these models are not well suited for studying the dynamics of dislocation pattern formation and evolution. Simulating the emergent walls with these methods requires positing both the existence and the dynam-

ics of these structures. Simulating individual dislocations (as in other 'discrete dislocation' simulations [76, 24, 12]) poses challenges of scale in simulating the massively collective behaviors of interest here.

The other approach is to use partial differential equations representing the dynamics of the density of dislocations. This still requires physical knowledge of the dynamics of dislocations, but these are much better understood than the collective behaviors of dislocation structures. To name a few, Groma et al. [26], Zaiser et al. [89], Rickman et al. [73], Parks and Arsenlis [5], Acharya et al. [1], and Limkumnerd et al. [49] and Chen et al. (Chapter 2) have worked on different variety of continuum dislocation dynamics models.

In this chapter, we explore how best to numerically simulate a system of continuum dislocation dynamics, discussing issues that arise and resolutions we have found.

In sections 4.2 and 4.3, we introduce the formalism of hyperbolic conservation laws and explore the mathematical aspects of our continuum dislocation dynamics model as a hyperbolic conservation law. In section 4.4, we explain the numerical methods that we implement and apply to solve our continuum dislocation dynamics (CDD) models [49, 17] (also Chapter 2) and justify the approximations made in the process. Section 4.5 illustrates the results and interpretations of the simulations, particularly with focus on validating that our method(s) provides physically sensible results. Lastly, we discuss conclusions in section 4.6.

4.2 Hyperbolic Conservation Laws

Continuum dislocation dynamics models are often written as partial differential equations that prescribe the evolution of the dislocation densities over time. In general it could include three different types of terms: a transport (flux) term, a source and sink term, and a regularization term. Some or all of these appear in different forms for each physical model, but to study the dislocation patterning, transport of dislocations should be the dominant term[1].

Hyperbolic partial differential equations (or hyperbolic conservation laws) are commonly used to describe transport behavior of many physical systems. For example, the wave equation, Euler equation for fluid flow, magnetohydrodynamics (MHD), shallow water equations are hyperbolic partial differential equations. Navier-Stokes equations include a parabolic viscosity term, but is dominated by the hyperbolic term in high Reynolds number cases.

Note that dislocation line density is not conserved per se, even with only transport. A single dislocation loop can expand or shrink, increasing or decreasing in length and hence changing the dislocation line density. It is the "net charge" (Burgers vector density) that is conserved, rather than the total line density. Similar behavior is exhibited with magnetic field lines in magnetohydrodyamics, where the lines can lengthen while each component of the line density vector is conserved.

[1]The source term dominates common phenomenological plasticity models, which however do not exhibit dislocation patterning.

4.2.1 Burgers Equation

The simplest example of a nonlinear conservation law is the Burgers equation. It also is a simplification of the Euler equations for fluid flow – guaranteeing it to be an interesting and worthy toy problem for us to start with:

$$\partial_t u + \partial_x(\tfrac{1}{2}u^2) = 0 \tag{4.1}$$

The key issue in these models is that shocks develop in a finite amount of time where the derivatives become ill-defined. One can address subsequent singularity evolution by multiplying the equation of motion by a smooth function and integrating over t and x. Integrating by parts, one eliminates the ill-defined derivatives and therefore now define an integrated version of the problem. This integrated version of the equations does not fully define a unique solution; families of *weak solutions* exist. For many problems including the Burgers equation and Euler equations, adding an explicit numerical viscosity term $\nu\partial_{xx}^2 u$ and taking $\nu \to 0$ is deemed to give the correct physical and unique weak solution to the problem, and most – if not all – methods are designed to (at the very least try to) converge to the vanishing viscosity solution. The vanishing viscosity solution is likely not physically appropriate for the dislocation dynamics models discussed here, but we defer that discussion to another place (see chapter 6).

4.2.2 Shocks and δ-shocks

Shocks, *i.e.* spatial jumps in conserved quantities, appear as a singularity in many explicit models, such as the Euler equation for fluid flow, shallow water equations, traffic jam equations, etc. The simplest PDE that forms shocks is

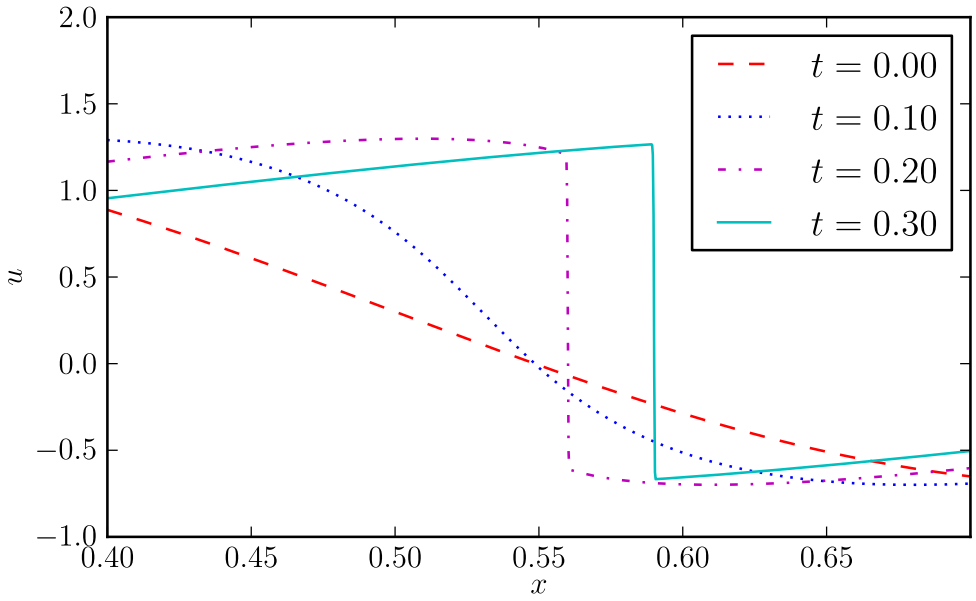

Figure 4.1: **Numerical simulation of Burgers equation**. A smooth profile evolves into a discontinuous one at later times, with a moving and decaying discontinuity. Evolved from an initial condition $u(x, t = 0) = sin(2\pi x) + 0.3$ with a periodic domain $x \in [0, 1)$.

the (inviscid) Burgers equation (4.1).

The Burgers equation has been studied extensively, leading to the development of suitable mathematical methods which have been applied to realistic problems.

How do shocks develop in the Burgers equation (4.1)? In Eq. (4.1), u is a conserved quantity similar to momentum density. Let's consider that for $z < 0$ there is a right-moving blob (hence with positive u), and for $z > 0$ there is a left-moving blob (with negative u). In finite time the clouds collide, and unless they pass through each other, they form an interface. Across this sharp interface there is a finite positive density on the left and negative density on the right, forming a moving jump in density. Figure 4.1 shows a numerical solution of the Burgers equation, forming a moving shock as described.

The problem with solving equation (4.1) is that a jump in u renders the derivatives ill-defined: the motion of the shock is not determined by the continuum equations, because they were derived assuming gradients were small. Shocks naturally arise from the continuum equations however, and the equation needs additional care once a shock is formed and the derivatives are ill-defined.

The usual method to attack this problem is to integrate the equations over a small window in space and time to get rid of the dangerous derivatives. By multiplying the whole equation with an arbitrary smooth test function $\phi(z,t)$ and integrating the equation, we get a problem that we can now tackle.

$$\begin{aligned} 0 &= \int dzdt\phi(z,t)\left[\partial_t u + \partial_z(\tfrac{1}{2}u^2)\right] \\ &= -\int dzdt\left[u\partial_t\phi(z,t) + \tfrac{1}{2}u^2\partial_z\phi(z,t)\right] + \int dt\left[\phi(z,t)\tfrac{1}{2}u^2\right]_{\partial Z} + \int dz\left[\phi(z,t)u\right]_{\partial T} \end{aligned} \tag{4.2}$$

where ∂Z and ∂T refers to the boundaries (the limits of integrations) in z and t. By choosing a test function $\phi(z,t)$ that vanishes at the boundaries, we find an integrated equation:

$$\int dzdt\left[u(z,t)\partial_t\phi(z,t) + \tfrac{1}{2}u(z,t)^2\partial_z\phi(z,t)\right] = 0 \tag{4.3}$$

The solutions to the integrated Eq. (4.3) are called the "weak solutions" to Eq. (4.1). It must be noted that weak solutions must satisfy Eq. (4.3) for any smooth function $\phi(z,t)$. Weak solutions are in general not unique; a shock, once formed, can evolve into (or stay as) either a shock, a rarefaction, or a mixture of both [46]. For many problems (including Burgers equation), however, a particular subset of weak solutions are most commonly studied. This so-called "vanishing viscosity solution" is achieved by adding a small regularizing diffusion term to the problem to smooth the shock, and then taking the limit of this

diffusion going to zero,

$$\partial_t u + \partial_z(\tfrac{1}{2}u^2) = \nu\partial_z^2 u \tag{4.4}$$

with $\nu \to 0$. In the case of fluid dynamics (i.e. sonic booms) the vanishing viscosity solution is the correct physical solution, satisfying the "entropy condition" that information is not created at the shock.

In addition to shocks in conserved quantities, there can appear higher-order singularities, such as δ-shocks (point masses in space) of the conserved quantity. They are less common in well studied problems (not appearing in most fluid-dynamics models), but they are mathematically well-defined [81, 48, 21] and represent physical solutions in some cases.

A simple example is exhibited in a straightforward extension of the Burgers equation,

$$\begin{aligned} \partial_t u + \partial_z(\tfrac{1}{2}u^2) &= 0 \\ \partial_t v + \partial_z(\tfrac{1}{2}uv) &= 0 \end{aligned} \tag{4.5}$$

where we added an equation for component v that is driven by u. v represents a passive scalar density that is convected with the flow of u. Let's consider the initial condition for u as before, but also consider additional tracer particles, or dust, of uniform density $v(t = 0)$. Then, the particles are dragged toward the shock in u and accumulate at the interface, forming a δ-shock (Figure 4.2) We will later (in section 4.3.3, and also chapter 5) show that this kind of entrainment exists in our continuum dislocation dynamics hence leading to dislocation wall structures. For the system of equations (4.5), wherever a shock appears in u, a δ-shock forms in v. Similar numerical or analytical techniques to those developed

for ordinary shocks can be used to treat these shocks, but it is more challenging, especially in higher dimensions [48].

4.3 Continuum Dislocation Dynamics

Our interest is of course not with Burgers equation dragging dust, but with a model of continuum dislocation dynamics with remarkable analogies to the simpler problem. Continuum theories of dislocations are of great interest, as it may fill the gap of the "missing length scales" between macroscopic crystal plasticity (used to design airplanes) and microscopic dislocation dynamics (now based on atomic-scale microphysics). As mentioned earlier, there exist many theories that attempt to bridge the gap: we study one particular construction [1, 49] (also see Chapter 2) which for simplicity and generality neglects many material specific properties and does not incorporate known phenomenological evolution laws.

In general, the nine-component dislocation density tensor ϱ_{ij} must satisfy

$$\partial_t \varrho_{ij} = \epsilon_{ilm} \partial_l J_{mj} \tag{4.6}$$

where the dislocation current J_{mj} is also $J_{mj} = \partial_t \beta^P_{mj}$ since

$$\varrho_{ij} = \epsilon_{ilm} \partial_l \beta^P_{mj} \tag{4.7}$$

(β^P_{mj} is the plastic distortion tensor [49]). The model we study depends on the constraints that are chosen; with only a constraint on the elastic energy that it must not increase, J_{ij} can be defined as

$$J_{ij} = \partial_t \beta^P_{ij} = \mathcal{V}_\ell \varrho_{\ell ij} = D(\rho) \varrho_{\ell mn} \sigma_{mn} \varrho_{\ell ij} \tag{4.8}$$

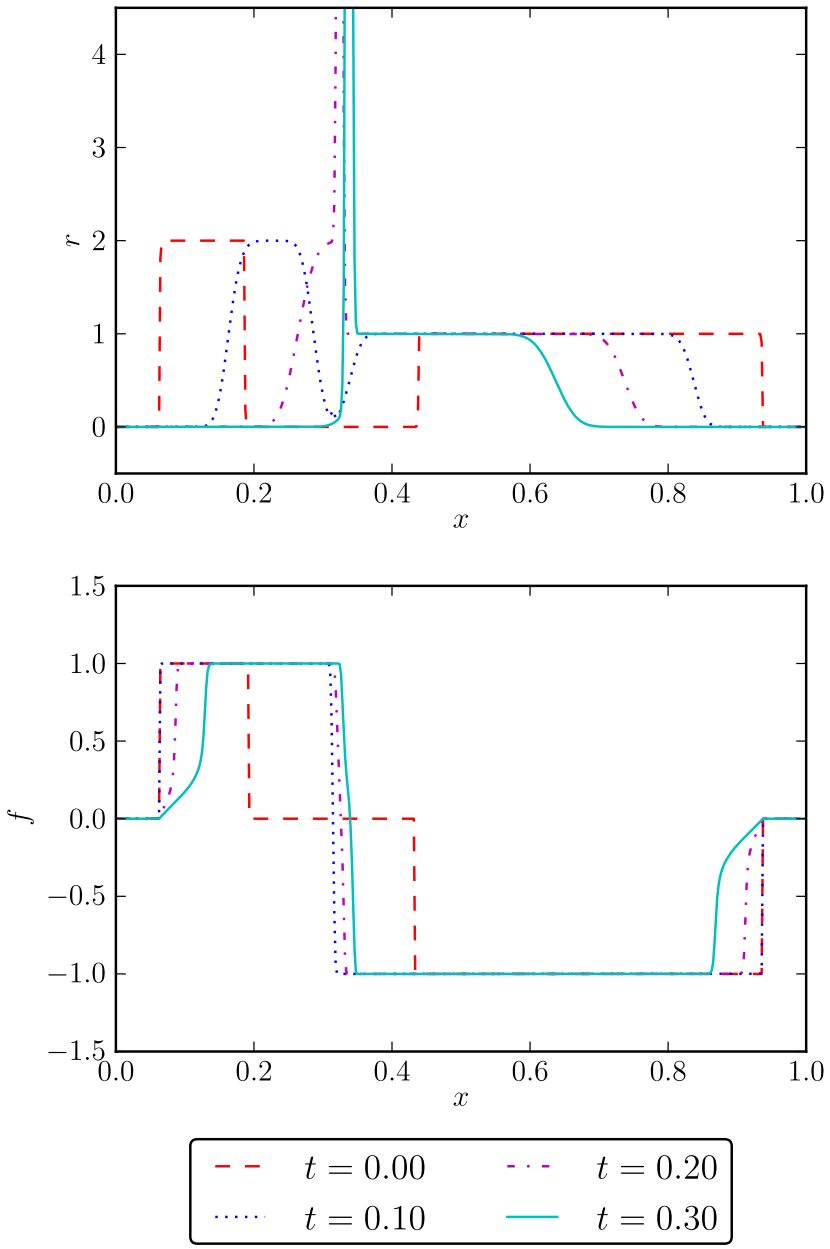

Figure 4.2: **δ-shock formation in pressureless gas equation**. Equations as presented in [48], representing pressure-less gas dynamics. (Top) Dust density r. (Bottom) Momentum density. f

(as implemented for grain boundary formation) where $\mathcal{V}_\ell$ is the local velocity of dislocations proportional to the Peach-Koehler force (see chapter 2); at low temperature where climb is forbidden, one may write

$$J_{ij} = \partial_t \beta^P_{ij} = \mathcal{V}_\ell \varrho'_{\ell ij} = D(\rho) \varrho'_{\ell mn} \sigma_{mn} \varrho'_{\ell ij} \tag{4.9}$$

where $\varrho'_{\ell ij} = \varrho_{\ell ij} - \frac{1}{3}\delta_{ij}\varrho_{\ell kk}$, also satisfying the *glide-only* (i.e. local material volume preserving) constraint. σ_{mn} represents the local stress field from both dislocation induced strain and external stress (or boundary conditions) and $D(\rho)$ prescribes dislocation mobility. We most commonly use

$$D(\rho) \propto 1/|\rho| \tag{4.10}$$

for thickness-independent wall behavior (Chapter 2): other choices, such as

$$D(\rho) = \text{Const.}, \tag{4.11}$$

will be used and discussed later however (see Chapter 5). There are also other variants that modify the climb behavior by introducing pressure due to vacancies [17], and modifications to include other energy terms, we leave the discussion on the other variants for a later publication.

Unfortunately, both equations (4.8) and (4.9) pose various challenges to the application of well-known methods for hyperbolic conservation laws. First, due to the long range interaction between dislocations, σ is a non-local function of ρ and therefore the equations (4.8) and (4.9) are not local equations of ρ. We discuss and justify the applicability of the methods to nonlocal problems in section 4.3.1. In section 4.3.2, we show that the equations are likely hyperbolic but not strictly hyperbolic based on numerical and approximate analytical evidences. Lastly, dislocations in experiments are known to form δ-function like singularities in the form of dislocation walls, and earlier studies [49, 51] observed that

δ-function dislocation walls were exhibited by these equations; such δ-shocks form a far less understood area within the field of hyperbolic conservation laws. In section 4.3.3 we explain that the studies of δ-shocks indeed are directly relevant to our equations. In the present section (4.3), we discuss these potential issues in applying a numerical method to our CDD equations, and (after some scrutiny) conclude that while mathematical proofs do not exist, it is reasonable to expect the methods to work.

4.3.1 Nonlocality

The first of the potential issues is that our continuum dislocation dynamics has nonlocal interaction between dislocations. Dislocations interact via (local) elastic deformation; but we leave elastic degrees of freedom out of the dynamics, justified by the relatively fast elastic relaxation. Were we to include all elastic degrees of freedom into our equations, nonlocality will disappear. The separation of time scales, however, would then pose challenges; most of the simulation time will be spent in relaxing elastic degrees of freedom, dissipating phonon energies from dislocation movements, etc. Thus, integrating out the elastic degrees of freedom and replacing them with an instantaneously updating stress field is a crucial step.

Dislocation density conservation is local. Long-range interactions make mathematical proofs much more complicated. Rigorously showing that elastically mediated interactions are harmless, for applying conventional mathematical and numerical methods, is not easy. However, the long distance elastic interaction usually dominates the stress field in our continuum model; the

strain field is thus quite smooth and slowly varying within a finite difference element. Theorems applicable to constant external stresses are thus physically likely to be applicable to our slowly varying stress. Fortunately, also, there are some analysis on non-local Eikonal equations (sometimes used indeed for dislocation dynamics) proving that the behaviors of non-local Eikonal equations are not different from that of the local Eikonal equations [4].

4.3.2 Hyperbolicity

The evolution laws of conserved densities are often formulated as (strictly) hyperbolic PDEs, which have a rich mathematical and numerical literature to guide simulations. When the conservation equation mixes hyperbolic and parabolic features, it becomes mathematically, and sometimes numerically challenging [39]. Is equation (4.6) strictly hyperbolic?

One can determine the nature of the system of equations by taking the Jacobian of the flux function and diagonalizing it. If it contains distinct real eigenvalues only, then it is strictly hyperbolic, if it contains degenerate real eigenvalues, it is not-strictly hyperbolic. Unfortunately, the Jacobian of Eq. (4.6) is nonlocal and hence very large and messy - albeit there being a very symmetric pattern - and is not feasible to analytically diagonalize.

There are several approximations we can take. First and foremost is to assume that σ_{mn} is independent of the local (and nonlocal) values of ρ_{ij}. This is motivated by our discussion above about the smoothness of σ_{mn}, presuming that long-range interaction dominates the stress field.

Once we make this first approximation, we can numerically diagonalize the Jacobian $J^{(\alpha)}_{ij,mn}$ (where α denotes the direction of the flux, i.e. $\alpha = x, y, z$ for three dimensions) within a simulation. The diagonalization consistently yields eigenvalues consisting of three zeros and six $\mathcal{V}_\alpha$s. This implies that the equation might be *non-strictly* hyperbolic, i.e. have degenerate real eigenvalues.

Analytical diagonalization of the flux Jacobian $J^{(\alpha)}_{ij,mn}$ is not feasible; however, we can make a second approximation assuming that the velocity part $\mathcal{V}_\ell$ is altogether independent of local ρ, i.e. ignoring local variations in ρ. Under this (somewhat) crude approximation

$$\partial_t \beta^P_{ij} = \mathcal{V}_\ell \varrho_{\ell ij} \tag{4.12}$$

the Jacobian to Eq. (4.12), a 9×9 matrix, can be analytically diagonalized, and it leads to three 0s and six $\mathcal{V}_z$ for the 1D problem. For two and three dimensions, each of the flux Jacobians yields three 0s and six $\mathcal{V}_\alpha$ respectively; when ϱ_{ij} is expanded into β^P_{mj},

$$\partial_t \beta^P_{ij} = \mathcal{V}_\ell \epsilon_{\ell ik} \epsilon_{kmn} \partial_m \beta^P m j \tag{4.13}$$

it is easy to see that different js are decoupled from each other, except through $\mathcal{V}_\ell$ – which is assumed independent of β^P for this calculation. Hence, we can fix j and reduce it into a three-component problem (i.e. Jacobian is block-diagonalized into three blocks of 3×3 matrices). Using $\epsilon_{\ell ik}\epsilon_{kmn} = \delta_{\ell m}\delta_{in} - \delta_{\ell n}\delta_{im}$, we can find the ($j$-block) Jacobian matrix in the z direction:

$$J^{(z)}_{uj,vj} = \frac{\partial(\partial_t \beta^P_{uj})}{\partial(\partial_z \beta^P_{vj})} = \begin{pmatrix} \mathcal{V}_z & 0 & 0 \\ 0 & \mathcal{V}_z & 0 \\ -\mathcal{V}_x & -\mathcal{V}_y & 0 \end{pmatrix} \tag{4.14}$$

Eigenvalues of this matrix are easy to find: 0 and two $\mathcal{V}_z$. Repeating this for all j leads to the exact same results and therefore yields three 0s and six $\mathcal{V}_z$. Flux in

x and y directions can be treated the same way to yield $\mathcal{V}_x$ and $\mathcal{V}_y$.

Another simplification we can make is to take single and few component versions of equation (4.8) and see what the eigenvalues turn out to be. For example, taking a single component the equation becomes

$$\partial_t \gamma = \sigma \text{sign}(\rho) \rho \tag{4.15}$$

where γ is the slip parameter (a component of β^P) and ρ is the dislocation density on that slip system (i.e. derivatives of the component).

In this version of the equation, the "Jacobian" – the only eigenvalue – is $\sigma \text{sign}(\rho)$ where σ is the shear stress resolved to the particular slip direction for γ.

In summary, although it is not possible to directly prove hyperbolicity, there is enough evidence to believe that our continuum dislocation dynamics is hyperbolic, but not strictly hyperbolic. The characteristic velocities(eigenvalues) likely consist of zeros and $\mathcal{V}_\ell$s and we will make use of this observation later for numerical methods.

4.3.3 Mapping to δ-shock Formation

Where and when derivatives are well defined, finding a solution to a partial differential equation is relatively straightforward. Therefore, the difficulty in finding solutions to a hyperbolic conservation law come from where the singularities occur. In one dimension, our singularities remain separated by smoothly varying regions except during collisions, so we can focus on the behavior of a single singularity, *i.e.* a discontinuity in conserved quantities, and try to un-

derstand its evolution. This so called Riemann problem provides the basis of understanding and solving hyperbolic conservation laws.

Traditionally studied conservation laws – such as Burgers Eq., Euler Eqs., traffic jam models, etc. – have relatively simple solutions to the Riemann problem. The "Riemann solutions" to these problems consist of (moving) shocks (contact discontinuities being subset of shocks) and rarefaction waves. However, this is not always the case, even for strictly hyperbolic problems, and multi-component systems have been shown to exhibit singular shocks such as $\delta, \delta', \ldots$ shocks [21].

We apply second order central upwind methods for Hamilton-Jacobi equations (for β^P) and conservation laws (for ρ) as proposed by Kurganov *et al.* [44] and we get very sharp dislocation walls forming in the simulations (shown in Figure 4.3). Both equations (4.8) and (4.9)[2] have been numerically shown to form jumps in β^P [49].

It is important to note though, that β^P is not a conserved quantity. In terms of the conserved quantity ρ which is a derivative of β^P, our evolution law is forming δ-shocks rather than Riemann shocks. It has been shown in Ref. [51] that in 1D, equation (4.8) maps onto the Burgers equation (4.1), assuming dislocation mobility $D(\rho) = \text{const.}$, where the local dislocation velocity $\mathcal{V}_z$ is equivalent to u of the Burgers equation:

$$\partial_t \mathcal{V}_z = -\partial_z(\mathcal{V}_z^2) \tag{4.16}$$

Note this equation (4.16) is not the same as the Burgers equation (4.1); there is a factor 2 difference. However, this discrepancy disappears under a simple

[2]The original work by Limkumnerd[49] uses a slightly different construction, which does not make the elastic energy always go downhill. This however does not change the fact that it forms shocks.

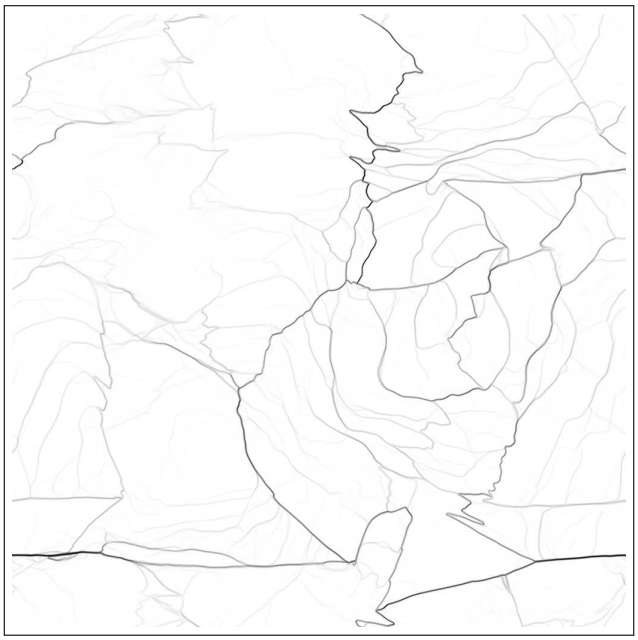

(a) **Dislocation density** black representing high dislocation density

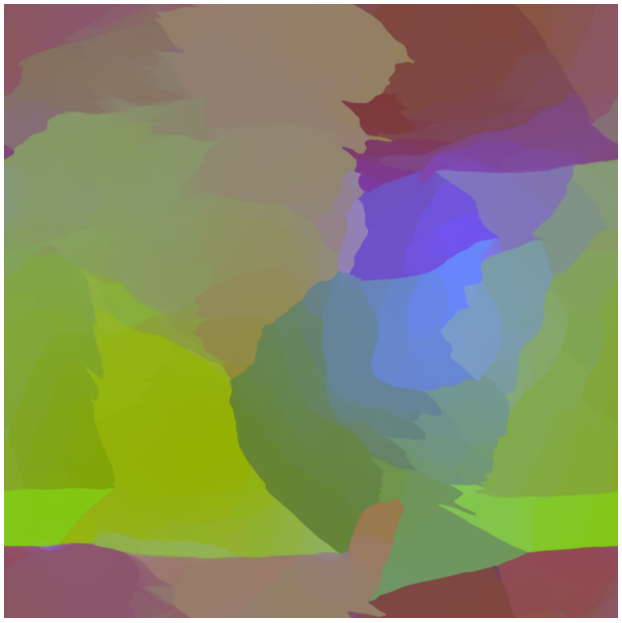

(b) **Orientation map** different colors represent different orientation

Figure 4.3: **Dislocation density and local orientation after relaxation** Smooth random initial condition relaxed into dislocation wall structures, forming δ functions in dislocation density. These dislocations mediate change in local orientation and thus coincide with the boundaries of the orientation map where the orientation jumps.

rescaling of $t' = t/2$.

It can be further shown in 1D that ρ_{xz},ρ_{yz}, and ρ_{xx}+ρ_{yy} do not affect the velocity and hence are passive: these passively advect (see Chapter 5), *i.e.*

$$\partial_t \tilde{\rho} = -\partial_z(\mathcal{V}_z \tilde{\rho}) \tag{4.17}$$

for $\tilde{\rho} = \rho_{xz}, \rho_{yz},$ or $\rho_{xx} + \rho_{yy}$.

Combining these two equations (4.16) and (4.17), you get a set of equations that are precisely the same as the Burgers dust equations (4.5) we discussed in the previous section. Figure 4.4 shows the δ-shocks formed in ρ for a 1D simulation, corresponding to jumps in β^P and cusps in $\mathcal{E}$ (In 1D, $\partial_z \mathcal{E} = \mathcal{V}_z$, [51] therefore these cusps represent shocks in $\mathcal{V}_z$.)

It is worth noting that although this mapping is precise only under special circumstances and in 1D, the qualitative behavior of δ-shock formation is very robust and generic. The form of Eq. (4.16) will depend on the model details greatly, but generically one expects shocks, and while most components of ρ will not be completely passive, all components of ρ will still follow Eq. (4.17) while also contributing part of the velocity in Eq. (4.16). Detailed discussion of why the δ-shocks are (or should be) generic is given in chapters 5 and 6.

4.4 Numerical Methods

Understanding the solutions to a partial differential equation with only analytical tools is not an easy task. Indeed, the solutions to the Navier-Stokes equations (and the Euler equations for fluid flow for that matter) still remains an

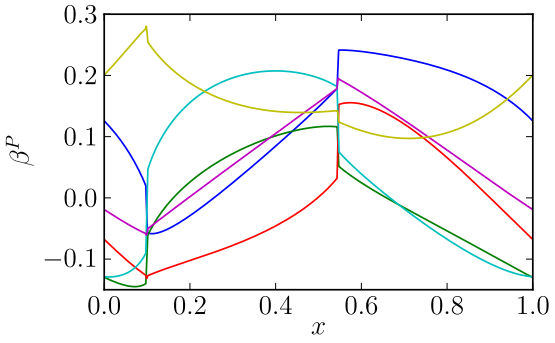

(a) **Shocks** in deformation gradient β^P

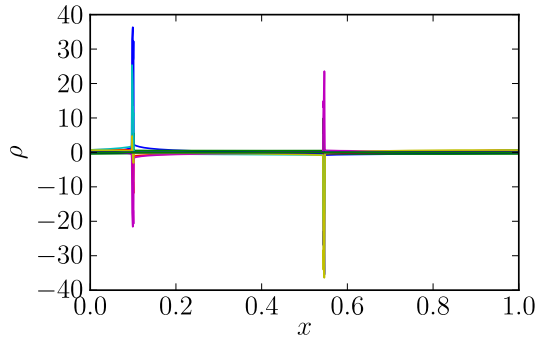

(b) δ**-shocks** in dislocation density ρ

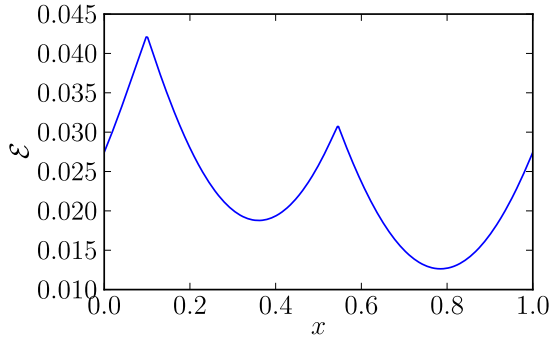

(c) **Cusps** in energy density $\mathcal{E}$

Figure 4.4: **Singularities in continuum dislocation dynamics.** Continuum dislocation dynamics exhibit several types of singularities, (a) shocks in plastic distortion tensor β^P which corresponds to (b) δ-shocks in dislocation density ρ, and (c) cusps that form in the elastic energy density $\mathcal{E}$. All of these singularities are coupled. It is interesting to know that, in terms of the conserved quantities, (a) and (b) both corresponds to a δ-shock in ρ, whereas (c) represents a shock in $\mathcal{F}$, the force density.

unsolved problem[3]. While the analytical solutions to these problems are not possible to extract, many of the equations have great practical use and fundamental importance, motivating careful numerical investigations.

Because of the ill-defined (or diverging) derivatives at the shocks, however, numerical integration of the equations is subject to instabilities without intelligent algorithms. In this section, we discuss the algorithms that we use to solve our continuum dislocation dynamics. We start with the de facto standard artificial viscosity method which has its root connected to the vanishing viscosity solutions. This method was used for the first stages of our exploration [49], but unfortunately it suffers from unnecessarily excessive diffusion (or viscosity)[4]. We then discuss the less-dissipative algorithms that are more sophisticated but provide much higher resolution by using interpolations and limiting the diffusion (or viscosity) to as little as possible.

Although the high resolution numerical methods are well established for standard strictly hyperbolic conservation laws, we should question carefully the applicability of the methods to a problem in higher dimensions (three dimensions in particular) and with the subtle properties discussed in section 4.2.

4.4.1 Artificial viscosity method

The most straightforward – and mathematically relevant – way of solving a PDE with shock discontinuities – is to add a regularizing term that smooths, either

[3]This is one of the "Millennium Problems".

[4]Depending on the simulation resolution and local values of the field, diffusion (or viscosity) must be in a range so that it is big enough to not cause numerical instabilities globally. Practically, this inevitably leads to more dissipation than necessary at a large fraction of the simulation volume in both space and time.

by diffusion or viscosity, the order parameter field and therefore avoids the numerical and mathematical issues associated with the ill-defined derivatives. In the case of our continuum dislocation dynamics, we can apply a quadratic or a quartic diffusion term as follows:

$$\partial_t \beta_{ij}^P = J_{ij} + \eta \nabla^n \beta_{ij}^P \tag{4.18}$$

where $n = 2$ or 4. This is analogous to solving Navier-Stokes equations with finite viscosity instead of solving inviscid Euler equations. Earlier investigation of our CDD using this method is presented in Refs. [49, 51]. However, there is a crucial problem with this method: physical magnitude of η is expected to be at the atomic scale, while the value needed for numerical stability must be at the (much larger) grid spacing scale. With the value of η needed for numerical stability, the wall structures are blurred over many grid spacings, making the emergent fractal patterns difficult to resolve.

For these reasons, it is imperative that we adopt, develop, and use minimally diffusive methods developed by mathematicians and scientists for many conservation laws to deal with the shock-forming nature of the inviscid versions of our equations.

4.4.2 Godunov-type schemes: Central upwind method

An alternative to the artificial viscosity method is to use a scheme that has built-in diffusion terms. The Lax-Friedrichs method is the first and the simplest of such methods, where a grid of u_i^j evolve as

$$u_i^{j+1} = \frac{1}{2}(u_{i+1}^j + u_{i-1}^j) - \frac{\Delta t}{2\Delta x}(f(u_{i+1}^j) - f(u_{i-1}^j)) \tag{4.19}$$

to solve $u_t + f(u)_x = 0$ where i and j represent spatial and temporal coordinates. This method is stable only if the maximum characteristic velocity[5] $c_{\max}$ satisfies the condition[6] $\frac{\Delta x}{\Delta t} \geq c_{\max}$; that is, within a single time step all physical characteristic waves must not affect any grid point other than the immediate nearest neighbors for this method to be stable. In general, this method is still overly diffusive. When $c_{\max}$ is constant and independent of the local field values (the case of simple advection with velocity a), this method can do a reasonable job. But when it is not the case (*i.e.* for most nonlinear problems) there will be regions where the effective diffusion is unnecessarily large.

Local and higher order methods have been developed to minimize diffusion and gain maximum resolution without causing instabilities (Refs. [63, 78, 43] to list a few). We will discuss the central ideas involved in these schemes, and how they apply to our implementation for our CDD equations.

For solving hyperbolic conservation laws, it is crucial to understand the "characteristics" of the equations. When full knowledge of characteristics and the Riemann solutions are acquired, good numerical methods exist to yield general solutions. Even with partial knowledge of characteristics, approximate Riemann solvers can retrieve approximate solutions to some hyperbolic problems[46, 43], but without some understanding of the hyperbolic characters of the equations one cannot expect to obtain a solution.

Our continuum dislocation dynamics model – as discussed in Section 4.3.2 – can not be fully diagonalized, and very likely is not strictly hyperbolic. Furthermore, Riemann solution to the problem (likely) contain δ-shocks that are

[5]For a strictly hyperbolic system, characteristic velocity c is a velocity that a certain "wave" propagates with: for example, the sound wave.

[6]This condition, the CFL (Courant-Friedrichs-Lewy) condition, is thus used to determine the time step Δt so that it is stable for a grid spacing Δx.

not very well explored. However, it can be argued that the only quantity that is transported – and carries information – is the components of the dislocation density tensor, and their physical velocity is given by the net Peach-Koehler force which is essentially a projection of the stress onto the characteristic glide directions of the dislocation, and therefore can not exceed a "norm" of the stress field. We utilize the characteristic velocity analysis presented in section 4.3.2, and assume that the maximum characteristic velocities are given by $\mathcal{V}_t$.

Central upwind methods are very well suited for this case, because the method demands knowledge of a maximum characteristic velocity but not much more. Essentially, it works by solving for the evolution of the smooth region and diffuses the "Riemann jump" with the widest Riemann fan[7] dictated by the maximum characteristic velocity.

4.4.3 Conservation Laws and Hamilton-Jacobi equations

Despite the fact that we have discussed conservation laws and dislocation density, there is another way to describe the system, which is to prescribe the instantaneous state by the use of the plastic distortion tensor β^P_{ij}. The dislocation density ρ_{ij} is related to β^P_{kj} by $\rho_{ij} = \epsilon_{ilk}\partial_l\beta^P_{kj}$. Thus, the dynamics of β^P_{kj} defines that of ρ_{ij}, and β^P_{kj} can be chosen as an order parameter instead of ρ_{ij}.

What are the pros and cons of choosing β^P_{ij} over the ρ_{ij} as the order parameter? There is a close analogy in electromagnetism, with ρ_{ij} like the magnetic field $\vec{B}$ and β^P_{ij} like the magnetic vector potential $\vec{A}$ (see Eq. 4.7). Because the magnetic field must satisfy the condition $\nabla \cdot \vec{B} = 0$, it is often convenient to use the vector

[7] The Riemann fan is the fan spanned by the shocks and rarefaction waves propagating outward from the Riemann shock.

potential $\vec{A}$ for designing initial conditions and for performing simulations [22]; $\vec{B}$ is written in terms of $\vec{A}$ as

$$\vec{B} = \nabla \times \vec{A}. \tag{4.20}$$

If we write the dynamics of $\vec{A}$ as

$$\partial_t \vec{A} = \vec{J}, \tag{4.21}$$

then it naturally follows from the relation (eqn 4.20) that

$$\partial_t \vec{B} = \partial_t \nabla \times \vec{A} = \nabla \times \vec{J}. \tag{4.22}$$

This equation (eq. 4.22), because the "flux" term has a derivative in front (although it is a curl, fiddling with the indices allows the equation to be transformed to look like a divergence[8]), is a conservation law, whereas Eq. (4.21) is not. This type of equations (often Hamilton-Jacobi equations) are commonly studied in relation to conservation laws [43].

As with the case of simulating $\vec{B}$ vs $\vec{A}$, we encounter the same pros and cons in simulating ρ_{ij} vs β^P_{ij}. We have implemented both approaches and the simulation results are nearly identical. However, due to the appearance of δ-shocks in ρ (challenging to represent on a grid) and due to the complexities associated with correcting the $\partial_i \rho_{ij} = 0$ condition, we opt to use the β^P_{ij} as our basic degree of freedom. All simulation results reported in this work are from simulating the β^P_{ij} equation.

It is interesting to note that one of the most interesting things about the vector potentials is that there is a gauge freedom in defining the vector potential for a given magnetic field. A similar gauge freedom exists in defining a β^P_{ij} field

[8] $\partial_t B_i = \epsilon_{ijk}\partial_j \partial_t A_k = \partial_j(\epsilon_{jki}\partial_t A_k) = \partial_j \mathcal{F}_j$ where $\mathcal{F}_j = \epsilon_{jki}\partial_t A_k$ is the "current flux" of the magnetic field.

for a given ρ_{ij} field, which corresponds to freedom of adding the derivatives of an arbitrary spatial functions ϕ_j to β^P_{ij}, i.e. $\beta^P_{ij} \to \beta^P_{ij} + \partial_i \phi_j$. This "gauge freedom" amounts to adding a component β^P_{ij} that does not generate any dislocations; it is initial condition and history dependent, but dislocation-free (see Ref. [17]).

4.5 Convergence and validation of the numerical method

In this section, we will examine the validity of the numerical method we employ to solve our continuum dislocation dynamics, and discuss the implications and outcomes of the results. This section previews the discussion of the results reported in chapter 3, with more numerical details that were not included in the previously published report.

Numerically, differential equations are often solved on a grid in space, or sometimes on a "grid" in time, or sometimes both. When doing so, it becomes essential to make sure that the "imposed" grid does not affect the solution, i.e. that the solution is independent of the (unphysical numerical) grid.

A common method of validating the correctness of a numerical scheme is to use a well-known – preferably analytically solved – problem as a test problem, comparing the simulation results to the analytical solution and confirming that it converges as the grid size (grid spacing) is taken to infinity (zero). Different metrics can be used to compare the solutions, but a standard convention is to look at the L_n norm between the solutions:

$$L_n = \langle (u_N - u_\infty)^n \rangle^{1/n} \tag{4.23}$$

When the solutions to the equations are smooth and continuous in space and

time, most methods do in fact converge as the grid spacing is taken to zero; the error terms can be shown to decay quickly due to the smoothness, for any n. However, whenever singularities appear, this convergence is not as natural.

For our CDD equations, unfortunately, the only analytically known solutions are trivial. Therefore, it is necessary to have a different measure of evaluating convergence. Because there is no u_∞ we can compare to, we examine the relative distance between terms $\langle (u_{2^m N} - u_{2^{m+1} N})^n \rangle^{1/n}$; if these vanish quickly, then we can use the Schwarz's inequality $\sum_{m=1\ldots} \langle (u_{2^m N} - u_{2^{m+1} N})^n \rangle^{1/n} \geq \langle (u_N - u_\infty)^n \rangle^{1/n}$ (true for $n \geq 1$) to argue for L_n norm convergence.

4.5.1 Spatio-temporal convergence in 1D

Using the central upwind method described in Section 4.4, we can implement the equations (4.8)) and (4.9). As has been discussed in previous work [49] (also Chapter 2), these models form sharp dislocation wall structures in all dimensions. Figure 4.5 shows the L_2 norm convergence as a function of time. In Ref. [18], in the interest of simplifying the discussion, instead of looking at the L_2 norms of β^P we looked at a variant smoothed version for ρ. With β^P the smoothing is actually unnecessary, as long as the solutions are properly interpolated.

As also can be verified in figure 4.6, in 1D, taking the limit to $N \to \infty$, the L_n norm sequence is a converging sequence at all times. Therefore the method is likely leading to a convergent real solution, as the grid spacing gets finer. In analogy with turbulence[9], we thus turn to statistical properties of the numerical solutions.

[9] See chapter 3 for the analogy.

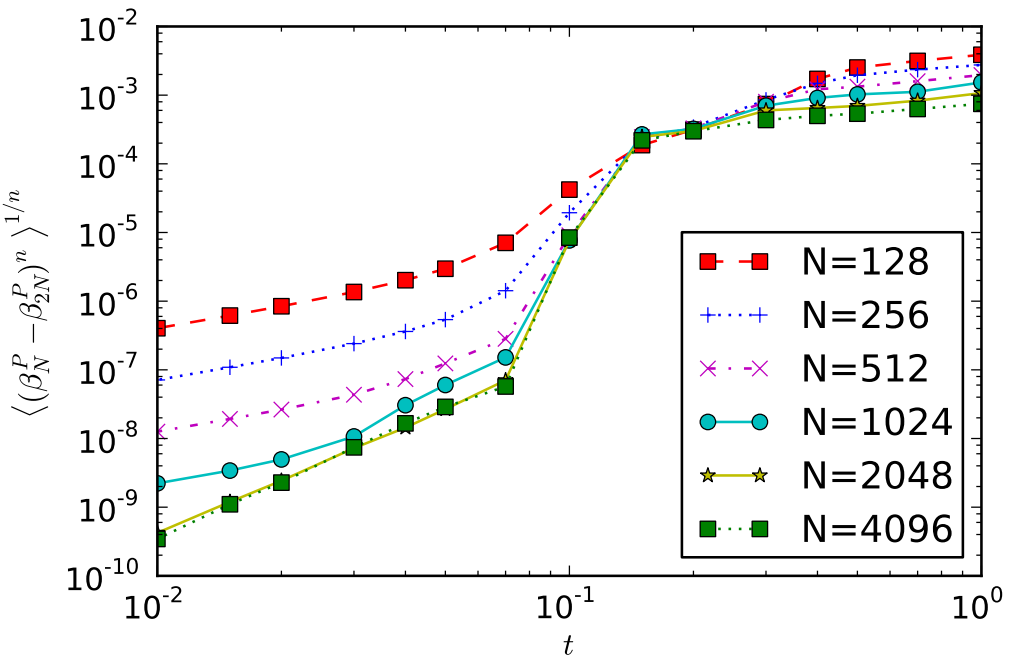

Figure 4.5: **Convergence of solutions in 1D**. L_2 norm differences between simulation results of grid sizes $N = 128, \cdots, 4096$ and $2N = 256, \cdots, 8192$ are plotted. Although at around $t = 0.1$ – when dislocation walls are formed the convergence becomes much worse, at later times the solutions again appear to converge.

4.5.2 Spatio-temporal non-convergence in 2D

However, this trend does not extend to higher dimensions. Figure 4.7 illustrates the L_2 norm non-convergence that arises as the dislocation wall structures are formed. A detailed discussion is available in chapter 3 and we will not delve into it deeply here; in essence, similar spatio-temporal non-convergence can be seen in simulations of Euler equations as well, we suggest it is a natural consequence of having fractal and chaotic solutions, as opposed to smooth "laminar" solutions.

The issue here is that this "turbulent" behavior is plausibly physically cor-

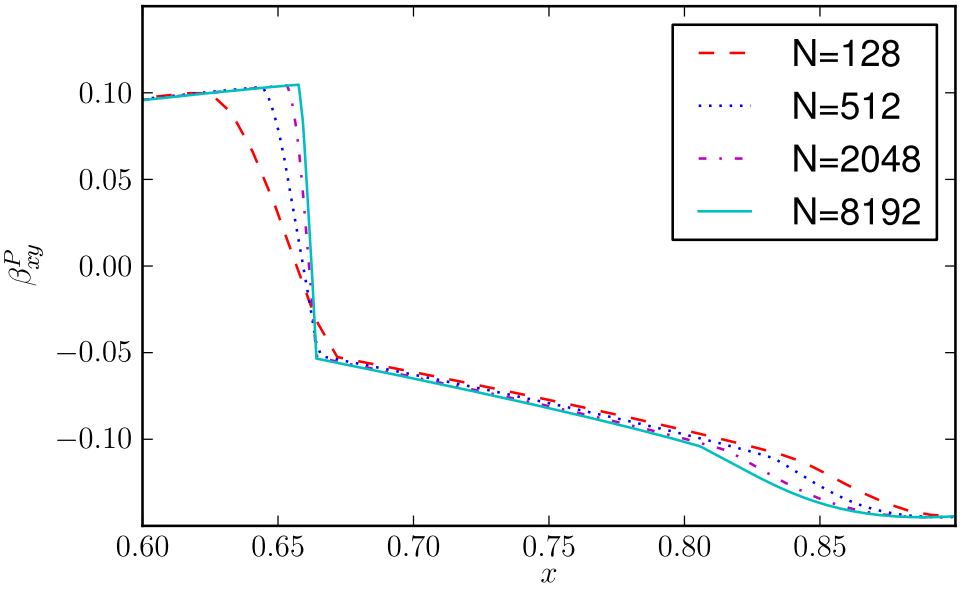

Figure 4.6: **Convergence of solutions in 1D, actual solutions**. β^P_{xy} at $t = 1.0$ for different simulation grid sizes $N = 128, 512, 2048, 8192$. Note that solutions appear to be converging as figure 4.5 implies at $t = 1.0$.

rect, but sabotages any possibility of naive numerical "convergence"!

4.5.3 Statistical properties and convergence

Despite the spatio-temporal non-convergence seen in the last subsection, dislocation cell walls form fractal patterns (Chapter 2) that are statistically identical and convergent as a function of the simulation grid size. Figure 4.8 shows the convergent (and robust) behavior of the dislocation density correlation function. This, in fact is consistently analogous with simulations of turbulence where statistical properties such as velocity correlations are expected to be meaningful even though the actual flow pattern is not realizing a limiting value. We discuss this analogy in detail in chapter 3. Various correlation functions and the

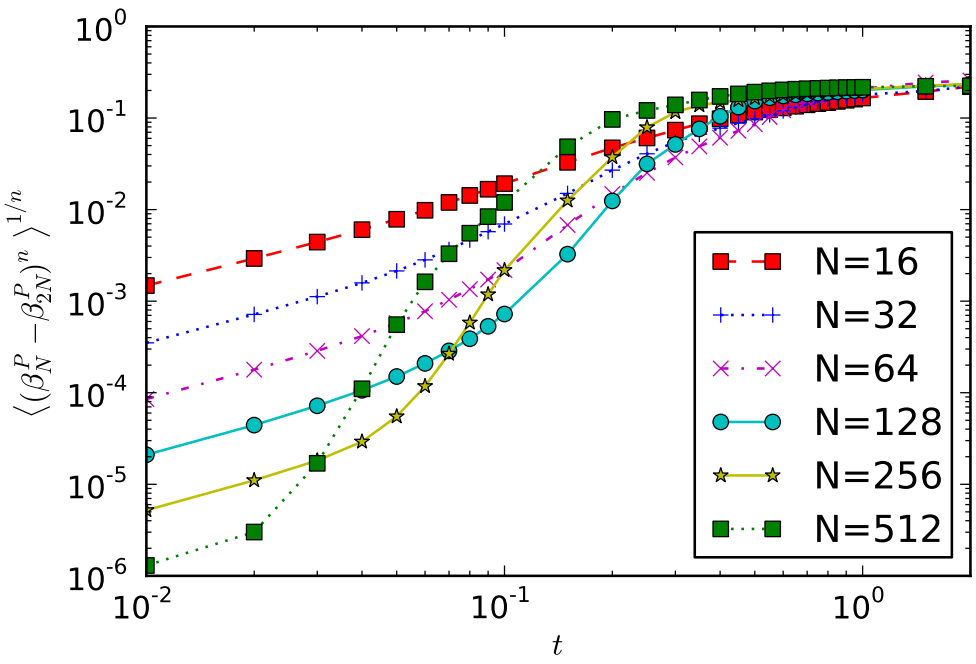

Figure 4.7: **Non-convergence of solutions in 2D**. At earlier times, e.g. $t = 0.01$ for the sizes being plotted, the L_2 norm differences are convergent. However, around $t = 0.1$, the differences become larger as the mesh refines, leading to spatio-temporal non-convergence. Figure reproduced from chapter 3 for detailed discussion.

relations between them are analyzed extensively in Ref. [17].

4.5.4 Convergence with finite viscosity

In the turbulence literature, although many simulations focus on looking at statistical properties and comparing them to that of experiments, it is rarely argued that the numerics might be causing problems. Perhaps a long history of experimental confirmation of theoretical prediction has led to confidence that the simulations are realistic. Another reason, though, is that fluids have viscos-

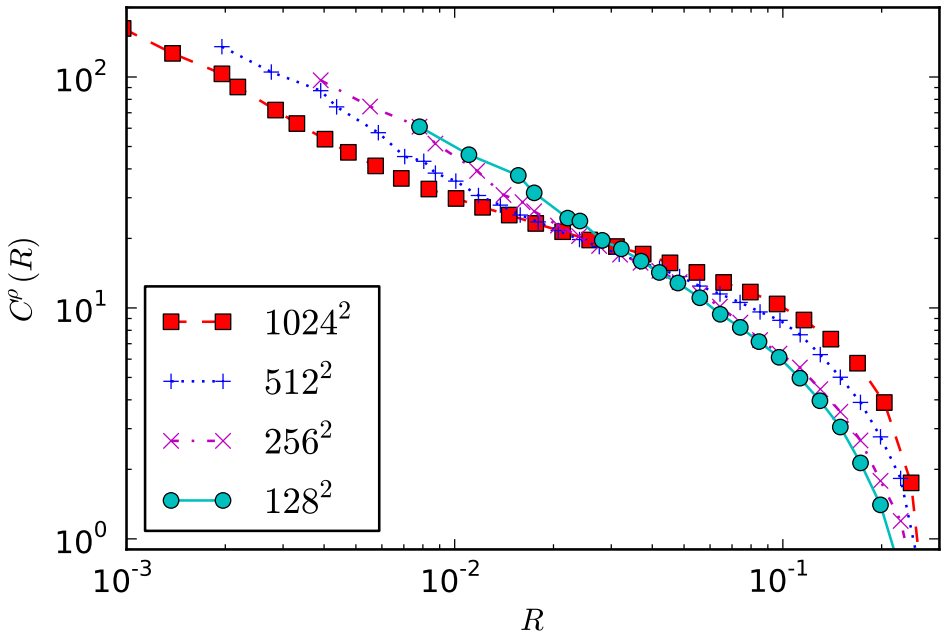

Figure 4.8: **Statistical Convergence**. While spatio-temporal convergence is lost in 2D, correlation functions of the relaxed dislocation structures exhibit convergent behavior. Figure reproduced from chapter 3 for detailed discussion.

ity (albeit small) which limits the short-length scale fractal fluctuations. Indeed, chaos limits the naive convergence of turbulence simulations at least as severely as does the fractal substructure.

Even for very high Reynolds number flows (small viscosity), while it may not be practically possible to fully resolve the resolution, it is commonly believed that if one could do a full-scale simulation that resolves the Kolmogorov length scale, it would lead to legitimate convergent solutions.

For our CDD, the situation is very similar. It is certainly argued that the dislocation cores should provide some sort of regularization [3], and the walls will not be mathematical singularities. On the other hand, for continuum dislocation

dynamics to be useful, we would like the core length scale to be much smaller than the numerical grid, as we hope to model the scale at which much more than 10^6 dislocations are evolving; when these dislocations are segmented into small pieces for simulation, the number of segments would defeat all current discrete dislocation dynamics simulations.

The convergence properties of turbulence simulations provides us a way of direct comparison, that could serve as a sanity check (or a similarity confirmation check). Instead of trying to solve the dislocation dynamics equation (4.6), we solve the equation (4.18) with $\eta \neq 0$, fixing η and checking the convergence as we increase the grid size.

Figure 4.9 shows the L_2 norm of the differences in 2D simulations of successive grid sizes, with a fixed viscosity $\eta = 10^{-3}$ and quartic viscosity $\tilde{\eta} = 10^{-7}$. It is immediately clear that once the grid spacing reaches the "viscosity length scale", the sequence becomes convergent and therefore is converging to a solution. This illustrates the fact that the behavior of our equations are indeed the same as most expect from the Navier-Stokes equations, and further reinforce the similarity between continuum dislocation dynamics and high Reynolds number turbulent fluid flow.

4.6 Conclusion

We have illustrated how the methods used for hyperbolic conservation laws can justifiably be applied to simulating our continuum theory of dislocations. The results still exhibit spatio-temporal nonconvergence in two and higher dimensions. However, we find that the behavior is consistent with that of turbulent

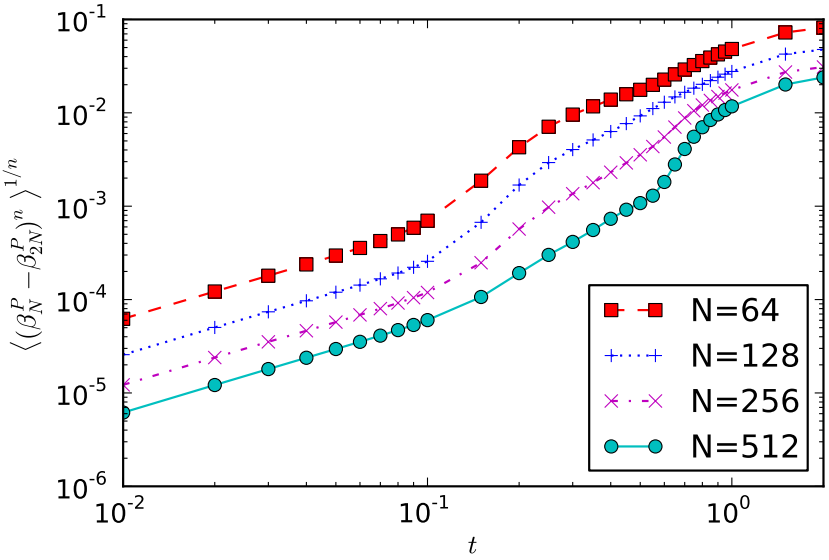

(a) With $\eta = 10^{-3}$

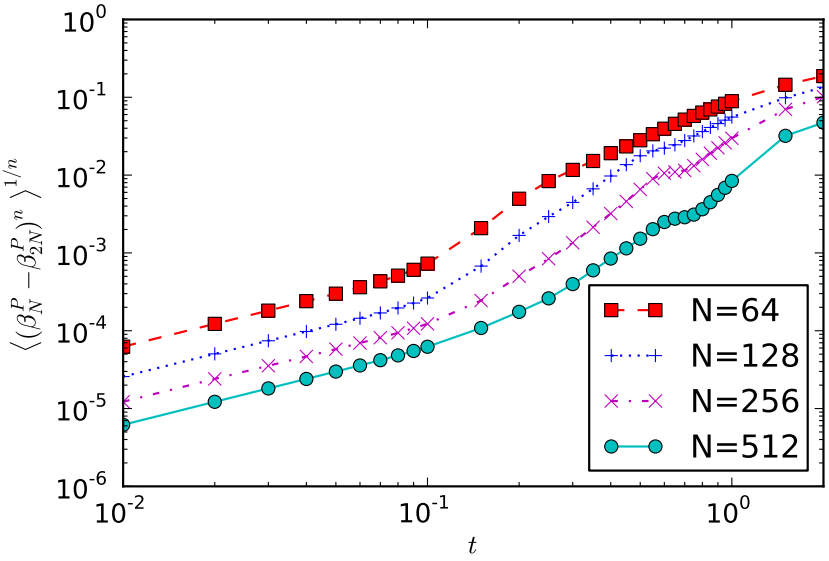

(b) With quartic viscosity $\tilde{\eta} = 10^{-7}$

Figure 4.9: **Convergence of solutions with fixed viscosity $\eta = 10^{-3}$ and quartic viscosity $\tilde{\eta} = 10^{-7}$.** Compare to figure 4.7. Same initial conditions in 2D with fixed viscosity $\eta = 10^{-3}$ (and quartic viscosity $\tilde{\eta} = 10^{-7}$) show convergent L_2 norms at all times.

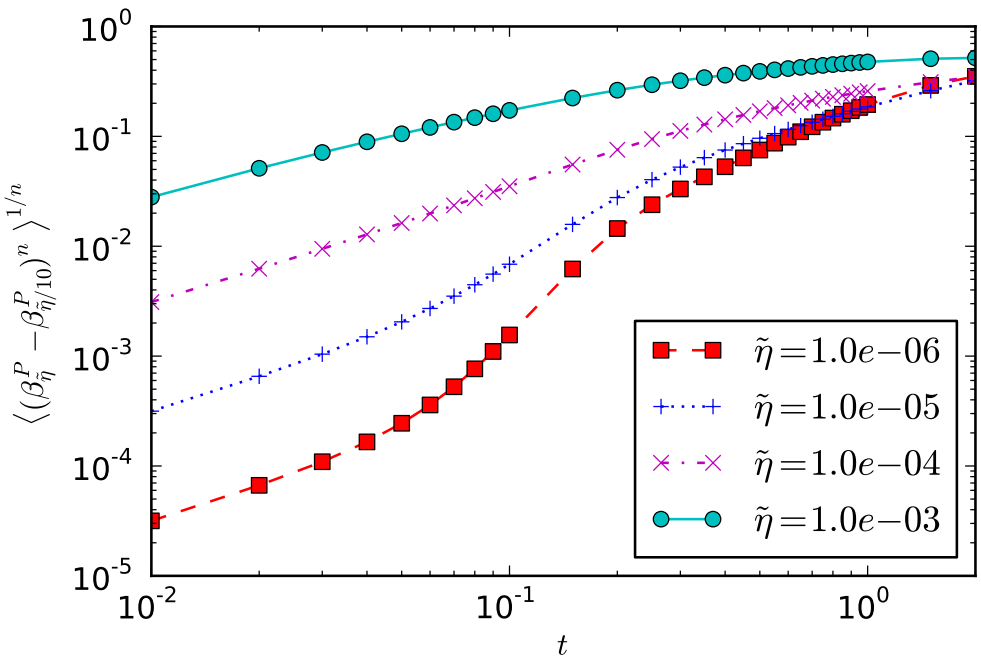

Figure 4.10: **Nonconvergence in the limit of $\eta \to 0$.** With the quartic viscosity, L_2 norm differences between the solutions with $\tilde{\eta}$ and $\tilde{\eta}/10$ are plotted for size $N = 1024^2$. Note that as seen in figure 4.9, $N = 1024^2$ appears convergent for all $\tilde{\eta}$ used for this plot. However, the solutions become nonconvergent in the limit of vanishing viscosity.

flow, and the fact that we get fractal dislocation wall patterns and the mapping to the passive-dust δ-shock equations complement the analogy.

This way of building a continuum dislocation dynamics is relatively new, and as shown in this chapter it is difficult to properly simulate the systems that exhibit δ-shocks that form *fractals*. Nevertheless, as both are experimentally readily observed, it will be necessary for theories to adopt and apply such methods to study the behaviors of dislocation walls.

Acknowledgement

We thank Alexander Vladimirsky and Randall LeVeque for helpful comments and guidance on hyperbolic conservation laws and numerical methods, and Chris Henley for comments and feedbacks that helped improved this article. This work was supported by US DOE/BES grant DE-FG02-07ER46393.

Appendix

Relation to Turbulence

Although we have made direct comparison of our continuum dislocation dynamics model to turbulence (comparing the plastic relaxation to the Rayleigh-Taylor instability, in chapter 3), there are obvious differences that exist between them. Turbulence is sustained only by constant supply of energy, and turbulent properties, such as velocity correlations, only hold while there is shear flow and dies away when relaxed. In contrast, our dislocation dynamics relax into fractal structures, and stay that way forever. So how is it directly analogous to turbulence?

The answer lies with passive scalar advection in turbulence. When there are dust particles advected with a turbulent fluid flow, the *scalar* dust particles also show turbulent behavior [33, 79]. Turbulent mixing of passive scalar dust is observed in many systems, such as astrophysical systems [38] and sedimentation [82]. Now recall the argument for δ-shocks presented above. In our dislocation dynamics, dislocation walls – that become fractal – are formed as a

result of the *flow* of the force density field dragging the dislocation density to segregate at the jumps of the force density. They are *passively* dragged there and stay there without diffusing. This makes a nice analogy to passive scalar advection in turbulent flows, except for the complication that dislocation walls are in general not completely passive and as they deform they can interact with itself and others as well.

CHAPTER 5

δ-SHOCKS IN CONTINUUM DISLOCATION DYNAMICS

5.1 Introduction

When metals are deformed, dislocations are known to nucleate, glide, entangle, and eventually form various patterns often comprised of wall-like structures. For decades it has been observed that the dislocation wall structures exhibit diverse features depending on the material property, loading conditions and history. Just as the yield stress is known to relate to the grain sizes (the Hall-Petch [30, 69] and reverse Hall-Petch [75] relations), the scaling of dislocation structures within cells are known to affect the yield stress and hardening [28]. It has also been observed that dislocation cell structures refine under strain [36]. However, theoretical and numerical understanding of the behaviors are yet incomplete as to why and how these dislocation wall structures are formed and how they affect the material properties.

Particularly, because of the collective nature of the dislocation wall and cell structure formation, it is deemed necessary to have a coarse-grained continuum description of the behavior. Traditionally, continuum theories of dislocations include features designed to capture macroscopic plasticity properties such as work hardening (statistically stored dislocations, yield stress, dislocation "forest" interactions) and anisotropic response (slip systems, yield surface). So far, these continuum models have not been observed to form walls. To form walls or other related dislocation structures, either stochasticity [27, 7] or direct simulations of the individual discrete dislocations [55] seemed necessary.

Recently, a class of fully deterministic continuum dislocation dynamics models (without discreteness or stochasticity), originally proposed by Acharya [1], have been shown to spontaneously develop dislocation wall structures and cellular patterns [49, 17] (see also Chapter 2 and Figure 5.1). Why do we form walls, where other more realistic theories do not? Does incorporating work hardening or other realistic features impede the formation of these wall structures somehow? Are the walls an artifact of our numerical methods? We shall show in section 5.2 that identical numerical methods applied to the traditional models, simplified to remove work hardening and other realism, do form jumps in dislocation density but do not exhibit wall formation. In section 5.3 we will introduce recent continuum dislocation dynamics theories that do exhibit wall formation; and we shall argue in section 5.4 that these walls are generally expected for multicomponent conserved systems that form jumps in the conserved density, whenever the velocities of the different components are directly coupled. However we observe that the dynamics of the different slip systems in the traditional theories are coupled only through the stress (a nonlocal function of the densities on the various slip systems) – hence no walls. In section 5.5 we propose various mechanisms that could couple these velocities, and we show that these proposed modifications of the traditional theories do indeed form wall-like structures, although the numerical methods we use smear these walls somewhat during their formation. In section 5.6, we show in detail why our isotropic model and the modified traditional models form wall structures.

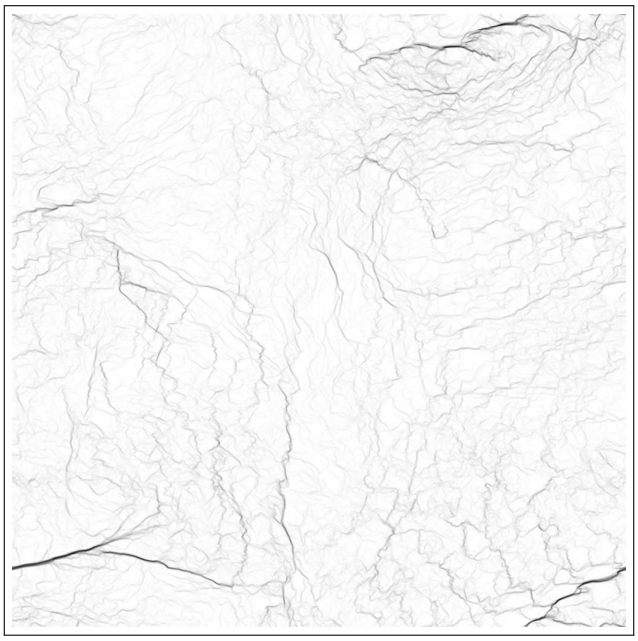

(a) Dislocation wall structures in 2D

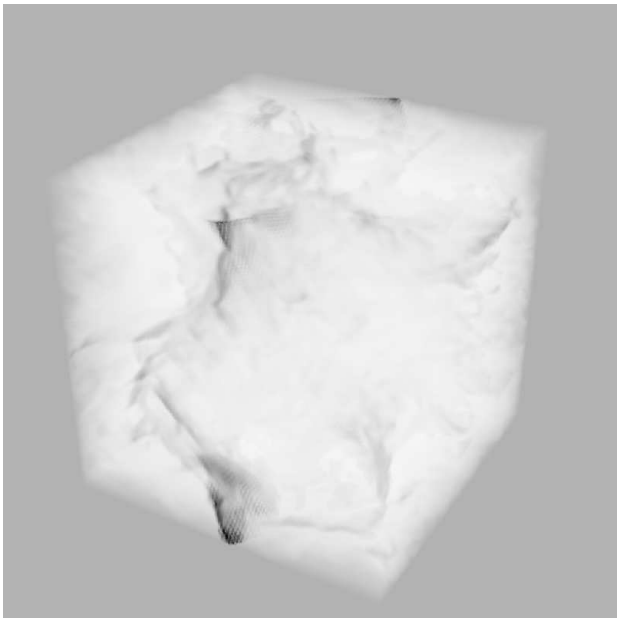

(b) Dislocation wall structures in 3D

Figure 5.1: **Dislocation wall structures formed in continuum dislocation dynamics**. Our continuum dislocation dynamics simulation exhibits complex dislocation wall structures evolved from a smooth random initial condition. Net local dislocation densities are plotted with black representing high dislocation density.

5.2 Continuum dislocation dynamics and dislocation patterning

The accurate prediction of macroscopic loading behaviors in stress-strain curves and their history dependence is the essence of the study of plasticity, the engineering theory underpinning the deformation of crystals and polycrystalline materials. For that reason, continuum theories of plasticity often incorporate many details of the particular targeted material[1]. The crystalline model is anisotropic, with specified active slip systems, contains (locally) canceling dislocations called statistically stored dislocations (SSDs)[2], whose velocities are given by complicated functions of local stresses and the local total dislocation density (mainly composed of SSDs).

These traditional theories [5, 6, 41, 37, 73] end up evolving a family of slip parameters $\gamma^{(\alpha)}$:

$$\partial_t \gamma^{(\alpha)} = \mathcal{V}(\sigma^{(\alpha)})\rho^{(\alpha)} \tag{5.1}$$

where α denotes different slip systems[3], $\gamma^{(\alpha)}$ denotes the local amount of slip on that system, $\sigma^{(\alpha)}$ denotes the resolved shear stress on that system, $\rho^{(\alpha)}$ is the dislocation density in the system, and $\gamma^{(\alpha)}$, $\sigma^{(\alpha)}$, and $\rho^{(\alpha)}$ are all functions of position. The velocity $\mathcal{V}(\sigma^{(\alpha)})$ is often a nonlinear function of the resolved shear stress, with the yield stress represented as a threshold [85], or as a high power

[1]This type of modeling is designed to bridge the gap between crystal plasticity, where a crystal is modeled with volume elements of different orientations, and microscopics effects of SSDs and their resulting hardening behaviors.

[2]Statistically stored dislocations are dislocations within the volume element of the continuum dislocation simulation whose Burgers vector densities cancel one another.

[3]Each slip system (α) is defined by a plane normal $\hat{n}^{(\alpha)}$ and the Burgers vector $\hat{b}^{(\alpha)}$. Most well-studied materials have fcc or bcc slip systems. For the simulations presented here, we use a cubic slip systems where both the slip plane normals and Burgers vectors are parallel to $\hat{x}, \hat{y}, \hat{z}$ directions for simplicity.

law in the stress [59], which may depend on the total densities of dislocations on other slip systems.

The simplest version of these theories, without yield surfaces or work hardening, would have the slip velocity proportional to the resolved shear stress:

$$\partial_t \gamma^{(\alpha)} = \sigma^{(\alpha)} \rho^{(\alpha)} \tag{5.2}$$

Ignoring all short range interactions – since they are tricky[4] to deal with – we get a simple PDE:

$$\partial_t \gamma^{(\alpha)} = \sigma^{(\alpha)} ||\nabla \gamma^{(\alpha)}|| \tag{5.3}$$

where we assume $\rho^{(\alpha)} = ||\nabla \gamma^{(\alpha)}||$. Here dislocation density $\rho^{(\alpha)}$ computed from the slip parameter $\gamma^{(\alpha)}$, i.e. $\rho^{(\alpha)} = ||\nabla \gamma^{(\alpha)}||$ could be either

$$||\nabla \gamma^{(\alpha)}|| = \sqrt{(\nabla \gamma^{(\alpha)}) \cdot (\nabla \gamma^{(\alpha)})} \tag{5.4}$$

or

$$||\nabla \gamma^{(\alpha)}|| = |\hat{b}^{(\alpha)} \dot{\nabla} \gamma^{(\alpha)}| + |(\hat{n} \times \hat{b})^{(\alpha)} \cdot \nabla \gamma^{(\alpha)}|, \tag{5.5}$$

depending on how one models the dislocation density[5]. Choosing the dislocation density based on the derivatives of the slip parameter results in SSDs becoming irrelevant; sub-grid scale local fluctuations in slip, which is related to SSDs, is neglected and only geometrically necessary dislocations (GNDs) resolved by the gradients in γ remain important. Finally, using Eq. (5.5), we can write equation (5.3) as:

$$\partial_t \gamma^{(\alpha)} = \hat{b} \cdot \vec{\mathcal{V}}^{(\alpha)}_{\text{edge}} (\hat{b} \cdot \nabla \gamma^{(\alpha)}) + \hat{p} \cdot \vec{\mathcal{V}}^{(\alpha)}_{\text{screw}} (\hat{p} \cdot \nabla \gamma^{(\alpha)}) \tag{5.6}$$

where $\hat{b}$ is the Burgers unit vector for (α) and $\hat{p} = \hat{b} \times \hat{n}$ where $\hat{n}$ is the slip plane normal unit vector for (α). $\vec{\mathcal{V}}^{(\alpha)}$ are the velocity of the edge and screw

[4] See Refs. [31, 23] for some approximate attempts at dealing with short-range interactions.
[5] Different ways of writing this density qualitatively do not change the behavior.

dislocations, which in the simplest form would be

$$\begin{aligned}\vec{V}^{(\alpha)}_{\text{edge}} &= \hat{b}\sigma^{(\alpha)}\text{sign}(\hat{b}\cdot\nabla\gamma^{(\alpha)})\\ \vec{V}^{(\alpha)}_{\text{screw}} &= \hat{p}\sigma^{(\alpha)}\text{sign}(\hat{p}\cdot\nabla\gamma^{(\alpha)}).\end{aligned} \tag{5.7}$$

Figure (5.2) shows the resulting evolution. The traditional slip-system models, simplified to Eq. (5.2), do not form dislocation wall structures. Starting from a smooth random distribution of dislocation density, the dislocation density forms jumps – shocks – in various places, but no sharp dislocation walls are observed (see Figure 5.3a for a one dimensional cut).

Why do the dislocation densities even form jumps in these traditional methods? Note that Fig. 5.2 depicts the net dislocation density. Consider the case of dislocations with Burgers vector along $\hat{x}$ with density $\rho(x)$ varying only along x. The long-range stresses between these dislocations cancel out (they form a continuous family of low-angle tilt boundaries along yz planes), but under an external resolved shear stress σ the positive densities will move to $+\hat{x}$ direction and the negative densities will move to $-\hat{x}$ direction, each with speed $|\mathcal{V}(\sigma)|$. Since models that evolve slip densities γ will automatically annihilate the positive and negative densities when they meet, such models will form a step discontinuity in density starting at every place where the density changes sign and the external stress pushes them together.

5.3 Cell wall structures in Continuum Dislocation Dynamics

Since the constitutive laws of these materials already include phenomenological models of work hardening, these traditional models are not designed to explain

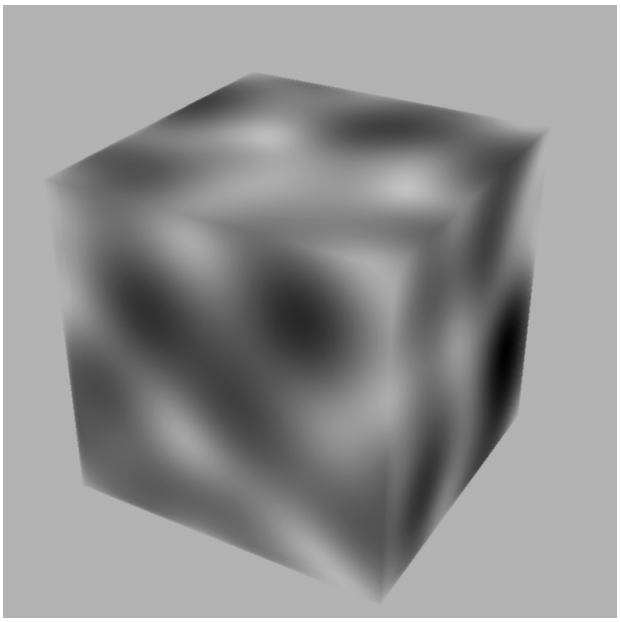

(a) $t = 0$

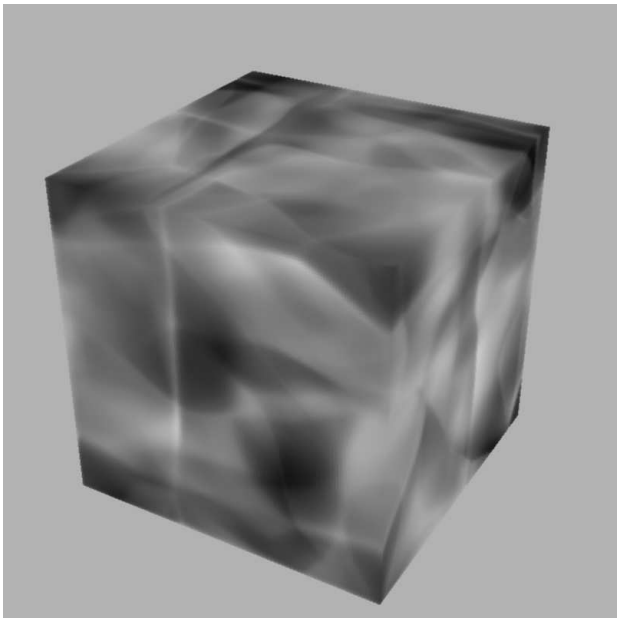

(b) $t = 20$

Figure 5.2: **Dislocation density evolved with slip dynamics**. The simplified slip dynamics forms jumps in the dislocation density, but no apparent walls are formed. The net dislocation densities are plotted with black representing high dislocation density. Note that the sharp white interfaces in (b) are not walls; the dislocation density jumps and goes through zero (see Figure 5.3).

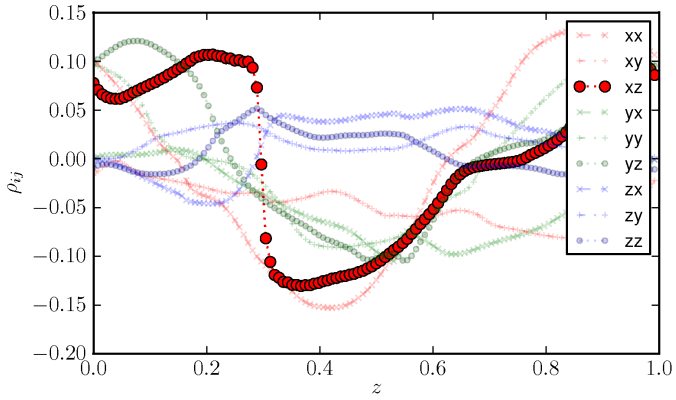

(a) $t = 20$, $f = 0$

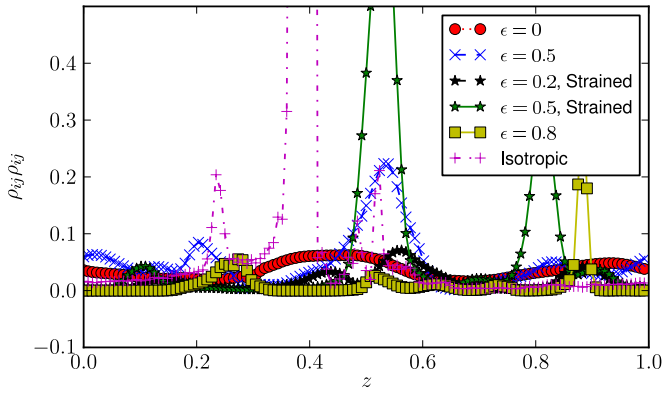

(b) Comparison of dynamics

Figure 5.3: **1D cross-sections of dislocation density components**. (a) Traditional model forms jumps, not walls. One-dimensional cross-sections along the z-axis showing all components of the Nye dislocation density tensor. See 5.2b and 5.4b for the full 3D plot. Note the jump in density of ρ_{xz} (large symbols); none of the components show wall formation. (b) Adding coupling forms walls. Total squared dislocation density along the same line, with (i) no coupling of velocity (ii) $f = 0.5$ (iii) $f = 0.2$ after loading to strain $\epsilon = 0.25$, (iv) $f = 0.5$ after loading to strain $\epsilon = 0.1$, (v) $f = 0.8$, and (vi) our isotropic continuum dislocation dynamics (CDD). The squared dislocation density $\rho_{ij}\rho_{ij}$ show no obvious hint of walls without the velocity coupling, but $f = 0.5$ and $f = 0.2$ after straining display wall formation (albeit smeared and wide). $f = 0.8$, $f = 0.5$ after straining, and our isotropic CDD show sharp walls.

the origins and evolution of the yield stress as it emerges from the collective physics of hardening at more microscopic length scales. But this regime of collective dynamics is without question interesting, as it harbors the explanations of the whys and hows of the macroscopic behavior. To address these questions, one can move towards directly coarse graining the microscopic physical behavior without incorporating phenomenological macroscopic relations. There are several approximate schemes that have been pursued: Groma *et al.* [27] started by assuming that only one (or a few) slip system(s) is(are) activated and relevant, but did not neglect the effect of statistically stored dislocations that arise in the process of coarse graining. Acharya [1] and later[6] Limkumnerd and Sethna [49] developed models of isotropic plasticity; they neglected the statistically stored dislocations under the assumption that at mesoscopic scales geometrically necessary dislocations dominate the dynamics.

These last recent theories are based on the dynamic evolution of the Nye dislocation density tensor ρ_{ij}[7] as [1, 49] (also Chapter 2):

$$\partial_t \rho_{ij} = f_{iuv} \partial_u J_{vj} \tag{5.8}$$

Here the conserved current $J_{vj} = \partial_t \beta^P_{vj}$ is given by:

$$\partial_t \beta^P_{ij} = f_{\ell ik} \mathcal{V}_\ell \rho_{kj} = \mathcal{V}_\ell \rho_{\ell ij} \tag{5.9}$$

where $\rho_{ij} = f_{imn} \partial_m \beta^P_{nj}$ and $\rho_{\ell ij} = f_{\ell ik} \rho_{kj}$. The overdamped velocity assumption gives $\mathcal{V}_\ell = D(\rho) \mathcal{F}_\ell$, where $\mathcal{F}$ is the net Peach-Koehler force on the local dislocation density.

Chapter 2 and Ref. [17] discuss how $\mathcal{V}_l$ can be defined in terms of ρ in detail.

[6] Acharya [1] had previously written the same isotropic theory, but most of their early work focused on GNDs in a single slip system, and they did not notice that their theories formed walls.

[7] Also often denoted α_{ji}.

In one of the two glide-only versions, we force the local material volume to be conserved and also ensure that the dynamics guarantees that the energy goes strictly downhill. These constraints lead to the dynamics (see Chapter 2)

$$\partial_t \beta^P_{ij} = \mathcal{V}'_\ell \rho'_{\ell ij} = D(\rho)\rho'_{\ell mn}\sigma_{mn}\rho'_{\ell ij} \tag{5.10}$$

where $\rho'_{\ell ij} = \rho_{\ell ij} - \frac{1}{3}\delta_{ij}\rho_{\ell kk}$ and where $D(\rho)$ is a mobility function[8]. (The glide-only condition can be imposed also in a different way, as a vacancy pressure induced by the vacancy generation/absorption associated with the climb process, in the limit of infinitely expensive vacancies [2, 17]. The differences between these two dynamics are not important within the scope of this paper as both share the same qualitative behaviors. We will focus here on the first glide-only dynamics.)

How do the traditional methods (Eq. 5.2) and the new methods (Eq. 5.9) compare? They are not all that different: β^P_{ij} is the same physical quantity as $\gamma^{(\alpha)}$, and the currents in both cases are given by a force: the shear-resolved stress on the dislocations times the dislocation density. How are they different? For Eq. (5.2), all types of dislocations – edge and screw in various slip systems – each have their own velocity and move independently, except by interacting through the stress. For Eq. (5.9), in contrast, there is a single velocity for all components of the dislocation density tensor: the net stress is not separated into stresses on the different slip systems, but applied to the local dislocation density, which moves 'as a unit'. But, the most central distinction is in the resulting behavior. As noted above, the traditional models form steps in the dislocation density but no walls (Fig. 5.2), whereas Eq. (5.9) – isotropic continuum dislocation dynamics (CDD)

[8]We use $D(\rho) = 1/|\rho|$ where $|\rho| = \sqrt{\rho_{ij}\rho_{ij}}$ for the dislocation wall velocity to be physical, i.e. independent of the wall thickness. Variants such as $D(\rho) = 1$ are used as well for mapping the equation into the Burgers equation [51]. Note that $D(\rho) = 1$ and $D(\rho) = 1/|\rho|$ are dimensionally incompatible. All PDEs discussed in this manuscript must have a constant factor that can be attributed to rescaling of time that gives the terms proper dimensionality. For simplicity, and consistency with preceding work, we neglect such constants in our discussion here.

– forms striking wall structures (Fig. 5.1).

5.4 Physics behind wall formation

How do we explain why walls form in the new theories? Let us presume that steps in dislocation density form naturally (as for the traditional theories, depicted in Fig. 5.2). Each of the components of the dislocation density tensor is conserved. Let us restrict our attention to the problem in one-dimension; in higher dimensions, the jumps form with co-dimension one and similar argument can be made [9]. Generally it is presumed that, at steps in the density of conserved quantities, the velocity s at the step must satisfy the Rankine-Hugoniot condition:

$$s = \frac{\mathcal{V}_+\rho_+ - \mathcal{V}_-\rho_-}{\rho_+ - \rho_-} \tag{5.11}$$

balancing the volume $s(\rho_- - \rho_+)\Delta t$ of the rectangle filled in by the moving step with the net flux $\mathcal{V}_+\rho_+ - \mathcal{V}_-\rho_-$ of conserved material impinging on the step. This is not a physical necessity: indeed, violation of the Rankine-Hugoniot condition would precisely imply the deposition of a finite density of new material at the step – forming a wall.

Now, in a multicomponent system there is a separate Rankine-Hugoniot front velocity condition $s_{\ell ij}$ for each of the nine independent component of the conserved dislocation density tensor $\rho_{\ell ij}$, where $\mathcal{V}_{\ell ij}$ depends in general on all components ρ_{mno}. Since these velocities ordinarily do not agree, wall formation is natural. (In the particular case of the new theories exemplified by Eq. (5.10), all dislocations share the same *dislocation* velocity $\mathcal{V}$, but will have different

[9] Rigorous mathematical proofs in higher dimensions are typically difficult or impossible, however.

Rankine-Hugoniot *step* velocity criteria.) Multicomponent systems do not generally have simple evolving step solutions; although other solutions are possible (e.g., breakup into multiple steps [46]), developments of walls in the conserved quantity must be considered generic when physically reasonable.

How do we explain that the traditional (multicomponent) systems do *not* form walls? First, the stress tensor (and hence the shear-resolved stress) is a nonlocal function of the dislocation density – basically an integral. A step discontinuity in the dislocation density generates only a cusp (derivative discontinuity) in the stress. For models (like Eq. (5.2)) where the dislocation velocity is a function of the local stress, the velocities $\mathcal{V}_+ = \mathcal{V}_-$ at the two sides of the jump; hence all components share the same Rankine-Hugoniot velocity $s = \mathcal{V}_+ = \mathcal{V}_-$. Second, for models where the dislocation velocity depends directly on the local dislocation density, the models usually do not incorporate annihilation; the positive and negative components of the dislocation density evolve independently, and steps may not arise. Whether the lack of wall formation in these theories is an asset or a handicap depends upon whether the new theories have the correct mechanism underlying the physical process.

5.5 Modification to traditional continuum models

In section 5.4, we have discussed the essence of why and how dislocation walls are being formed in the models presented in section 5.3. These models [49] (also Chapter 2) exhibit intriguing fractal morphology akin to those seen in experiments, yet are very minimalistic and missing most material dependent features. Conversely, the traditional continuum models are missing the dynami-

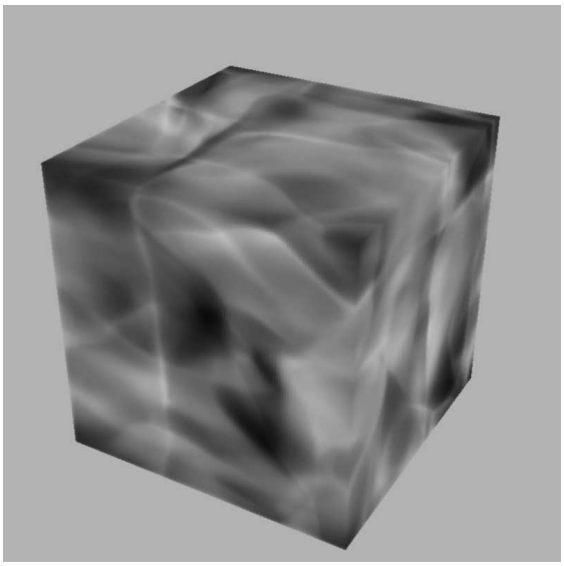

(a) With $f = 0.2$, relaxed

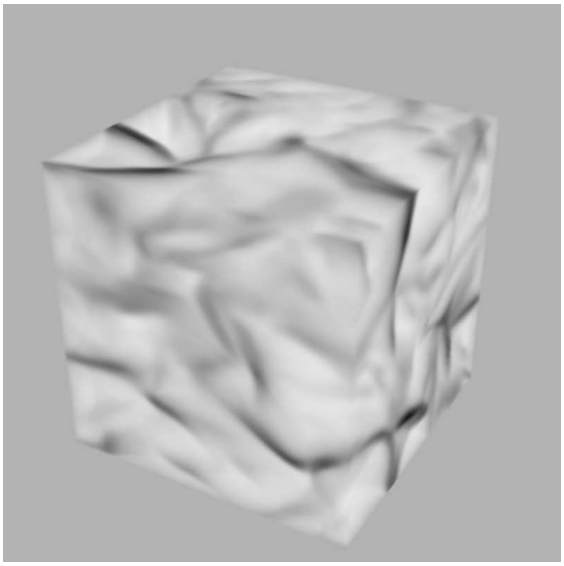

(b) With $f = 0.5$, relaxed

Figure 5.4: **Relaxed dislocation wall structures formed in modified slip dynamics**. Traditional slip dynamics with the dislocation velocity modified to add velocity coupling between slip systems, which leads to sharp dislocation wall structures driven by jumps in some components. Compare (a) and (b) to Fig. 5.2: although $f = 0.2$ does not make a big difference, $f = 0.5$ clearly leads to sharp dislocation wall structures.

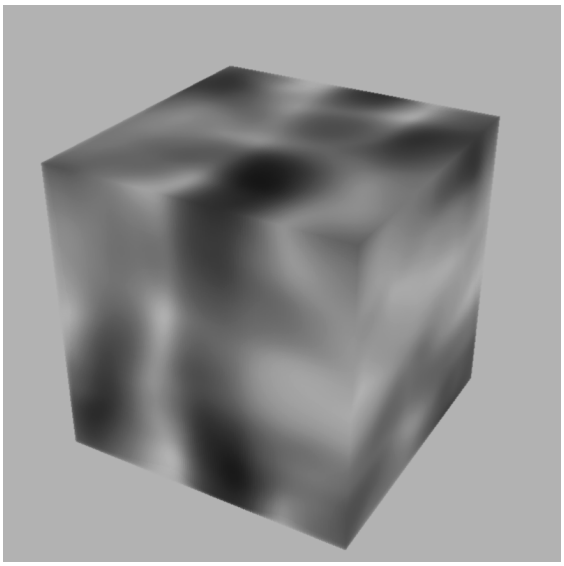

(a) Without coupling ($f = 0$), strained to $\epsilon = 0.5$

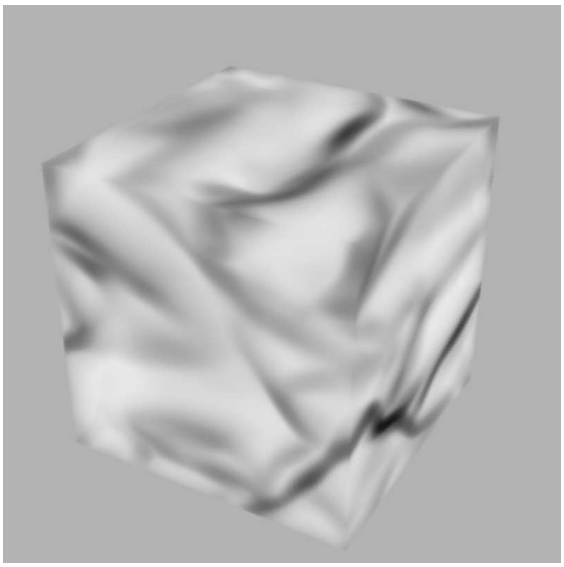

(b) With $f = 0.2$, strained to $\epsilon = 0.5$

Figure 5.5: **Strained dislocation wall structure formed with small velocity coupling under load**. Compare to figure 5.4 where $f = 0.2$ does not seem to have significant wall formation. Under load, it becomes much more clear that even small couplings can still lead to dislocation wall structures.

cally formed dislocation wall structures.

The discussion of the previous section hints at what they maybe missing;

when velocities of different slip systems are directly coupled, jumps in one slip system may lead to dislocation walls in other slip systems. Many physical (microscopic) mechanisms may lead to this effect: e.g. cross slip (velocities coupled through cross-slipped segments), mobile double junctions, ... Here we propose a simple model of mobile double junctions leading to cross-coupled velocities.

Consider the case when two dislocations intersect and form a double junction as they cross each other. One can easily envision that this junction will act as a binding force that will effectively "mix" the velocities of the two dislocations. Physically, this interaction will be rather complicated, depending on the anisotropy of the crystal and the geometry of the intersection, the junctions will have sophisticated physics [42, 54, 13, 14]. We will choose a zeroth-order minimalistic description where the interaction drags each dislocation to partly move with the other, depending only on whether the lines are close enough and share glide directions. The equations prescribing this added term can be written as:

$$\begin{aligned}\partial_t \gamma^{(\alpha)} =& (1-f)\sigma^{(\alpha)} \|\nabla \gamma^{(\alpha)}\| \\ &+ f\left[(\hat{b}\cdot\vec{\mathcal{V}})(\hat{b}\cdot\nabla) + (\hat{p}\cdot\vec{\mathcal{V}})(\hat{p}\cdot\nabla)\right]\gamma^{(\alpha)}\end{aligned} \tag{5.12}$$

where

$$\vec{\mathcal{V}} = \frac{\sum_\beta \vec{\mathcal{V}}^{(\beta)}_{\text{edge}} |\rho^{(\beta)}_{\text{screw}}| + \vec{\mathcal{V}}^{(\beta)}_{\text{screw}} |\rho^{(\beta)}_{\text{screw}}|}{\sum_\beta |\rho^{(\beta)}_{\text{screw}}| + |\rho^{(\beta)}_{\text{edge}}|}.$$

$\mathcal{V}^{(\beta)}_{\text{edge}}$ and $\mathcal{V}^{(\beta)}_{\text{screw}}$ are defined in Eq. (5.7). Velocity coupling coefficient f ($0 \leq f \leq 1$) represents the strength of velocity coupling, and for $f = 0$ Eq. (5.12) is equivalent to Eq. (5.3).

Simulation results solving Eq. (5.12) are shown in figure 5.4. With $f = 0.2$ the dislocation density shows jumps (valleys) as in figure 5.2b, however with $f = 0.5$, dislocation wall structures are formed. Because the velocity coupling term is very similar in this case to Eq. (5.10), this may not be so striking as

half ($f = 0.5$) of the dynamics can be attributed to the velocity coupling term which, considering the resemblance to Eq. (5.10), likely leads to walls by itself. However, upon loading the relaxed specimen to strain $\epsilon = 0.25$, smaller values of f that does not exhibit walls under only relaxation, e.g. $f = 0.2$ is enough to display wall formation while the absence of this term leads to no walls (Figure 5.5).

Figure 5.3 illustrates the behavior in 1D cross-sections of the 3D simulations comparing several f values, some relaxed and some strained states. It is clearly observed that the absence of velocity coupling yields smoothly varying dislocation density whereas increasing velocity coupling term and also straining afterwards in the presence of coupling leads to sharper wall structures.

5.6 Description of wall formation

The wall formation mechanism explained through sections 5.3 and 5.5 appears to be both simple and general; but how do we ascertain that the mechanism is indeed mathematically correct for the models, apart from the evidence provided by the simulations (see Chapters 3 and 4)? In this section, we will elaborate on the details of the wall formation mechanism in Eqs. (5.9) and (5.10); we will show that the equations are directly related to equations that are mathematically proven to form δ-shocks [81].

In Ref. [51] it was shown that our CDD equation in 1D with free boundary condition and the choice of $D(\rho) = 1$ can be transformed to the Burgers equation. The Burgers order parameter is the velocity $\mathcal{V}_z$ (or equivalently the force density). Burgers equation is the prototypical model equation for conservation

laws that form shocks:

$$\partial_t \mathcal{V}_z + \partial_z(\mathcal{V}_z^2) = 0 \tag{5.13}$$

We start with a nine component set of equations for the Nye dislocation density tensor and this is only one particular combination of them; what happens to the other 8 (independent) components? This turns out to have a simple answer. Because the dislocation density has a single velocity field shared among the components in this model, given by the net Peach-Koehler force, each component ρ_{ij} evolves as:

$$\partial_t \rho_{ij} + \partial_z(\mathcal{V}_z \rho_{ij}) = 0 \tag{5.14}$$

Equations (5.13) and (5.14) turn out to be a rather well-studied set of equations (in the two-component case) for a simplified pressureless gas dynamics [81, 48], which is known to form δ-shocks (*i.e.*, our dislocation walls). We defer the detailed discussion of the solutions to the references [81, 48, 21]; but in essence, when $\mathcal{V}$ develops an ordinary jump, ρ_{ij} is passively dragged by $\mathcal{V}$ toward the jump and is forced there to form a δ-shock. This type of singular-shocks has not been commonly observed in fluid dynamics. But when microscopic physics – such as short range interactions between microscopic entities – governs the behaviors of singularities, singular-shocks may appear quite generically in physical systems (see chapter 6).

Note that this mapping is only achievable in a particular setting, where $D(\rho) = 1$ with free boundary condition and in 1D. However, the passive advection of ρ_{ij} seen in Eqs. (5.14) generalizes much more broadly to the new theories, leading to δ-shock walls robustly, independently of how exactly the equation is written.

We have shown that (slightly smeared) walls naturally form within the traditional slip-system dynamics models when the velocities are coupled. We have pointed out that these models naturally form jumps in some components of the order parameter, and that these jumps (when the velocities are coupled in any way) will naturally build up walls of the other order parameters at the jump. In the new theories, we showed that these multiple components all are swept into the shock with the same velocity field – as passive scalars, they form a δ-shock at the moving jump.

But a final question arises: why are the walls smeared in the traditional slip-system models (Figs. 5.2, 5.3, and 5.4), rather than forming the elaborate, fractal structures exhibited by the new theories (Fig. 5.1)? The wall components themselves have dynamics: they move according to their (now coupled) resolved shear stresses, and will in general move in different directions and velocities than the jump that formed them. The smeared walls may be an artifact of the simulational method, that imposes the continuum evolution laws (as 'weak solutions') onto regions whose densities and gradients are too high for those laws to be valid (we discuss this further in Chapter 6). Physical grain boundaries and cell walls would presumably maintain their integrity once formed – evolving according to their mobility and the applied traction. But even within the current dynamical evolution algorithms, we see clear indication that wall-formation physics is generic for multicomponent dislocation dynamics models, except when the velocities for different slip systems are entirely free of local coupling.

5.7 Conclusion

We have illustrated the inner workings behind the dislocation wall structure formation as given by a minimalistic isotropic continuum dislocation dynamics theory [49, 1] (also Chapter 2). In essence, all dislocation dynamics models have Burgers equation-like behavior through which the dislocation velocity evolves and form shocks where there is "annihilation" of dislocation components. In models where dislocations of different flavors interact and can drag other types to some extent, it will lead to pile-up of dislocations where the jump is formed. This is a completely different, novel physical mechanism for wall formation, that does not rely on the energetic preference of dislocations to form stress-free walls. We do not claim to have proven that this mechanism is operative in real systems; experiments are needed to distinguish our mechanism from (say) stochastic and discreteness driven mechanisms [55, 27, 7].

Acknowledgement

We thank Alexander Vladimirsky, Randall LeVeque, and Chris L. Henley for helpful discussions and suggestions. This work was supported by US DOE/BES grant DE-FG02-07ER46393.

CHAPTER 6

REGULARIZATION AND SINGULAR SHOCKS IN CONSERVATION LAWS

6.1 Introduction

The existence and uniqueness theorems of ordinary differential equations are not applicable to many partial differential equations: indeed, the latter often form singularities in finite time. Continuum theories in materials physics also form singularities. Vacancies, dislocations, cracks, and grain boundaries in crystals, steps and facets on surfaces, disclinations and focal conic structures in liquid crystals all form and evolve as systems minimize their free energies and/or respond to external stresses, fields, and boundary conditions. How do we evolve our equations after these singularities arise?

In physics, it is understood that the continuum equations must be supplemented by separate evolution laws for the defects. Vacancies have diffusion constants and effective electromigration charges, dislocations have glide and climb mobilities, cracks have critical stress intensities and growth laws [32] – all dependent upon geometry and temperature through their atomic-scale structures. In the mathematical study of shock-forming partial differential equations (PDEs), this indeterminacy is partially manifested through a multiplicity of *weak solutions*, although the primary focus has historically been on a particular class, satisfying entropy conditions or defined by the vanishing of a regularizing diffusive viscosity.

Here we argue for a broader approach to singularity evolution than these

vanishing viscosity solutions; we propose a new class of problems and solutions that require different methods and treatments to find the physical solutions. The historical focus on vanishing viscosity solutions is justified by the fact that the leading ignored microscopic corrections to many continuum laws are indeed diffusive. This is commonly true of fluid systems, where the Navier-Stokes equations[1] simplify(or complexify) to shock-forming systems describing (e.g.) sonic booms, tidal waves [46], and galactic matter [22]. Indeed, in fluid systems one may derive an entropy condition from the microphysics, which in turn can be shown to imply the vanishing viscosity limit as the appropriate weak solution. But these vanishing viscosity solutions are not the obvious choice in other physical systems, such as traffic models [47], continuum theories of dislocation dynamics [49, 16] and facet growth on grown or etched surfaces [72, 88], where viscosity, entropy, and weak solutions are not relevant to the microscopic behavior. Here we bring ideas from materials physics to inspire new applied mathematics approaches for singularity evolution.

Indeed, we shall argue that the appropriate weak-limits that define the physically reasonable solutions of these physical systems are not typically weak solutions as commonly defined. The singularities in weak solutions must obey the continuum laws in integral form; we argue that the continuum equations are simply inapplicable in singular regions where high densities and gradients violate the continuum assumptions. In particular, for dislocation dynamics the physical systems develop sharp walls of dislocations (grain boundaries and cell walls), corresponding to *δ-shocks* in the continuum partial differential equation [81, 16].

[1] It is not known whether the Navier-Stokes equations have finite-time singularities for smooth initial conditions. There are conjectures that the Euler equations (Navier-Stokes without viscosity) do have such singularities [71, 80].

We begin in section 6.2 by discussing the solutions of the Burgers equation in conservation-law form. We also note the known fact [81] that δ-shocks arise even in the viscosity solutions for some multicomponent systems. We note that in multicomponent systems the Rankine-Hugoniot conditions for general jump discontinuities are not soluble, and that some other mechanism like δ-shocks must arise. In subsection 6.2.3, generalizing the Rankine-Hugoniot condition on the jump discontinuities to allow for δ-shocks will be seen to decouple the jump velocity from the continuum equations, allowing for a family of physical solutions that could be tuned to reflect the microphysics. And we discuss other known families of solutions in subsection 6.2.4, explaining the distinction between these and the proposed singular solutions. In section 6.3 we discuss these shock-forming systems more broadly in the context of numerical methods for evolving defects and defect structures.

6.2 Burgers equation and δ-shocks

Hyperbolic conservation laws and the entropy solutions are the traditional focus of hyperbolic partial differential equations community. We will first introduce the basic ideas of hyperbolic conservation laws and their (entropy) solutions. Then, we will propose and argue that when the singularities' dynamics are not determined by the continuum equations, the physical solutions are different from the traditional weak solutions and therefore need a new class of mathematical and numerical methods to probe the solutions corresponding to the correct microscopic physics of singularities.

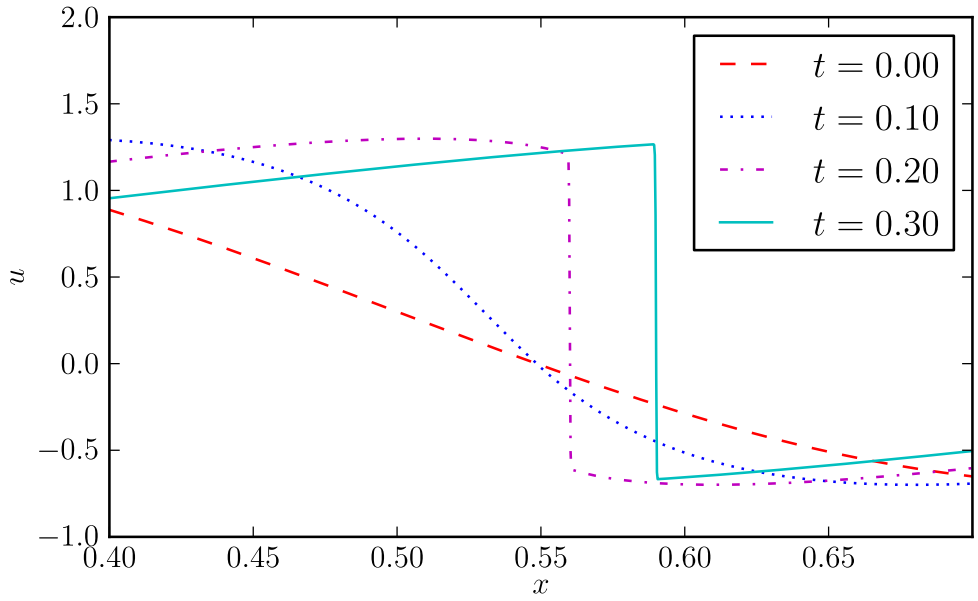

Figure 6.1: **Solutions to the Burgers equation**. At $t = 0$, initial condition is chosen to be a smooth profile as $u(x, t = 0) = \sin(2\pi x) + 0.3$ with $x \in [0, 1)$ and periodic boundaries. At around $t = 1/2\pi \sim 0.159$, sharp jump(or shock) is formed.

6.2.1 Solutions to the Burgers equation

We begin with the conservation-law form of Burgers equation, the classic shock-forming partial differential equation

$$\partial_t u + \partial_x f(u) = \partial_t u + \tfrac{1}{2}\partial_x(u^2) = 0, \tag{6.1}$$

where $f(u) = \frac{1}{2}u^2$ is the flux of the conserved quantity u (It can also be thought of as a 1-D simplified version of the Euler equation for fluid dynamics [46].). It is straightforward to see that the Burgers equation can develop shocks in finite time: a linear region of negative slope $u = \alpha(0)x$ will evolve $\dot{\alpha} = \alpha^2$ yielding $\alpha = 1/(t_c - t)$ with a divergence at $t = t_c$.

Once there is a shock, there is no straightforward solution to the equation

(6.1) because of the diverging derivatives. Indeed, it is clear that we cannot converge pointwise to the traditional jump-singularity solution expected for the Burgers equation (Fig. 6.1); any error in the jump position $x_0(t)$ leads to a large discrepancy (albeit in a small region). Instead, it is physically and mathematically sensible to insist on what is known as *weak limits*. Loosely, a sequence of smooth functions $u_n(x,t)$ converges weakly to the singular solution $u(x,t)$ if

$$\lim_{n\to\infty} \int \phi(x,t) u_n(x,t) \mathrm{d}x\mathrm{d}t \to \int \phi(x,t) u(x,t) \mathrm{d}x\mathrm{d}t \tag{6.2}$$

for all smooth functions $\phi(x,t)$ vanishing at infinite time and space (similar to how a δ function is defined as a *generalized function* and a sequence of smooth *regular functions* is a "solution in the sense of distribution.") This solution should of course obey the equations of motion (Eq. 6.1) everywhere away from the shock at $x_0(t)$. It is also important to insist upon satisfying the conservation law in the vicinity of the singularity: for any $\epsilon > 0$ the flow f into the singularity region minus the flow out must be reflected in the amount near the singularity

$$\begin{aligned} \frac{\partial}{\partial t} \int_{x_0-\epsilon}^{x_0+\epsilon} u(x,t)\mathrm{d}x &= f(x-\epsilon) - f(x+\epsilon) \\ &= \tfrac{1}{2}u^2(x-\epsilon) - \tfrac{1}{2}u^2(x+\epsilon). \end{aligned} \tag{6.3}$$

These conditions are combined in the PDE community into a single seemingly equivalent criterion: a *weak solution* to a differential equation is one which *solves the equation of motion* in a weak sense. Consider multiplying the equation of motion by a smooth function $\phi(x,t)$ which vanishes as $x, t \to \pm\infty$, and integrating over time and space,

$$\begin{aligned} \int \phi \partial_t u &= \int \phi \tfrac{1}{2} \partial_x (u^2), \\ -\int u \partial_t \phi &= -\int \tfrac{1}{2} u^2 \partial_x \phi, \end{aligned} \tag{6.4}$$

where the second equation is formed by integrating by parts. A function $u(x,t)$ which satisfies Eq. (6.4) is said to be a weak solution. The definition of the weak

solution elegantly avoids the specification of the location of the singularity $x_0(t)$. However, we shall see that it does not allow for many physically reasonable solutions that both form weak limits (eqn 6.2) and satisfy the conservation laws (eqn 6.3). The weak solution demands that the continuum equations apply also to the singularity (during the limiting procedure) – whereas physically the evolution of the singularity should be governed by different microphysics.

Even within this restricted class of solutions (the "weak solutions" as defined above, which is much more restricted than the "weak limits" discussed ahead in that the singularities in the weak solutions obey the continuum equations through a limit), there can be many weak solutions of the same initial value problem. The one most commonly studied is the *vanishing viscosity solution*, found by adding a 'viscous' diffusive term to the equations of motion (eqn 6.1),

$$\partial_t u + \tfrac{1}{2}\partial_x(u^2) = \nu \partial_{xx} u \tag{6.5}$$

and then taking the viscosity ν to zero. As long as the viscosity is non-zero, it smoothens the sharp interfaces and allows for a mathematically well-defined and numerically tractable differential equation.

The properties of the vanishing viscosity solutions for the Burgers equation can be understood by studying the associated *Riemann problem*. Consider an initial value problem with a single jump at $x = 0$ from u_- to u_+. To the left ($x < 0$) the flux into the jump is $f(u_-) = \frac{1}{2}u_-^2$; to the right the flux away from the jump is $f(u_+) = \frac{1}{2}u_+^2$. If we presume that the solution remains a jump moving with velocity s, then after a small time Δt there is a hole of size $s\Delta t(u_- - u_+)$ of new conserved u that needs to be filled behind the moving front. Matching the net flux in to the growth rate, we find the Rankine-Hugoniot condition for the

velocity

$$s_{\mathrm{RH}} = \frac{f(u_-) - f(u_+)}{u_- - u_+}. \tag{6.6}$$

The presumption that the singularity remains a single jump, plus the Rankine-Hugoniot condition, provides a complete specification of a weak solution for the Burgers equation for smooth initial conditions. Is it the same as the vanishing viscosity solution? One can show that for negative jumps $u_- > u_+$ the vanishing viscosity solution does indeed remain jump-like, but for positive jumps an initial step will smoothen into a *rarefaction wave*. Smooth initial conditions evolving under Burgers equations never develop positive jumps, though, so the Riemann solution is completely equivalent to the vanishing viscosity solution for smooth initial conditions. Indeed, many numerical methods are based on the correct implementation of the corresponding Riemann problems [46].

The fact that the vanishing viscosity solution in Burgers equation basically agrees with the Rankine-Hugoniot condition, and can be justified for fluid problems based on the 'entropy condition' (not discussed here), has led the numerical analysis community to focus on developing efficient algorithms for extracting the limit of small viscosity in an efficient manner.

6.2.2 Multi-component nonlinear problems with genuine δ-shocks

In many physically interesting problems, however, the problem is often not described by a single component equation; the models are generically multi-component and nonlinear. What happens with multi-component nonlinear problems? Let us generate a two-component equation from Burgers equation

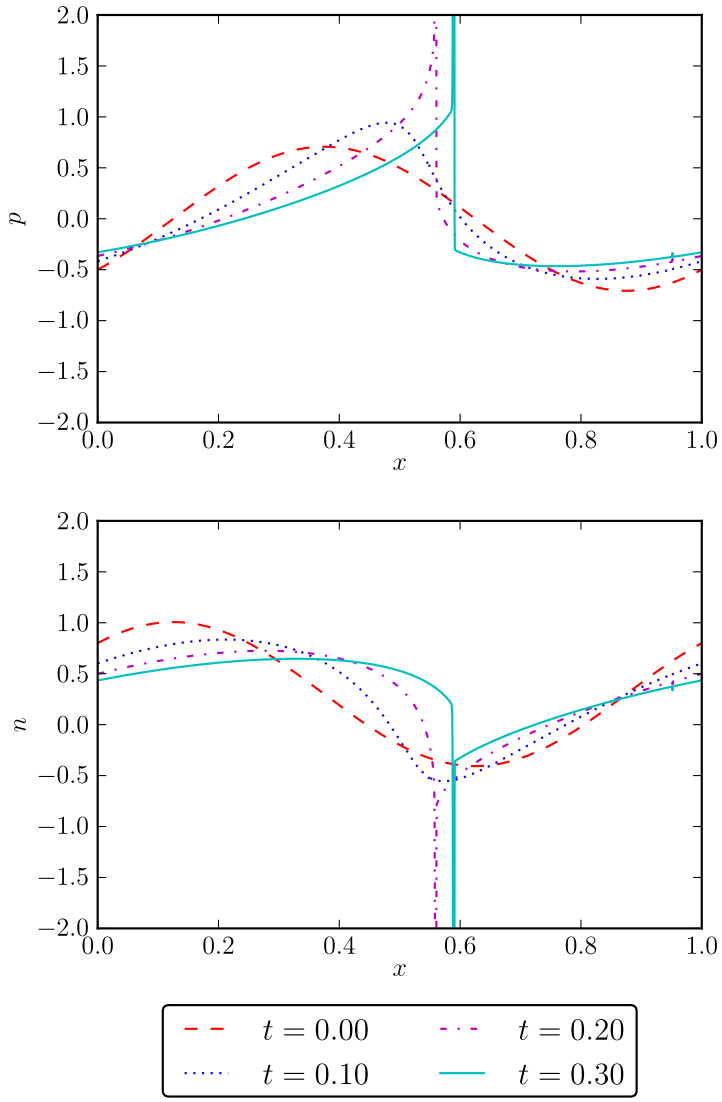

Figure 6.2: **Solutions to** $p_t + (\frac{1}{2}(p+n)p)_x = 0$ **and** $n_t + (\frac{1}{2}(p+n)n)_x = 0$, equations (6.7) and (6.8). Note that both p and n develop δ-shocks as they evolve, starting from a smooth initial condition.

by writing $u = p + n$, with p and n two separately conserved quantities. Suppose that overall the dynamics is still the same, i.e. each component flows with

velocity $u = p + n$. This leads to a set of equations:

$$\partial_t p + \tfrac{1}{2}\partial_x[(p+n)p] = \nu\partial_x^2 p \tag{6.7}$$

$$\partial_t n + \tfrac{1}{2}\partial_x[(p+n)n] = \nu\partial_x^2 n \tag{6.8}$$

Adding and subtracting equation (6.8) to equation (6.7) respectively can also be written as

$$\begin{aligned} \partial_t u + \tfrac{1}{2}\partial_x(u^2) &= \nu\partial_x^2 u \\ \partial_t v + \tfrac{1}{2}\partial_x(uv) &= \nu\partial_x^2 v \end{aligned} \tag{6.9}$$

where $u = p + n$ and $v = p - n$.

We immediately see a serious problem: the Rankine-Hugoniot velocity for u does not agree with that for v

$$\begin{aligned} s_u &= \tfrac{1}{2}(u_-^2 - u_+^2)/(u_- - u_+) = \tfrac{1}{2}(u_- + u_+) \\ s_v &= \tfrac{1}{2}(u_- v_- - u_+ v_+)/(v_- - v_+) \end{aligned} \tag{6.10}$$

except when the additional jump condition $v_+/v_- = u_+/u_-$ happens to be satisfied (not true in general). Since u satisfies the original Burgers equation and v is slave to u, v will remain smooth until u forms cusps, at which point something must happen.

How does the vanishing viscosity solution deal with this conundrum? It turns out that variants on the set of equations (6.9) have been rather well studied, and that they form δ-shocks [81, 21, 48]. That is, the vanishing viscosity solutions to this problem contain δ-functions in v and conventional shocks in u. However, if one looks at the components p and n, both would contain δ-shocks.

Figure 6.2 illustrates what happens with the equations (6.7) and (6.8). Notice that both p and n develop δ-shocks. Figure 6.3 instead simulates the equations (6.9), where it is seen that only v develops a δ-shock where u forms a

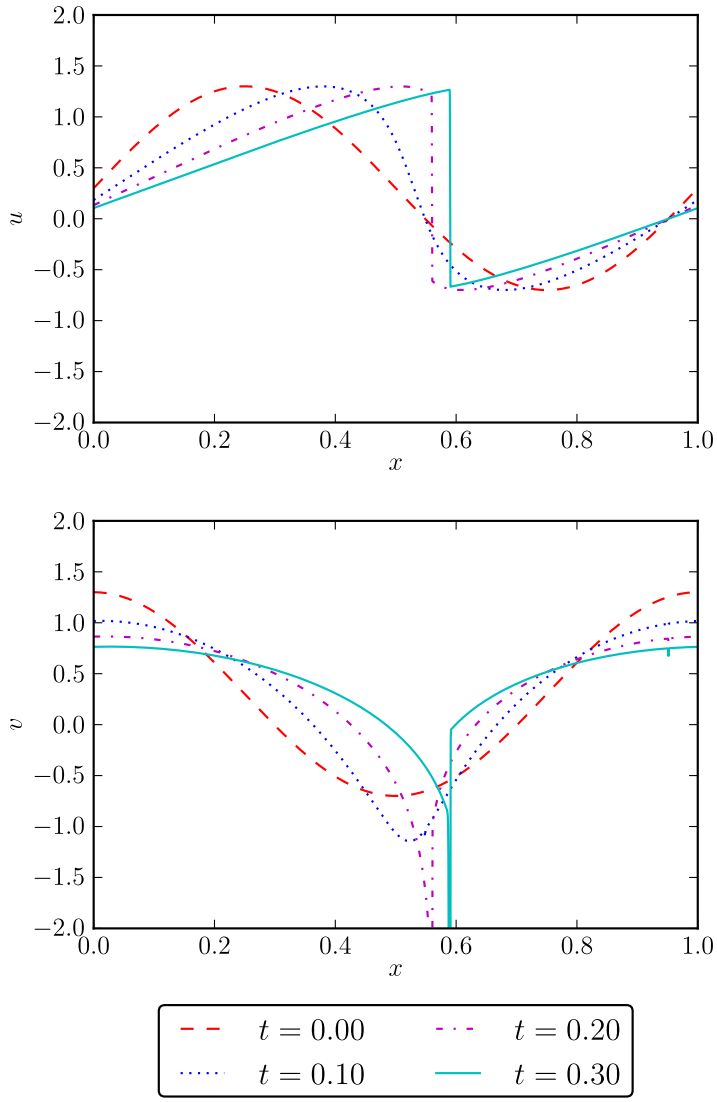

Figure 6.3: **Solutions to** $u_t + (\frac{1}{2}u^2)_x = 0$ **and** $v_t + (\frac{1}{2}uv)_x = 0$, equations (6.9). These are the same set of equations discussed in Ref. [81] albeit simulated with central upwind method [43] rather than an explicit vanishing viscosity solution. Note that on the one hand the central upwind method is not proven to yield the vanishing viscosity solution for this problem, and also that (as discussed in Ref. [18]) the vanishing viscosity solution may not exist.

jump(shock). Note that this is (likely) a vanishing viscosity solution, and also (likely) a weak solution, although we have not proven either fact.

Some of the theorems and algorithms demand strict hyperbolicity [46]. Note that eqn (6.9) is not strictly hyperbolic: the two eigenvalues u and $2u$ become degenerate when $u = 0$, the umbilic point of the equations. However, this is not the root cause of the δ-shocks, as they arise even for initial conditions which avoid these umbilical points. Indeed, there are other strictly-hyperbolic PDEs which are known to form δ-shocks in their vanishing viscosity solutions [81].

Note also that our argument is generic. In some systems, such as magnetohydrodynamics, such a jump is known [22] to split up into multiple "wave" components which each obey the relevant extra conditions. (Such a decomposition is not possible for eqns. (6.10); partial jumps in u have velocities which cause them to merge so long as $u_- > u_+$.) Only when this happens, and the *waves* conspire to each satisfy its Rankine-Hugoniot condition, will the system not form δ-shocks. In general, however, conforming to all R-K conditions at the same time everywhere may not be possible. Hence, we see that δ-shocks likely will arise, even as weak solutions for many multi-component systems.

6.2.3 Physically sensible singular solutions

But physically, even for a single component model, the vanishing viscosity solutions with shocks are not the only physically sensible solutions; in some cases a mismatch of the flow of the conserved quantity at a boundary can lead not only to boundary motion, but also to a pile-up of the conserved order parameter at the boundary. (This is a sensible model to the physical problem of the accumu-

lation of dislocations into moving grain boundaries during polygonization in crystals at high temperature [9, 51], and is the proposed mechanism for the formation of the typical 'cell boundary' dislocation patterns in crystals deformed at low temperatures [16].) In such a case, the solution to the Riemann initial value problem u_- for $x < 0$ and u_+ for $x > 0$ would at short times be approximately

$$u(x,t) = \begin{cases} u_-(x,t) & x < st \\ u_+(x,t) & x > st \\ \Delta_s(t)\delta(x-st) & x = st. \end{cases} \tag{6.11}$$

where $\delta(x - st)$ is a Dirac δ-function[2] at the moving interface. The amplitude of the δ-shock evolves as

$$\begin{aligned} \frac{d\Delta_s}{dt} &= (\text{flow in}) - (\text{hole filled}) \\ &= f(u_-) - f(u_+) - s(u_- - u_+). \end{aligned} \tag{6.12}$$

This is called the generalized Rankine-Hugoniot condition (originally derived for multi-component equations developing δ-shocks as vanishing viscosity solutions [81, 48]), incorporating the δ-shock pile-up at the boundary. A physicist must then turn to a more microscopic theory to determine the evolution law for the defect velocity s:

$$s = s(u_-, u_+, \Delta_s). \tag{6.13}$$

(Insofar as s depends on Δ_s, eqn (6.11) is an approximation; the true equation should have the shock not at st moving linearly with time, but at position $\hat{x}(t)$ with $d\hat{x}/dt = s(u_-, u_+, \Delta_s)$.) For the Burgers equation, we only need an equation for $u_- > u_+$ (since these are the only shocks that spontaneously arise), and we probably expect that $0 \le s \le s_{\mathrm{RH}}$, but otherwise the jump velocity is undetermined.

[2] A δ-function can be viewed as a point mass at the origin: $\int_A^B f(x)\delta(x)\mathrm{d}x = f(0)$ if $A < 0 < B$.

However, we argue that δ-shocks should be not just tolerated when necessary. Rather, they should be considered as legitimate solutions whenever physically indicated, even when viscosity or other regularizations can avoid them.

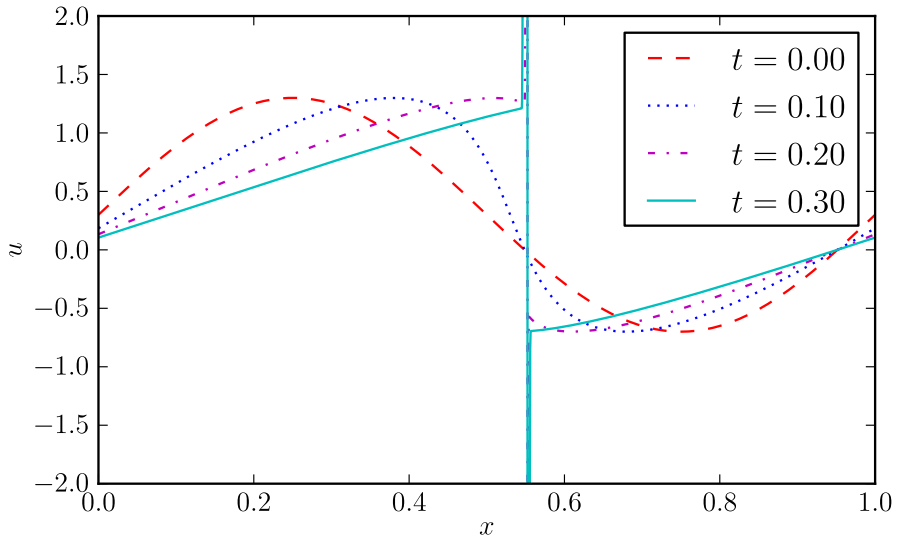

Figure 6.4: **Burgers equation with modified singularity dynamics**. Simulated with $N = 4096$ and $\epsilon = 5/N^2$. Equation (6.14) is the same as the Burgers equation in the limit of $\epsilon \to 0$; smooth parts evolve according to the Burgers equation. However, as the shock forms and progresses, shock velocity (zero) differs from Rankine-Hugoniot condition and δ functions pieces grow at the shock as $\epsilon \to 0$. (The net strength of the δ-shock is the difference between the positive and negative spikes, which remains fixed as $\epsilon \to 0$.)

As an explicit example of a PDE wth 'microphysics' that leads, as $\epsilon \to 0$, to a version of the Burgers equation which violates the Rankine-Hugoniot condition, consider

$$\partial_t u + \partial_x \left(\tfrac{1}{2} u^2 \exp(-\epsilon (\partial_x u)^2) \right) = 0 \tag{6.14}$$

In the limit, it is clear that the solution obeys the Burgers equation where it is smooth, away from the singularity. However, where there are shocks, the flux is suppressed to zero and the shocks, once formed, do not move ($s = 0$). Figure 6.4 illustrates the solutions to equation (6.14); because the shock does not obey

its Rankine-Hugoniot condition, it develops a δ function at the position of the shock.

6.2.4 Previous variants on shock dynamics

There are two well known ways that seemingly benign alterations of a PDE can generate different solutions; we will show that our weak limits do not belong to these categories. In this subsection, we will discuss and explain that our weak limit solutions described in subsection 6.2.3 (prescribed with Eqns. 6.11, 6.12, and 6.13) do not belong to these categories. The category of solutions we propose are neither a solution conserving a different physical quantity, nor another weak solution.

Solutions conserving different quantities

First, our solution (eqns. 6.11, 6.12, 6.13) obeys the conservation law. It is known that harmless-seeming rewritings of the continuum equations can lead to distinct front velocities, but these change the conserved quantity. Multiplying eqn (6.1) by u and rearranging, we produce the classic example of this:

$$\tfrac{1}{2}\partial_t u^2 + \tfrac{1}{3}\partial_x u^3 = 0 \tag{6.15}$$

for which the Rankine-Hugoniot condition yields a front velocity of $s = \tfrac{2}{3}(u_-^2 + u_+^2 - u_- u_+)/(u_- + u_+)$ rather than the Burger's velocity of $s_{\mathrm{RH}} = \tfrac{1}{2}(u_- + u_+)$. This change in the velocity is due to the fact that eqn (6.15) locally conserves not the density u, but rather the density u^2.

Our proposed δ-shock solution by construction conserves the same density

as the standard Burgers equation: it is a different, physically sensible solution to the same continuum evolution law for the same conserved quantity.

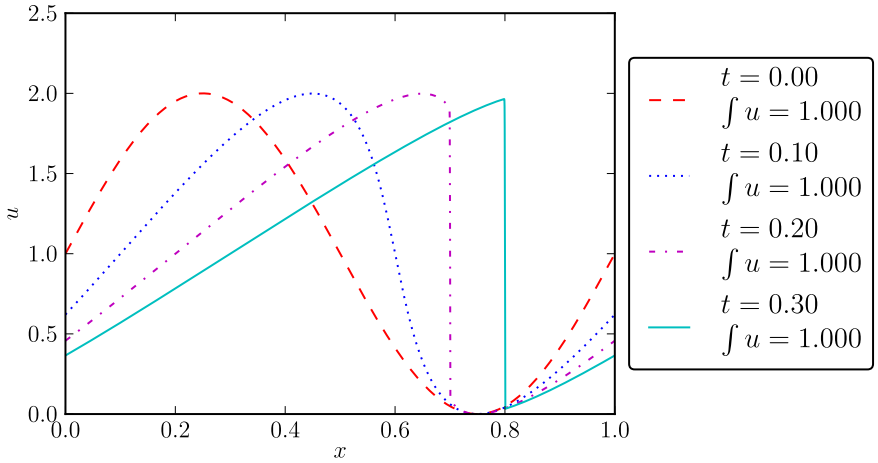

(a) Solutions to Burgers Equation

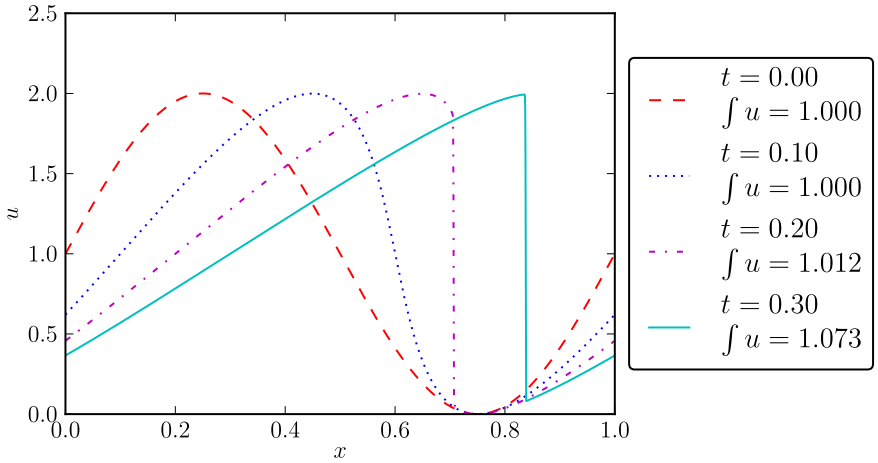

(b) Solutions to Modified Burgers Equation

Figure 6.5: **Weak solutions of the Burgers Equation and its modified form**. Note that the vanishing viscosity solutions of the Burgers equation conserves $\int |u|$ whereas the vanishing viscosity solutions of the modified form does not.

Other weak solutions

Second, our solution is not another weak solution. For many problems, the entropy solution (or the vanishing viscosity solution) is not the unique weak solution and the supplementary entropy condition decides between multiple allowed weak solutions. However, the "entropy condition" does not give physical solutions to all problems (see Ref. [47] for an example in traffic flow). The solution discussed in 6.2.3 is not a weak solution; in eqn (6.4), our δ-shock makes the integral of $\frac{1}{2}u^2\partial_x\phi$ badly defined. This reflects the fact that the velocity of the pile-up at the interface is completely unrelated to the velocity at normal densities, and does not need to be described in a limiting sense by the continuum equations valid for the latter. Thus our proposed solution is not a weak solution as commonly defined. To encompass the variety of physically allowed solutions, we need a broader category of weak limits which solve the differential equation (everywhere it is defined), but which are not weak solutions of the differential equation.

We argued that there can be physically sensible δ-shock solutions to shock-forming equations, that invalidate the traditional Rankine-Hugoniot condition determining the shock velocities – demanding that microscopically determined defect evolution laws enter into the continuum physics. We note that these Rankine-Hugoniot conditions do not naturally generalize to multi-component systems, and indeed that the traditional vanishing viscosity solution can generate δ-shock solutions violating them when two different components are coupled.

6.3 Conclusion: Shocks, singularities, and numerical methods

There are several approaches in the broad field of numerical simulations of singularity dynamics, especially in the field of condensed-matter physics. When the interstitial medium between the defects is linear, one can remove it in favor of effective long-range interactions between defects. Such simulations are most useful for point defects and line defects, where the complexities of topology change during the evolution are limited. For surface and interface evolution (crystalline grain growth, evolution of magnetic domain walls, and martensitic morphologies, surface growth and surface etching), there are two approaches. First, specialized tools have been developed [11] to cope with these topological complexities. Alternative formulations such as phase-field [87] and level-set methods [67] re-introduce fields between singularities and reformulate the problem again as a PDE. These interpolating fields typically have no physical significance. Finally, there are hybrid methods [56, 10] which track both defect and continuum. In all of these cases, the methods are flexibly designed to implement the defect equations of motion suited for the material system at hand.

The shock-forming features of hyperbolic and related PDEs pose unusual challenges which make these explicit defect-tracking methods less attractive. The continuum separating the defects is itself nonlinear in an essential way, and new defects arise from the continuum evolution[3], we want methods like the upwind schemes that evolve nonlinear continuum and defects simultaneously.

However, we have seen that existing formulations are too rigid to encompass sensible weak-limiting physical solutions to these differential equations,

[3]New defects often arise in other physical systems through thermal or even quantum nucleation, but these represent stochastic deviations from the continuum laws. Shock-forming PDEs develop new defects through their intrinsic evolution laws.

allowing for the defect evolution laws to evolve according to rules determined by the microphysics. Existing numerical methods for solving these partial differential equations relies on the properties of the vanishing viscosity solutions, essentially demanding that the dynamics of the singularities be governed by the continuum equation. This, however, is prohibiting the possibility of incorporating separate defect dynamics whose rules are determined by the microphysics at the shock not extrapolating from the continuum laws. We thus call for new mathematical and numerical approaches for these systems.

Acknowledgement

We thank Alexander Vladimirsky, Randall LeVeque, and Chris L. Henley for helpful comments and guidance on hyperbolic conservation laws and numerical methods. This work was supported by US DOE/BES grant DE-FG02-07ER46393.

APPENDIX A

CUDA MASSIVELY PARALLEL IMPLEMENTATION OF PDE SIMULATIONS

A.1 Introduction

The most amazing advancement in technology during the last several decades, undoubtedly, is the invention of computer technologies. Since the development of semiconductor devices started following the Moore's law, it has penetrated virtually all parts of mankind's lives, including physics. Physics and materials science greatly benefited from the appearance and evolution of computer technologies, as it has allowed scientists to view nature in unprecedented ways in both experimental and numerical fronts.

Along the frontier of this development is the new paradigm of computing that utilizes many simple (and cheap) cores instead of using smaller number of more complex (and expensive) cores that was at the height of the technology until last decade. In scientific computing, two main avenues have been pursued in many-core programming. In the first, many individual computers are networked to form a cooperative group of processors with a high memory latency due to network bandwidth. The second, a more recent development, has been the use of graphics processing units (GPUs). These peripheral cards are designed to rotate, project, and render millions of vertices of three dimensional objects as quickly as possible for the gaming industry. Due to the parallel nature of the operations performed on each data element, they have been since adopted as a generalized parallel platform called general purpose graphics processing units (GPGPU).

After some years of developers' interest, several graphics chipset manufacturers grew interest in this potentially new business area, and nVidia came up with a computing hardware and software architecture (CUDA) framework that enables numerical computation on their new generations of graphics cards. With roughly 100× pure floating point operation capacity compared to a single core on a CPU, many algorithms have been shown to achieve 20 ~ 100 times speed-up relative to their single CPU counterparts. With the cost of a GPU roughly similar to 8 conventional CPU cores, GPUs cost much less per FLOP taking into account the workstation box, peripherals, real estate, and operating costs, making them an extremely useful hardware for numerical simulations.

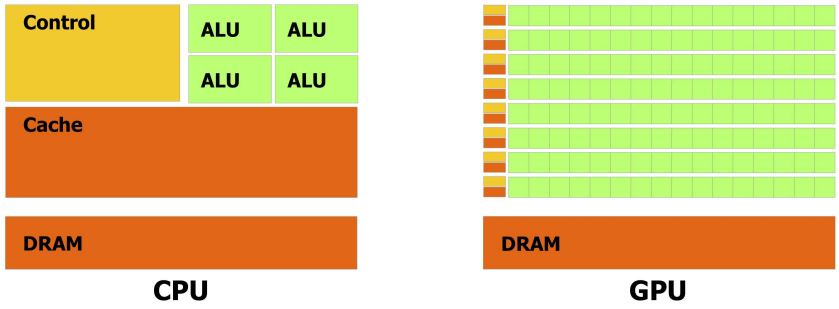

Figure A.1: **Schematic comparison of CPU and GPU**. [a] GPU has many more simpler arithmetic units for computation allowing fast computation on data. Current generation GPU commonly employ SIMT(Single Instruction Multiple Thread) to maximize arithmetic performance while limiting the types of computation for which the architecture is effective.

[a] Figure reproduced from NVIDIA CUDA C Programming Guide [20].

Nevertheless, the technology has its limitations. GPUs have more restrictions as to what individual threads can do, how they can be synchronized, and how the full hierarchy of memories should be handled. Much of these traditionally have been automatically taken care of the (sophisticated) hardware without

the necessity of the programmer stepping into the swamp[1], but with the current generation hardwares, to get best performance, fiddling with the algorithm is unavoidable.

In this chapter we describe a CUDA implementation of yet another simulation that achieves significant speedup compared to the single thread implementation run on a CPU.

A.2 Continuum Dislocation Dynamics

The model that we try to simulate is explained and motivated in detail in Ref. [49] and Chapters 2 and 4. We implement a second-order central upwind method as developed by Kurganov et al.[44] for the partial differential equation:

$$\partial_t \beta_{ij} = \epsilon_{lms} \rho_{sn} \sigma_{mn} \epsilon_{lik} \rho_{kj} \tag{A.1}$$

where $\rho_{kj} = \epsilon_{kuv} \partial_u \beta_{vj}$, and $\sigma_{mn}(r) = \int K_{mnuv}(r - r')\rho(r')dr$ with a kernel function $K_{mnuv}(r - r')$ representing the stress field generated by dislocations. Einstein convention is used for summation of repeated indices.

In general, computing the stress field is likely the most computationally expensive part of the calculation as it involves a spatial convolution, whereas the rest of the calculation is relatively local. For discrete dislocation simulations (where each dislocation line segment is tracked individually like molecular dynamics), fast multi-pole expansion [45] is used to achieve fast computation of the stress field [86]. For continuum simulations (where a partial dif-

[1]This is for the most part true, although a good number of programmers spent their lives optimizing codes that could have orders of magnitudes difference in performance, if one did not think carefully about the hardware architecture.

ferential simulation is solved on a grid), similar multi-pole expansion on the density could be applicable, but are rendered less crucial on a regular grid with fast Fourier transforms. Since a spatial convolution is a simple multiplication in Fourier space, we have $\tilde{\sigma}_{mn} = \tilde{K}_{mnuv}\tilde{\rho}_{uv}$ where tilde denotes spatial Fourier transforms.

Time evolution of the PDE is dealt with by applying a second order central upwind method with total-variance diminishing (TVD) integrators, as described in chapter 4. For the purpose of this chapter, it is only important to note that combinations of right and left derivatives are used in each dimension for evaluating the correct right hand side leading to 2^d combinations of right/left derivatives that are evaluated and mixed to get the final value. This can be repeated multiple times to yield a higher-order TVD integration, but all steps are analogous to each other.

A.3 CUDA algorithm

In this section, we will describe the design decisions made to implement an effective simulation of the continuum dislocation dynamics PDE presented in the previous section. There are three main issues in designing a CUDA algorithm: effectively using hierarchal memory, aligning memory accesses to consolidate memory read and write, and avoiding divergence (branching of different cases).

Figure A.2 illustrates the different types of memory that can be utilized in CUDA architecture. Constant, texture, global, local, shared memories and registers all have different properties pertaining to the types of tasks they are designed for. Global, texture, and constant cache all reside in the global memory

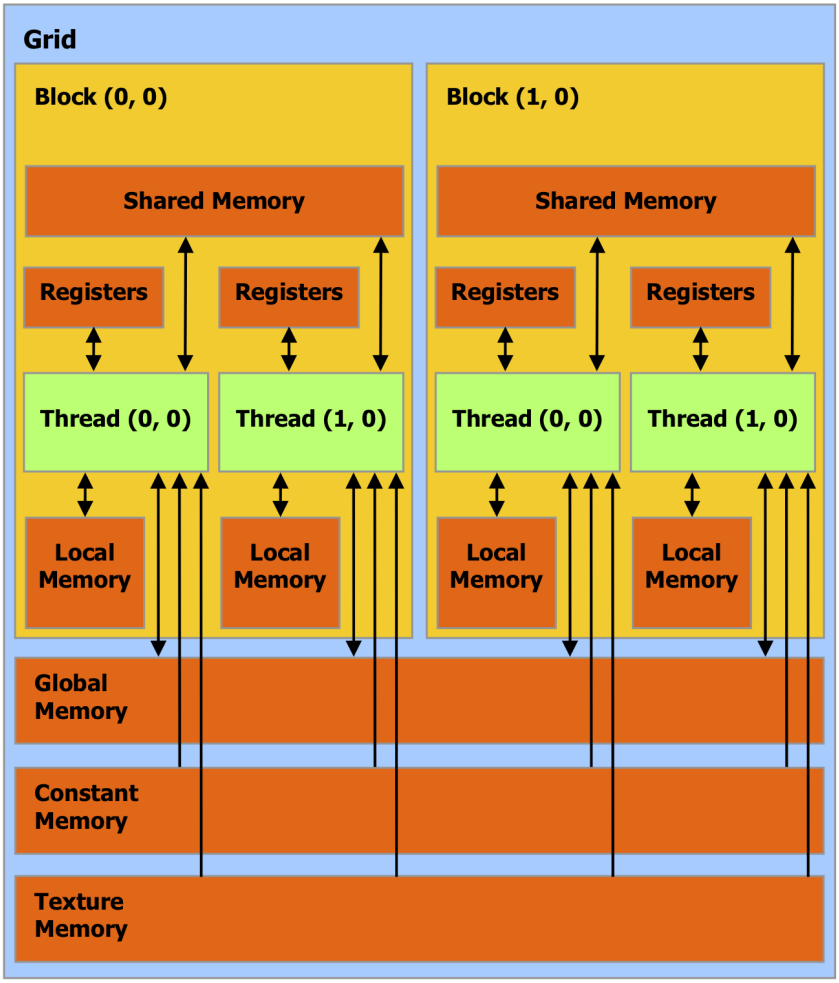

Figure A.2: **Hierarchy of Memory in CUDA architecture** [a]. Global, texture, and constant memory reside outside each multiprocessor, while registers, local memory and shared memory live inside. Each type of memory has different properties, in general on-chip memory are faster but limited in size. Registers, local, and shared memory are allocated from within the same block in current generation hardware.

[a] Figure reproduced from NVIDIA CUDA Programming Guide 0.8.2

and in general are relatively slow, whereas registers, local and shared memories are located within the microprocessors and are faster, but are smaller and volatile – not persistent between kernel executions.

Likewise, accessing these different types of memory in a multi-thread setting is also complicated; when accessing global or shared memory, threads must read from or write to a contiguous aligned block of memory (for global memory) or without bank conflicts (for shared memory). This sometimes necessitates counterintuitive design, such as using oddly sized arrays (see [19] for examples), to achieve maximum performance.

This is much more complicated than the counterparts of a CPU architecture: typically there are the registers, memory, and several levels of cache, but the caches are completely hardware controlled and automatic for the most part, and compilers take care of the registers. Although there are circumstances where one needs to worry about the cache structure, and manually manipulate how the registers are used, for most cases modern sophisticated compilers have made it much less necessary to delve into the complicated affair of performance tuning on this hardware level forceps. However, when programming for CUDA architecture, utilizing the correct memory hierarchy can lead to orders of magnitudes difference in performance providing strong incentive for programmers to understand the details of the architecture and the hardware.

A.3.1 Algorithm overview

The main persistent object in our computation is the order parameter field, β^P. During each time step, we calculate intermediates such as the stress, σ, and derivatives of the distortion field, u that are used to determine the right hand side. Then a central upwinding scheme is used to determine the final RHS and it is added to our order parameter field.

A.3.2 Thread block design issues

As explained in section A.2, the stress field is calculated with spatial convolutions performed in Fourier space. Because this part of the computation takes place in Fourier space (Fourier transform, multiply by $\tilde{K}$, an inverse Fourier transform) it is computed as a preparation step for the main algorithm. The Fourier transforms are performed component-by-component using CUFFT, and the computation of the stress is relatively straight forward.

Implementing the central upwind method it is a little more tricky. There are 9 components of β^P on the right hand side, and 6 components of σ to be read in and eventually written to the global memory. There are also 3 components of the local velocity field $\mathcal{V}$, maximum speeds in each direction for the Riemann fan, and the total dislocation density $\|\rho\| = \sqrt{\rho_{ij}\rho_{ij}}$ to be computed as intermediate fields used in the method. These are (mostly) not written to the global memory, but each involve all components of the derivatives of β^P.

It is also important to note that these steps should preferably done within a single kernel, not as separate steps. Because shared memory is not persistent over separate kernel executions, splitting the kernel demands intermediate values to be stored, and therefore is costly and should be avoided if possible.

A.3.3 Memory usage design issues

It is often tempting to encapsulate a vector or a tensor quantity into a struct that contains the components of the field at a spatial location. For CPU implementations, this helps the design in many ways, and because the components are

consecutive in memory it also is beneficial for maximized cache performance in many cases, especially if there are many local Einstein summation style component contractions. However, on the GPU, this is not necessarily the case. If each thread performs an Einstein summation with data stored in this struct data type they become *non-coalesced* when reading form global memory, and when the field size is a multiple of the *warp size*(or for this matter the number of banks) shared memory accesses have *bank conflicts*. Both of these can result in severe performance loss for applications which are memory access bound.

Thus, the arrays are stored with spatially consecutive values of the same component (along the fastest running index) residing contiguously in the memory. This makes local component access much more effective.

A.3.4 Description of the code

As explained earlier, computing the stress field from the β^P field is straight forward, albeit only on a finite difference grid. Once the Fast Fourier Transforms (FFTs) are performed, it then becomes a local multiplication with a tensor prescribed by its k-space "position". The inverse Fourier transform then returns the stress field to be used in the computation of the dynamics.

The most expensive – and important – part of the problem is to perform the central upwind method and integrating the equations with it. The code consists mainly of three blocks:

1. (Component-wise) Load the order parameter β^P and other local fields, such as σ, into the shared memory.

2. (Component-wise) Compute the derivatives of β^P in $2d$ directions where d is the number of dimensions.
3. (Quadrant-wise) Compute the velocity $\mathcal{V}$ and other quantities that mix multiple components, such as $|\rho|$.
4. (Component-wise) Based on the velocity and other values computed, compute the right hand side($= -h$).

where (Component-wise) refers to kernel operations where different threads work on different components of u and (Quadrant-wise) refers to kernel operations where different threads work on different Cartesian "quadrants".

A.4 Benchmark results

Figure A.3 illustrates the relative speed-up of the CUDA implementation, compared to a single-core python implementation using numpy. Python implementation is without question not the most efficient CPU implementation, and can be further tuned to gain $2 \sim 3\times$ performance [2], but for convenience is used here as the reference implementation.

It is without a doubt very efficient as it achieves $100\times$ speed-up compared to the python implementation: it translates to $30 + \times$ speed-up even comparing to an efficient CPU implementation written in C. Theoretical maximum between the compared platform tells it can be $200\times$ faster if the computation is purely instruction bound, but practically lower for most purposes.

[2] This has been tried and implemented, compared to an optimized C implementation and confirmed that this is close to the maximum performance that can be achieved.

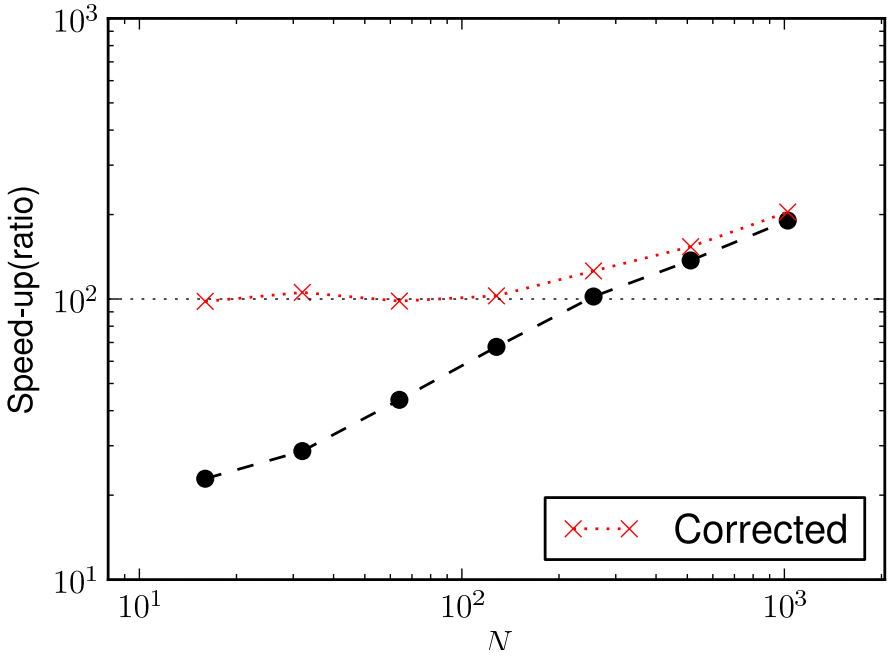

Figure A.3: **Relative speed-up of the CUDA code**. Compared to a single core implementations in python, executed with a Xeon E5520 CPU and a Tesla C2070 CUDA compute unit. The python implementation is obviously not the most efficient implementation on CPU and is $2 \sim 3\times$ slow compared to an optimized CPU code. Theoretically, Tesla C2070 has 515.2 GFLOPS double precision peak processing power while Xeon E5520 can perform 1.9 GFLOPS double precision per core. CUDA benchmark runs contain constant time offset spent in initializing and setting up the system, shown in red is the estimate speed-up correcting for this offset [a].

[a] Obviously, python implementation also has such offset, but because the main routine is so much slower it becomes negligible.

A.5 Remarks

As science and technology advanced at tremendous rates, computer simulations and scientific computing have become an integral part of research in every field of science and engineering. Due to the current limitations of the traditional hardware and CPU architectures, it is becoming increasingly important to

utilize many-core parallel platforms. Many-core massively parallel computing platforms have been in the domain of extremely expensive super computing until very recently, but during the last decade we have seen fast growth of smaller scale and personal computing clusters, and now with the appearance of GPU and many-core processor computing these methods are becoming more accessible and mainstream. In this chapter we have illustrated how such platform could be utilized very efficiently to simulate partial differential equations modeling dynamics of dislocations. Widespread usage of this technology will bring the cost of large-scale simulations down by orders of magnitudes – as the top notch GPUs with similar costs to CPUs have potentially orders of magnitudes better performance – this will surely help advance our understanding of the physics.

APPENDIX B

THE MAPPING TO THE BURGERS EQUATION AND DEVIATING SOLUTIONS

One of the early fascinating results found with this theory was that under certain conditions – 1D and $D(\rho) = 1$ – our continuum dislocation dynamics equations has a direct mapping to the Burgers equation [51], which is the simplest and most studied conservation law. However, as described in chapter 6, the "physical" solutions to a partial differential equations may greatly depend on how the equations are presented[1] and how the singularities are regularized[2].

Clearly the mapping applies for times before the formation of the first singularity so the analytic argument justifies the numerical observation of wall formation. But it remains an interesting question, then, as to whether this mapping does in fact lead to different solutions or the same set of solutions for the dynamics after shock formation.

By calculating the force density $\mathcal{F}_x$ from the initial condition, we set up an initial value problem with the Burgers equation on the one hand, and on the other side we simulate the 1D, $D(\rho) = 1$ version of the equation explicitly, and plot the evolution of $\mathcal{F}_x$. The results as a function of time are plotted in figure B.1.

As shown in the figure, it becomes clear that the solutions – as soon as they develop shocks – do not agree; shocks move with different velocities than for the Burgers equation. Because it looks fuzzy near the shock when we solve

[1] As seen in the comparison of the solutions of the Burgers equations and the modified $\frac{1}{2}(u^2)_t + \frac{1}{3}(u^3)_x = 0$

[2] As argued in chapter 6.

the β^P equation, it's tempting to say that the resolution is causing the shocks to move at different velocities. However, it must be noted that 1D simulations are convergent (as shown in Figure 4.5) and the results presented in figure B.1 are obtained with $N = 4096$ where the solutions should become quite converged. These results are reminiscent of solving the Burgers equation and the modified form $\frac{1}{2}(u^2)_t + \frac{2}{3}(u^3)_x = 0$ (see chapter 6), although $\mathcal{F}$ is conserved for both solutions in our case. A closer examination of the two forms of the equations reveal that the effective artificial viscosity term for Burgers equation differs from that for $\mathcal{F}$ derived from the equations for β^P, and thus the equations must be differently regularized.

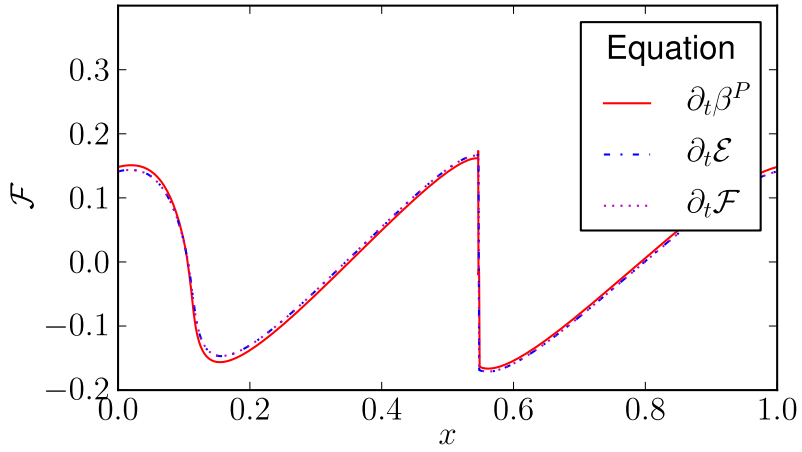

(a) At t = 0.30

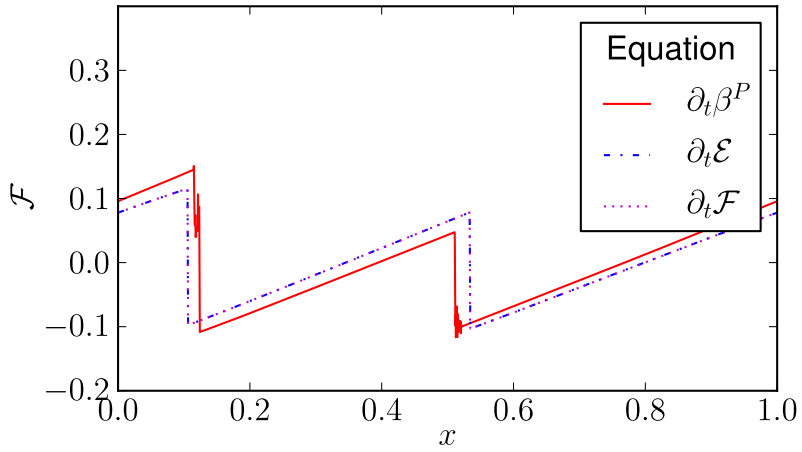

(b) At t = 1.00

Figure B.1: **Burgers equation solutions compared to a mapped results from the CDD equations**. Force density $\mathcal{F}$ plotted at times t = 0.30 and t = 1.00, comparing three different forms of the equations. Labels indicate the order parameter for the solved equation. Note that while it is almost identical when it is smooth, after it forms a jump, the multi-component simulation differs in kink velocity from Burgers equation. Note that the density of each component is conserved: these are legitimate weak solutions of a multicomponent 'microphysics' simulation which yields Burgers equation as its emergent continuum limit – but with a velocity that does not satisfy the Rankine-Hugoniot conditions.

BIBLIOGRAPHY

[1] A. Acharya. A model of crystal plasticity based on the theory of continuously distributed dislocations. *Journal of the Mechanics and Physics of Solids*, 49(4):761 – 784, 2001.

[2] A. Acharya and A. Roy. Size effects and idealized dislocation microstructure at small scales: predictions of a phenomenological model of mesoscopic field dislocation mechanics: Part i. *Journal of the Mechanics and Physics of Solids*, 54(8):1687–1710, 2006.

[3] A. Acharya and L. Tartar. On an equation from the theory of field dislocation mechanics. *Bollettino dell'Unione Matematica Italiana*, 2011.

[4] O. Alvarez, E. Carlini, R. Monneau, and E. Rouy. Convergence of a first order scheme for a non-local eikonal equation. *Applied Numerical Mathematics*, 56(9):1136 – 1146, 2006.

[5] A. Arsenlis and D. M. Parks. Crystallographic aspects of geometrically-necessary and statistically-stored dislocation density. *Acta Materialia*, 47(5):1597 – 1611, 1999.

[6] A. Arsenlis and D. M. Parks. Modeling the evolution of crystallographic dislocation density in crystal plasticity. *Journal of the Mechanics and Physics of Solids*, 50(9):1979 – 2009, 2002.

[7] B. Bakó, I. Groma, I. Mastorakos, and E. C. Aifantis. Investigation of dislocation patterning by stochastic integration of dislocation trajectories. *Modelling and Simulation in Materials Science and Engineering*, 13:671, 7 2005.

[8] C. Bardos and D. Lannes. Mathematics for 2d interfaces. *e-print arxiv:1005.5329*, 5 2010.

[9] D. B. Barts and A. E. Carlson. Simulation and theory of polygonization in single glide. *Philosophical Magazine A*, 75(2):541562, 8 1997.

[10] D. B. Barts and A. E. Carlsson. Order-n method for force calculation in many-dislocation systems. *Phys. Rev. E*, 52(3):3195–3204, 9 1995.

[11] K. A. Brakke. The surface evolver. *Experimental Mathematics*, 1(2):141–165, 1992.

[12] V. Bulatov, W. Cai, J. Fier, M. Hiratani, G. Hommes, T. Pierce, M. Tang, M. Rhee, K. Yates, and T. Arsenlis. Scalable line dynamics in paradis. In *Proceedings of the 2004 ACM/IEEE conference on Supercomputing*, SC '04, page 19, Washington, DC, USA, 2004. IEEE Computer Society.

[13] V. V. Bulatov and W. Cai. Nodal effects in dislocation mobility. *Phys. Rev. Lett.*, 89(11):115501, 8 2002.

[14] V. V. Bulatov, L. L. Hsiung, M. Tang, A. Arsenlis, M. C. Bartelt, W. Cai, J. N. Florando, M. Hiratani, M. Rhee, G. Hommes, T. G. Pierce, and T. Diaz de la Rubia. Dislocation multi-junctions and strain hardening. *Nature*, 440(7088):1174, 4 2006.

[15] L.-Q. . Q. Chen and W. Yang. Computer simulation of the domain dynamics of a quenched system with a large number of nonconserved order parameters: The grain-growth kinetics. *Phys. Rev. B*, 50(21):15752–15756, 12 1994.

[16] Y. S. Chen, W. Choi, S. Papanikolaou, and J. P. Sethna. Bending crystals: Emergence of fractal dislocation structures. *Phys. Rev. Lett.*, 105(10):105501, 9 2010.

[17] Y. S. Chen, W. Choi, S. Papanikolaou, and J. P. Sethna. Scaling theory of continuum dislocation dynamics in three dimensions: Self-organized fractal pattern formation. *e-print arxiv:1106.0195*, 6 2011.

[18] W. Choi, Y. Chen, S. Papanikolaou, and J. Sethna. Is dislocation flow turbulent in deformed crystals? *Computing in Science & Engineering*, 14(1):33–39, 2012.

[19] Nvidia cuda c best practices guide, 2012.

[20] Nvidia cuda c programming guide, 2012.

[21] V. G. Danilov and V. M. Shelkovich. Dynamics of propagation and interaction of [delta]-shock waves in conservation law systems. *Journal of Differential Equations*, 211(2):333 – 381, 2005.

[22] F. De Hoffmann and E. Teller. Magneto-hydrodynamic shocks. *Phys. Rev.*, 80(4):692–703, 11 1950.

[23] J. Deng and A. El-Azab. Temporal statistics and coarse graining of dislocation ensembles. *Philosophical Magazine*, 90(27-28):3651–3678, 8 2010.

[24] B. Devincre, L. P. Kubin, C. Lemarchand, and R. Madec. Mesoscopic simulations of plastic deformation. *Materials Science and Engineering A*, 309:211–219, 2001.

[25] U. F. Frisch and A. N. K. Kolmogorov. *Turbulence : the legacy of A.N. Kolmogorov*. Cambridge University Press, Cambridge, [Eng.] ; New York, illustrated, reprint edition, 1995.

[26] I. Groma. Link between the microscopic and mesoscopic length-scale description of the collective behavior of dislocations. *Phys. Rev. B*, 56(10):5807–5813, 9 1997.

[27] I. Groma and B. Bakó. Dislocation patterning: from micro- to mesoscale description. *Phys Rev Lett*, 84(7):1487–90, 2 2000.

[28] I. Gutierrez-Urrutia and D. Raabe. Dislocation and twin substructure evolution during strain hardening of an fe-22 wt.% mn-0.6 wt.% c twip steel observed by electron channeling contrast imaging. *Acta Materialia*, 59(16):6449 – 6462, 2011.

[29] P. Hähner, K. Bay, and M. Zaiser. Fractal dislocation patterning during plastic deformation. *Phys. Rev. Lett.*, 81(12):2470–2473, 9 1998.

[30] E. O. Hall. The deformation and ageing of mild steel: Iii discussion of results. *Proceedings of the Physical Society. Section B*, 64:747, 1951.

[31] T. Hochrainer, M. Zaiser, and P. Gumbsch. A three-dimensional continuum theory of dislocation systems: kinematics and mean-field formulation. *Philosophical Magazine*, 87(8-9):1261–1282, 2007.

[32] J. A. Hodgdon and J. P. Sethna. Derivation of a general three-dimensional crack-propagation law: A generalization of the principle of local symmetry. *Phys. Rev. B*, 47(9):4831–4840, 3 1993.

[33] M. Holzer and E. D. Siggia. Turbulent mixing of a passive scalar. *Physics of Fluids*, 6:1820, 1994.

[34] D. A. Hughes, D. C. Chrzan, Q. Liu, and N. Hansen. Scaling of misorientation angle distributions. *Phys. Rev. Lett.*, 81(21):4664–4667, 11 1998.

[35] D. A. Hughes and N. Hansen. Graded nanostructures produced by sliding and exhibiting universal behavior. *Phys. Rev. Lett.*, 87(13):135503, 9 2001.

[36] D. A. Hughes, Q. Liu, D. C. Chrzan, and N. Hansen. Scaling of microstructural parameters: misorientations of deformation induced boundaries. *Acta materialia*, 45(1):105–112, 1997.

[37] A. Hunter, H. Kavuri, and M. Koslowski. A continuum plasticity model that accounts for hardening and size effects in thin films. *Modelling and Simulation in Materials Science and Engineering*, 18:045012, 6 2010.

[38] A. Johansen, T. Henning, and H. Klahr. Dust sedimentation and self-sustained kelvin-helmholtz turbulence in protoplanetary disk midplanes. *The Astrophysical Journal*, 643:1219, 2006.

[39] L. E. Kidder, M. A. Scheel, and S. A. Teukolsky. Extending the lifetime of 3d black hole computations with a new hyperbolic system of evolution equations. *Phys. Rev. D*, 64(6):064017, 8 2001.

[40] R. Kobayashi, J. A. Warren, and W. C. Carter. A continuum model of grain boundaries. *Physica D: Nonlinear Phenomena*, 140(12):141 – 150, 2000.

[41] M. Koslowski, A. M. Cuitino, and M. Ortiz. A phase-field theory of dislocation dynamics, strain hardening and hysteresis in ductile single crystals. *Journal of the Mechanics and Physics of Solids*, 50(12):2597–2635, 2002.

[42] L. P. Kubin, B. Devincre, and M. Tang. Mesoscopic modelling and simulation of plasticity in fcc and bcc crystals: Dislocation intersections and mobility. *Journal of Computer-Aided Materials Design*, 5(1):31–54, 1998.

[43] A. Kurganov, S. Noelle, and G. Petrova. Semidiscrete central-upwind schemes for hyperbolic conservation laws and hamilton–jacobi equations. *SIAM J. Sci. Comput*, 23(3):707–740, 2001.

[44] A. Kurganov and G. Petrova. Adaptive central-upwind schemes for hamiltonjacobi equations with nonconvex hamiltonians. *Journal of Scientific Computing*, 27(1):323–333, 2006.

[45] G. L and R. V. A fast algorithm for particle simulations. *Journal of Computational Physics*, 73(2):325 – 348, 1987.

[46] R. J. LeVeque. *Numerical methods for conservation laws*. Birkhäuser, 1992.

[47] R. J. LeVeque. Some traffic flow models illustrating interesting hyperbolic behavior. *Minisymposium on traffic flow*, 2001.

[48] R. J. LeVeque. The dynamics of pressureless dust clouds and delta waves. *Journal of Hyperbolic Differential Equations*, 1:315–328, 2004.

[49] S. Limkumnerd and J. P. Sethna. Mesoscale theory of grains and cells: Crystal plasticity and coarsening. *Phys. Rev. Lett.*, 96(9):095503, 3 2006.

[50] S. Limkumnerd and J. P. Sethna. Stress-free states of continuum dislocation fields: Rotations, grain boundaries, and the nye dislocation density tensor. *Phys. Rev. B*, 75(22):224121, 6 2007.

[51] S. Limkumnerd and J. P. Sethna. Shocks and slip systems: Predictions from a mesoscale theory of continuum dislocation dynamics. *Journal of the Mechanics and Physics of Solids*, 56(4):1450–1459, 2008.

[52] A. E. Lobkovsky and J. A. Warren. Sharp interface limit of a phase-field model of crystal grains. *Phys. Rev. E*, 63(5):051605, 4 2001.

[53] J. C. Mach, A. J. Beaudoin, and A. Acharya. Continuity in the plastic strain rate and its influence on texture evolution. *Journal of the Mechanics and Physics of Solids*, 58(2):105 – 128, 2010.

[54] R. Madec, B. Devincre, and L. P. Kubin. From dislocation junctions to forest hardening. *Physical review letters*, 89(25):255508, 2002.

[55] R. Madec, B. Devincre, and L. P. Kubin. Simulation of dislocation patterns in multislip. *Scripta materialia*, 47(10):689–695, 2002.

[56] D. L. McDowell. A perspective on trends in multiscale plasticity. *International Journal of Plasticity*, 26(9):1280 – 1309, 2010.

[57] A. Mignone, G. Bodo, S. Massaglia, T. Matsakos, O. Tesileanu, C. Zanni, and A. Ferrari. Pluto: A numerical code for computational astrophysics. *The Astrophysical Journal Supplement Series*, 170:228, 5 2007.

[58] M. C. Miguel, A. Vespignani, S. Zapperi, J. Weiss, and J.-R. . R. Grasso. Intermittent dislocation flow in viscoplastic deformation. *Nature*, 410(6829):667, 4 2001.

[59] D. P. Mika and P. R. Dawson. Polycrystal plasticity modeling of intracrystalline boundary textures. *Acta Materialia*, 47(4):1355 – 1369, 1999.

[60] B. Morin, K. R. Elder, M. Sutton, and M. Grant. Model of the kinetics of polymorphous crystallization. *Phys. Rev. Lett.*, 75(11):2156–2159, 9 1995.

[61] H. Mughrabi, T. Ungár, W. Kienle, and M. Wilkens. Long-range internal stresses and asymmetric x-ray line-broadening in tensile-deformed [001]-orientated copper single crystals. *Philosophical Magazine A*, 53(6):793–813, 1986.

[62] T. Mura. *Micromechanics of defects in solids*. Springer, Dordrecht, Netherlands ; Boston, 2, illustrated, reprint edition, 1987.

[63] H. Nessyahu and E. Tadmor. Non-oscillatory central differencing for hyperbolic conservation laws. *Journal of Computational Physics*, 87(2):408 – 463, 1990.

[64] J. F. Nye. Some geometrical relations in dislocated crystals. *Acta Metallurgica*, 1(2):153 – 162, 1953.

[65] M. Ortiz, E. A. Repetto, and L. Stainier. A theory of subgrain dislocation structures. *Journal of the Mechanics and Physics of Solids*, 48(10):2077 – 2114, 2000.

[66] S. Osher and R. P. Fedkiw. Level set methods: An overview and some recent results. *Journal of Computational Physics*, 169(2):463 – 502, 2001.

[67] S. Osher and J. A. Sethian. Fronts propagating with curvature-dependent speed: Algorithms based on hamilton-jacobi formulations. *Journal of Computational Physics*, 79(1):12 – 49, 1988.

[68] W. Pantleon. On the statistical origin of disorientations in dislocation structures. *Acta Materialia*, 46(2):451 – 456, 1998.

[69] N. J. Petch. The cleavage strength of polycrystals. *J. Iron Steel Inst*, 174(1):25–28, 1953.

[70] A. Pumir and E. D. Siggia. Development of singular solutions to the axisymmetric euler equations. *Physics of Fluids*, 4:1472–1491, 7 1992.

[71] A. Pumir and E. D. Siggia. Finite-time singularities in the axisymmetric three-dimension euler equations. *Phys. Rev. Lett.*, 68(10):1511–1514, 3 1992.

[72] M. Rauscher, T. Cretegny, J. P. Sethna, R. A. Wind, and M. A. Hines. unpublished work.

[73] J. M. Rickman and J. Viñals. Modelling of dislocation structures in materials. *Philosophical Magazine A*, 75(5):1251–1262, 1997.

[74] A. Roy and A. Acharya. Finite element approximation of field dislocation mechanics. *Journal of the Mechanics and Physics of Solids*, 53(1):143 – 170, 2005.

[75] J. Schiøtz, F. D. Di Tolla, and K. W. Jacobsen. Softening of nanocrystalline metals at very small grain sizes. *Nature*, 391(6667):561–563, 2 1998.

[76] K. W. Schwarz. Simulation of dislocations on the mesoscopic scale. i. methods and examples. *Journal of Applied Physics*, 85(1):108–119, 1 1999.

[77] C. Schwink. Flow stress dependence on cell geometry in single crystals. *Scripta Metallurgica et Materialia*, 27(8):963 – 968, 1992.

[78] J. Shi, Y.-T. . T. Zhang, and C.-W. . W. Shu. Resolution of high order weno schemes for complicated flow structures. *Journal of Computational Physics*, 186(2):690 – 696, 2003.

[79] B. I. Shraiman and E. D. Siggia. Scalar turbulence. *Nature*, 405(6787):639–646, 2000.

[80] E. D. Siggia and A. Pumir. Incipient singularities in the navier-stokes equations. *Physical review letters*, 55(17):1749–1752, 1985.

[81] D. C. Tan, T. Zhang, T. Chang, and Y. X. Zheng. Delta-shock waves as limits of vanishing viscosity for hyperbolic systems of conservation laws. *Journal of Differential Equations*, 112(1):1 – 32, 1994.

[82] C. Teisson, O. Simonin, J. C. Galland, and D. Laurence. Turbulence and mud sedimentation: a reynolds stress model and a two-phase flow model. In *Proceedings of the International Conference on Coastal Engineering*, volume 1, 2011.

[83] V. Tikare, E. A. Holm, D. Fan, and L. Q. Chen. Comparison of phase-field and potts models for coarsening processes. *Acta materialia*, 47(1):363–371, 1998.

[84] M. D. Uchic, D. Dimiduk, J. N. Florando, and W. D. Nix. Sample dimensions influence strength and crystal plasticity. *Science*, 305(5686):986–989, 8 2004.

[85] R. von Mises. Mechanik der festen körper im plastisch deformablen zustand. *Göttin. Nachr. Math. Phys*, 1:582–592, 1913.

[86] H. Y. Wang and R. Lesar. O(n) algorithm for dislocation dynamics. *Philosophical Magazine A*, 71(1):149–164, 1995.

[87] J. A. Warren, R. Kobayashi, A. E. Lobkovsky, and W. C. Carter. Extending phase field models of solidification to polycrystalline materials. *Acta Materialia*, 51(20):6035 – 6058, 2003.

[88] R. A. Wind and M. A. Hines. Macroscopic etch anisotropies and microscopic reaction mechanisms: a micromachined structure for the rapid assay of etchant anisotropy. *Surface Science*, 460(13):21 – 38, 2000.

[89] M. Zaiser, M. C. Miguel, and I. Groma. Statistical dynamics of dislocation systems: The influence of dislocation-dislocation correlations. *Phys. Rev. B*, 64(22):224102, 11 2001.